Spring 1-1-2020

Interaction Between the Metabolism of Ketone Bodies In Brain Tissue And Neurological Disorders

Chan-chih Hsiao
Cleveland State University

INTERACTION BETWEEN
THE METABOLISM OF KETONE BODIES IN BRAIN TISSUE
AND
NEUROLOGICAL DISORDERS

CHAN-CHIH HSIAO

Bachelor of Science in Botany

National Taiwan University

June 2001

Mater of Science in Biomedical Engineering

National Yang-Ming University

June 2004

Submitted in partial fulfillment of requirements for the degree

DOCTOR OF PHILOSOPHY IN APPLIED BIOMEDICAL ENGINEERING

at the

CLEVELAND STATE UNIVERISTY

August 2020

We hereby approve this dissertation for

CHAN-CHIH HSIAO

Candidate for the DOCTOR OF PHILOSOPHY degree for the

Department of CHEMICAL AND BIOMEDICAL ENGINEERING

and the CLEVELAND STATE UNIVERSITY'S

College of Graduate Studies by

Committee Chairperson, JORGE E. GATICA, PH.D.

Department of Chemical and Biomedical Engineering, Sep 3, 2020

Committee Member, JOANNE M. BELOVICH, PH.D.

Department of Chemical and Biomedical Engineering, Sep 3, 2020

Committee Member, NOLAN B. HOLLAND, PH.D.

Department of Chemical and Biomedical Engineering, Sep 4, 2020

Committee Member, R. JEFFREY DEAN, PH.D.

Department of Biology, Sep 3, 2020

Committee Member, CHANDRA KOTHAPALLI, PH.D.

Department of Chemical and Biomedical Engineering, Sep 3, 2020

Student's Date of Defense: MAY 1, 2020

INTERACTION BETWEEN THE METABOLISM OF KETONE BODIES IN BRAIN TISSUE AND NEUROLOGICAL DISORDERS

CHAN-CHIH HSIAO

ABSTRACT

Regulation of brain metabolism and cerebral blood flow involves complex control systems with several interacting variables at both cellular and organ levels. Quantitative understanding of the spatially and temporally heterogeneous brain control mechanisms during internal and external stimuli requires the development and validation of a computational (mathematical) model of metabolic processes in brain tissue. A computational model of the biochemical pathways in brain is presented in this paper. The model structure consists of neurons, astrocytes, and a surrounding capillary network. Glucose is the major oxidative energy substrate in the brain. However, under hypoglycemic conditions such as during diet or fasting or other conditions induced by pathology, alternate energy substrates such as ketone bodies supplement glucose metabolism. In this study, the increased activity of the glutamate-glutamine shuttle is studied in conjunction with the observation that ketosis results in lower lactate levels in brain. A model of ketosis in brain is used to examine the partitioning of carbon units entering the tricarboxylic acid cycle at the level of acetyl-CoA. Using Flux Balance Analysis, we hypothesized that the carbon fluxes would shift towards an increase in flux rates stemming from the metabolism of ketone bodies with a proportional decrease in the flux of lactate derived from the astrocyte-neuron lactate shuttle. It was found that the model could predict an estimation of compartmentalized flux-balances (mitochondrial-cytosolic) in standard and ketogenic diet conditions. Ketone body metabolism was found

to be loosely coupled with glucose metabolism (astrocyte-neuron) suggesting important therapeutic implications.

TABLE OF CONTENTS

Page

LIST OF TABLES

LIST OF FIGURES

CHAPTER I

INTRODUCTION

A normal daily life diet consists of three main types of nutrients: carbohydrates (60%), lipids (20%), and proteins (20%). The process of digestion transforms carbohydrates into glucose (Kemppainen et al., 2005). Our brain consumes around 25% of whole body's glucose at rest, and 14% during exercise. This change occurs because a certain amount of glucose is needed to provide energy for the muscles. Neurons use not only glucose, but also lactate as a fuel. Astrocytes produce lactate from pyruvate and export it to neurons by means of the astrocyte-neuron lactate shuttle (ANLS).

In neurons, about 10% of pyruvate is derived from glycolysis and 90% from the lactate shuttle. Lipids are digested into fatty acids in the small intestine and then transported to the liver. The fatty acids can be converted into ketone bodies, including acetone, acetoacetate, and BHB (β-hydroxybutyrate). Acetone and acetoacetate are then metabolized into BHB, and BHB is delivered to the neurons and transformed into acetyl Co-A. 65% of acetyl Co-A is derived from pyruvate and 35% from BHB under normal diet. Acetyl Co-A, that is produced by metabolizing glucose, lactate, or ketones is then incorporated into tricarboxylic acid (TCA) cycle. Brain tissue main metabolic pathways are as shown schematically in Figure I.1 below.

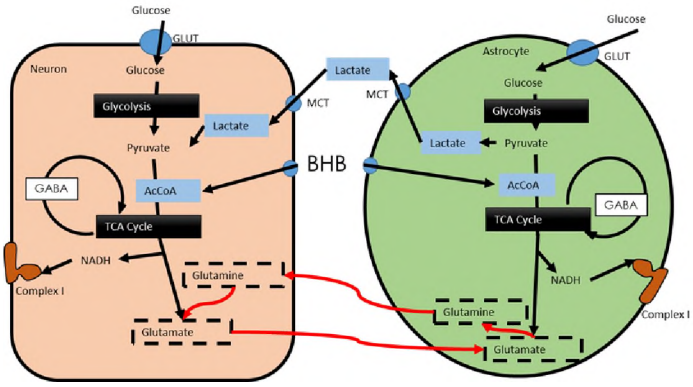

Figure I.1. Brain tissue main metabolic pathways. (Russell et al., 2002)

Glucose and brain tissue

Brain consists mostly of neurons and astrocytes. The function of neurons is sensing, while astrocytes are supporting cells that provide nutrients to neurons. Glucose enters the cells through glucose transporters, or GLUTs. While each individual astrocyte has the same glucose transporting rate than those of neurons, the number of astrocytes in the brain is ten times that of neurons. Therefore, the total astrocytic glucose intake is approximately ten times that of neurons. When glucose enters cells, it is metabolized through glycolysis and the TCA cycle, which generates NADH (reduced form of nicotinamide adenine dinucleotide), ATP (adenosine tri-phosphate), carbon dioxide, and water.

The glycolysis and TCA cycle (cf. Figure I.2) are metabolic pathways, which consist of more than twenty steps. In the process of glycolysis, free radicals, the molecules that contain an unpaired electron, are produced in the conversion of glyceraldehyde 3-phosphate (GADP) to 1,3-bisphosphoglyceric acid (1, 3 BPG). In the process of TCA cycle, the steps which produce NADH will generate free radicals when NADH metabolize to ATP.

A

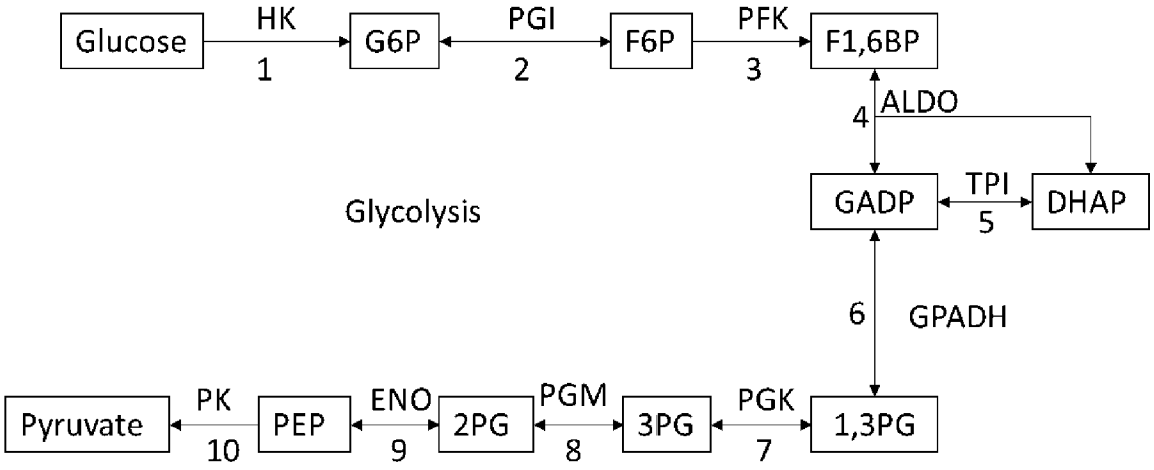

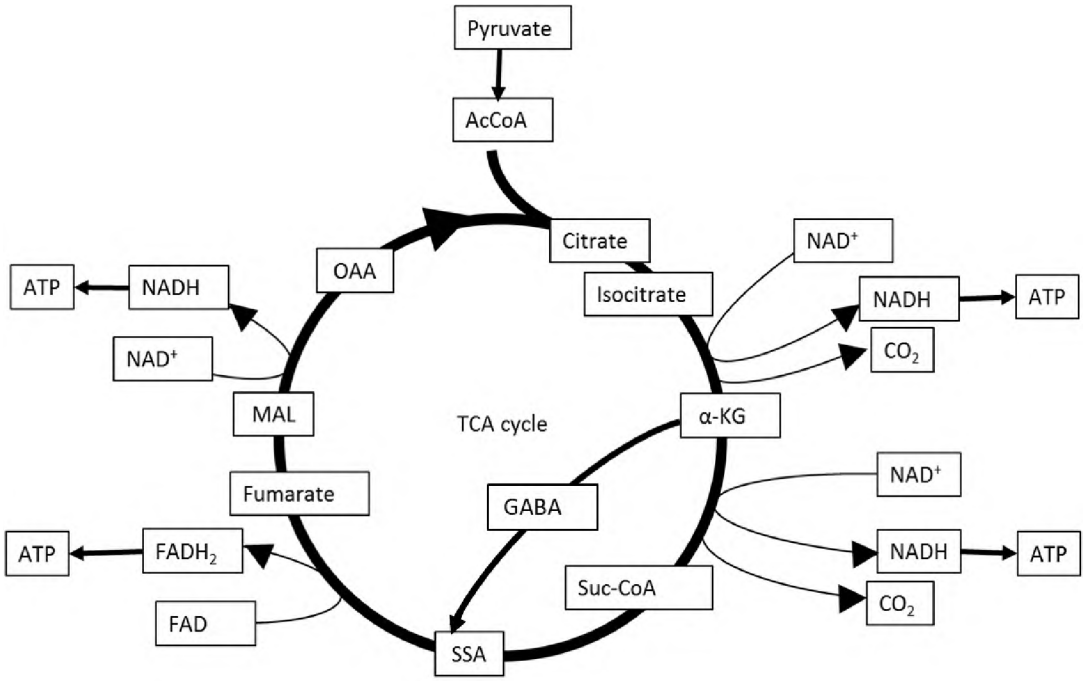

B

Figure I.2. (A) Glycolysis and (B) TCA cycle (Salim, 2017).

Statement of the Problem

The degeneration or loss of functionality of different parts of the brain is one of the reasons typically associated with a variety of neurological disorders, such as Parkinson's Disease (PD) and Alzheimer's disease. For instance, a widely accepted cause of PD is the degeneration of the substantia nigra, which secretes dopamine. However, the detailed mechanisms underlying cell death in the substantia nigra have not yet been elucidated (Chen et al., 2007). One possible mechanism that has been highlighted as a potential cause for the loss of functionality of neurons is the metabolism of glucose in these cells (or glycolysis) (Salim, 2017). Glycolysis typically produces significant levels of reactive oxygen species (ROS); which could lead to mitochondrial dysfunction in neurons (Salim, 2017). In order to find the interrelationship of free radicals and neuron dysfunction, it is need to find the free radicals dynamic and steady state level. One possible method would be to measure, directly or indirectly, the dynamic and steady state concentrations levels of GADP and 1, 3 BPG. It needs evaluate the dynamic and steady state concentrations in neuron. However, due to neurons are separated each other and surrounded by astrocytes, *in vivo* evaluation of neuronal glycolysis and TCA cycle is difficult (Kemppainen, 2005).

A valuable complement to experiments is the availability of predictive tools that connect levels of metabolites or specific fluxes whose values can be determined by already have well-established experimental techniques, with fluxes and dynamics of pathways that can potentially explain these losses in functionality. Modeling of brain tissue has been widely addressed in the literature (Aubert et al., 2005; Perrillat-Mercerot et al., 2019). These efforts, however, have focused on specific pathways or substrate

dynamics. Mulukutla (Mulukutla et al., 2015), for example, completed detailed models of the glycolysis and TCA cycle in rats ovary cells, but did not attempt to build communication pathways between neurons and astrocytes, nor they accounted for different dynamics in each cell. Patel and coworkers (Patel et al., 2004) concentrated their attention on some of the inter-compartment (cells) pathways, particularly the glutamate-glutamine cycle and GABA shunt, but simplified the basic intra-compartment pathways. These groups studied tissue metabolic dynamics for glucose as the main energy substrate, they did not consider the metabolic effect of ketone bodies (KB) in their models. Aubert and coworkers (Aubert & Costalat, 2005) developed a simplified model focusing on the lactate shuttle and transporters (GLUT and MCT); these authors, however, did not consider the potential of effect of lactate fluxes and levels on the transporters affinity, nor they accounted for different isoforms of these transporters (GLUT1-4 and MCT1-4). More recently, Heiske (Heiske et al., 2014) provided complex I modeling equations, but did not connect the model to the onset or progression of neurological disorders.

This study will combine different aspects of brain metabolism models, like those referred above, into an integrated model by adding the missing connections and interrelations. Since the most important aim of this study is to formulate and validate a metabolic model, which can replicate and shed light on experimental observations and phenomena; we envision a model with significantly increased complexity. Particular attention will be paid to the pathways that can explain the differences and limitations when ketone bodies are considered as a substitute or complementary substrate to sustain brain metabolism.

This model will enable *in silico* experiments, which will be validated by in *vivo* and *in vitro* results. There have been several Parkinson's disease-related studies, such as those examining mass flux transport between brain cells, as well as studies on membrane proteins. However, the results from all these studies have not yet been integrated in a mathematical model of brain metabolism.

A computer model can be formulated to integrate the major inter and intra-cellular pathways, it can be developed aimed to include all species, reactions, transporters, fluxes, and parameters of glycolysis and TCA cycle of neurons and astrocytes. Such a model will consist of more than 60 species, more than 100 fluxes, with more than 200 parameters. A model with such a high complexity may not be realizable or not robust due to the intricate interrelation between fluxes and parameter values that can affect the prediction of the dynamics for the concentrations and fluxes of the different model metabolites. Therefore, a balance between complexity and robustness is necessary. If the number of species, reactions, fluxes, and parameters could be reduced, without significantly affecting the model predictive ability, a more robust model will result.

Once a computer model is validated, this model will prove to be an efficient tool to study potential causes, which can accelerate or slow down brain deterioration phenomena associated to the onset and progression of neurological disorder. Moreover, the model can identify fluxes and species, either dynamic and steady state levels, that could be used to formulate or validate therapies to control the deterioration of areas of interest in brain tissue. For example, the model can be used to examine the link of Complex I denaturation and brain tissue deterioration rates, with ratios of glucose to KB in the diet. Similarly, and model can examine the inter-relation of tissue deterioration

rates with the activity of transport protein which control the flux of glucose and ketone-bodies into the brain cells.

Materials and Methods

This research will formulate a lumped-parameter *in silico* model to describe the dynamics of concentrations and mass transport fluxes under isothermal conditions in brain tissue. The model aims to predict fluxes and concentration levels for all the reactions (cf. Figure I.2) in the glycolysis and tri-carboxylic acid cycle, along the most significant pathways (cf. Figure I.1) accounting for inter-cellular transport in brain metabolism.

This model will be validated using literature data for selected concentration and fluxes levels collected during stimulated (dynamic) brain metabolism experiments as well as at steady-state. We will demonstrate how the model can be simplified, and highlight how models with different levels of complexity can be used to run *in-silico* experiments. These studies are anticipated to predict critical metabolic phenomena, formulate conditions for in-vivo experiments, and identify measurements required to elucidate the interrelation between metabolic pathways and cell functionality.

Initially, an *in silico* model including all species, fluxes, metabolisms, and transporters, for the glycolysis and TCA cycle, both in astrocytes and neurons, will be formulated.

This model will be completed by assistive metabolic pathways, such as the GABA shunt, the glutamate-glutamine cycle, and the astrocyte-neuron lactate shuttle. The resulting model is very high in complexity.

An essential goal in the formulation and development of in-silico models is their reliability and robustness as predictive tools. Cognizant that the reliability of these models is directly related to the number of adjustable parameters, the complexity of the model and uncertainty of its parameters will be examined sequentially as follows.

The first step is to the significance of each metabolic reaction under the light of its thermodynamic feasibility. Some reactions which have small reaction Gibb's free energy (ΔG) will be neglected. Because small ΔG reaction implies that it is a fast equilibrium reactions, and is not a rate determined step. The reaction ΔG is the difference of species formation ΔG. We find the standard formation from reference. Then we consider the enthalpy, change number of species, total number of hydrogen atoms in the species to calculate transformed ΔG. Due to ATP and NADH will involve in some reactions of glycolysis and TCA cycle, we will consider pH, ATP/ADP, NADH/NAD levels and calculate further transformed formation Gibbs energy in neuron and astrocyte. Here, we have the species formation ΔG, and we can calculate reaction ΔG by the difference of species formation ΔG. However, our system is in steady state and is not in equilibrium, we need consider the species steady state concentration to calibrate reaction ΔG. After these steps, the outputs are steady state reaction ΔG of every step of glycolysis and TCA cycle. Then next step is neglecting the reactions whose ΔG are close to zero. Because the reactions with small ΔG implies they are fast arriving equilibrium reactions. However, the

steps which produce NADH will not be neglected, because free radicals will be produced when NADH metabolizing to ATP. The free radicals producing steps are what we concerned, because free radicals might affect dysfunction of brain tissues.

Using Constrained Optimization to examine Enzymatic Activity.

In every steps of glycolysis, we know metabolic and transporter flux balance equation of Haldane relationship. This relationship includes rate constant of reaction and transportation, affinity of enzyme and transporter, species concentration, and reaction flux rate.

Next, using enzyme activity and minimum non-linear constrained optimization to determine thermodynamic driving force (ΔG) and concentrations. The steps of constrained optimization is based on Beard and Qian's research(Beard & Qian, 2005). In their research, we know the standard reaction ΔG, which is not calibrate by the steady state concentration, and we know all fluxes of all reactions under different modes, species partition coefficients, stoichiometric matrix of total reactions. The constraints are the outputs of each flux multiplies each calibrated reaction ΔG always small than zero. In method 3, the total outputs are the all species steady state concentrations and all reaction ΔG of different modes. Applying these concentrations and ΔG, and we know the affinity of enzymes and transporters, we can calculate all rate constants. Eventually, we can calculate the steady state concentrations and reaction ΔG, and no need of knowing the rate constants of all reactions. This means we can decrease the system complexity through decrease the parameter number, here, rate constants are parameters. Theoretically, we can neglect 2 parameters of each reaction of glycolysis, TCA cycle, and transportation, of each type cell

(astrocytes or neurons). The total number of neglected parameters will be different, based on metabolisms and tissues what we concerned.

After created a simplified model, we are going to try to run the model to output a reliable dynamic and steady state result, and the result can represent in vivo experimental data. However, in order to find specific issue, for example, the free radicals which produced from glycolysis, we need to keep some key steps which cannot neglect in too simplified model. How to neglect the minor steps and left the key metabolisms? We need to revise *in silico* model to represent the concerned issues.

As diets can effectively used to change the level of ketone bodies in blood. We can use the model to investigate the effect of lipid percentage in diet composition on metabolic processes in brain tissue. Special attention will be paid to examine the effect of three important transporters (Complex 1, GLUT, and MCT) in brain tissue metabolism.

CHAPTER II

LITERATURE REVIEW

Background

The human brain consists of three main structural entities: the cerebrum, the cerebellum, and the brain stem (Utsuki, 2015). The functions of these regions such as cognition, motion, and emotions are coordinated by signal delivery. The brainstem is formed by midbrain, pons, and medulla oblongata. The term basal ganglia refers to a functional unit consisting of a series of nuclei, and this structure connects the brainstem with the cerebral cortex and thalamus.

In order to initiate the movement of the body, the basal ganglia deliver a signal to the thalamus, and this signal is then transferred to the cerebral cortex and other parts of brain. The main function of the basal ganglia is to control voluntary movement. Furthermore, the basal ganglia are involved in high level cognitive functions, for instance, memory, emotion, and reward learning. Pathological changes in the basal ganglia will result in the limitation of movement and cognition, and may cause Parkinson's disease (PD) as well as Huntington's disease (LeWitt & Fahn, 2016).

The substantia nigra is a nucleus within the midbrain located between the midbrain tegmentum and the cerebral peduncle. It is not a homogeneous nucleus, and it can be divided into three regions that differ in structure and functions: substantia nigra pars compacta, SNpc; substantia nigra pars reticulata, SNpr; and substantia nigra pars lateralis. Substantia nigra is a subsidiary nucleus of the basal ganglia. Dopaminergic neurons in the substantia nigra secrete dopamine to the basal ganglia in the cerebrum.

The origin of PD is the dysfunction of the neurons in the substantia nigra. The neurons in the brain transfer signals via molecules called neurotransmitters. A neurotransmitter named dopamine, produced by substantia nigra cells, is essential for normal movement. When the cells in the substantia nigra cell lose functionality, dopamine is no longer produced or delivered to the basal ganglia, and the transmission of signals controlling body movement is blocked. Another molecule, called acetylcholine, is also regulated by dopamine. Insufficient levels of dopamine lead to excessive amounts of acetylcholine, which induce tremors and muscle stiffness, symptoms frequently present in patients with PD.

Biochemistry and Brain Metabolism

Normal daily life diet consists of three main types of nutrients: carbohydrates (60%), lipids (20%), and proteins (20%). The process of digestion transforms carbohydrates into glucose (Kemppainen et al., 2005). Our brain consumes around 25% of whole body's glucose at rest, and 14% during exercise. This change occurs because a certain amount of glucose is needed to provide energy for the muscles. Neurons use not only glucose, but also lactate as a fuel. Astrocytes produce lactate from pyruvate and

export it to neurons by means of the astrocyte-neuron lactate shuttle (ANLS, cf. Figure II.1).

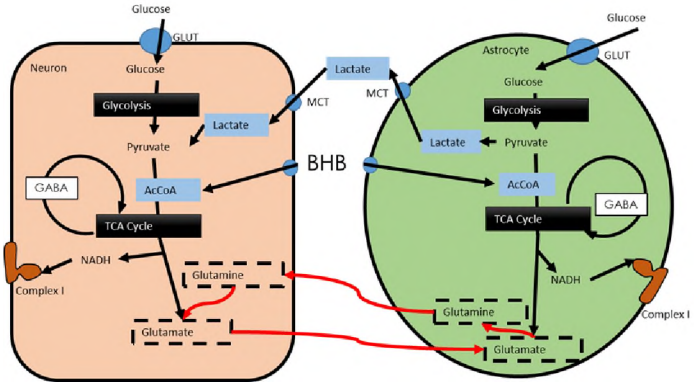

Figure II.3. Brain tissue main metabolic pathways. (Russell et al., 2002)

In neurons, about 10% of pyruvate is derived from glycolysis and 90% from the lactate shuttle. Lipids are digested into fatty acids in the small intestine and then transported to the liver. The fatty acids can be converted into ketone bodies, including acetone, acetoacetate, and BHB (β-hydroxybutyrate). Acetone and acetoacetate are then metabolized into BHB, and BHB is delivered to the neurons where is metabolized into acetyl Co-A. Under normal, or standard, diet conditions 65% of acetyl Co-A is derived from pyruvate, while the remaining 35% is derived from the metabolism of BHB. Acetyl Co-A, that is produced by metabolizing glucose, lactate, or ketones is then incorporated into the tricarboxylic acid (TCA) cycle. Brain tissue main metabolic pathways are shown schematically in Figure II.1.

Glucose as Brain Metabolism Substrate

The brain consists mostly of neurons and astrocytes. The function of neurons is sensing, while astrocytes are supporting cells that provide nutrients to neurons. Glucose enters the cells through glucose transporters, GLUTs. While each individual astrocyte has the same glucose transporting rate as a neuron, the number of astrocytes in the brain is ten times higher than that of neurons. Therefore, the total astrocytic glucose intake is approximately ten times that of neurons. When glucose enters the cells, it is metabolized through glycolysis and the TCA cycle, which generates NADH (reduced form of nicotinamide adenine dinucleotide), ATP (adenosine tri-phosphate), carbon dioxide, and water.

The glycolysis and TCA cycle are metabolic pathways consisting of more than twenty metabolic steps. In the process of glycolysis, free radicals, the molecules that contain an unpaired electron, are produced in the conversion of glyceraldehyde 3-phosphate (GADP) to 1,3-bisphosphoglyceric acid (1, 3 BPG) as shown in Figure II.2.

A

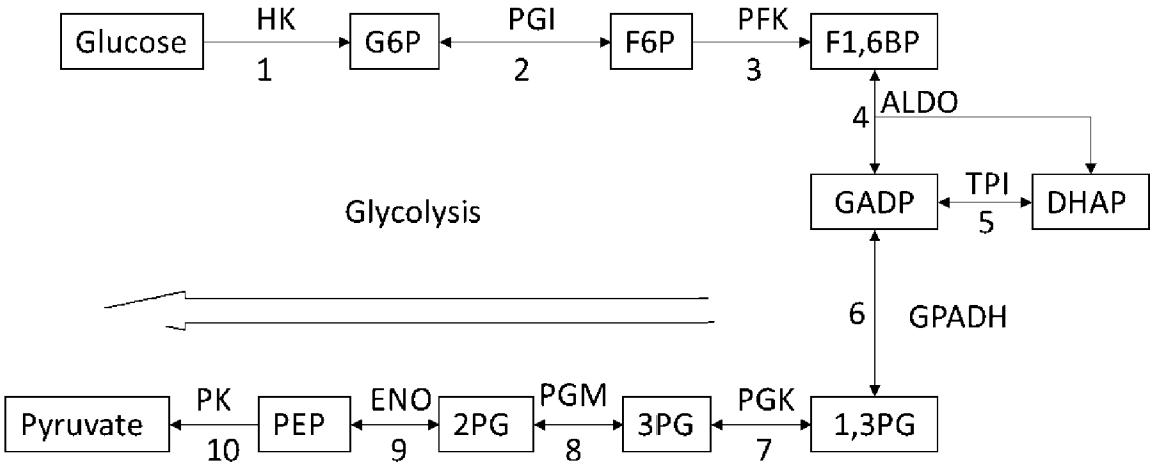

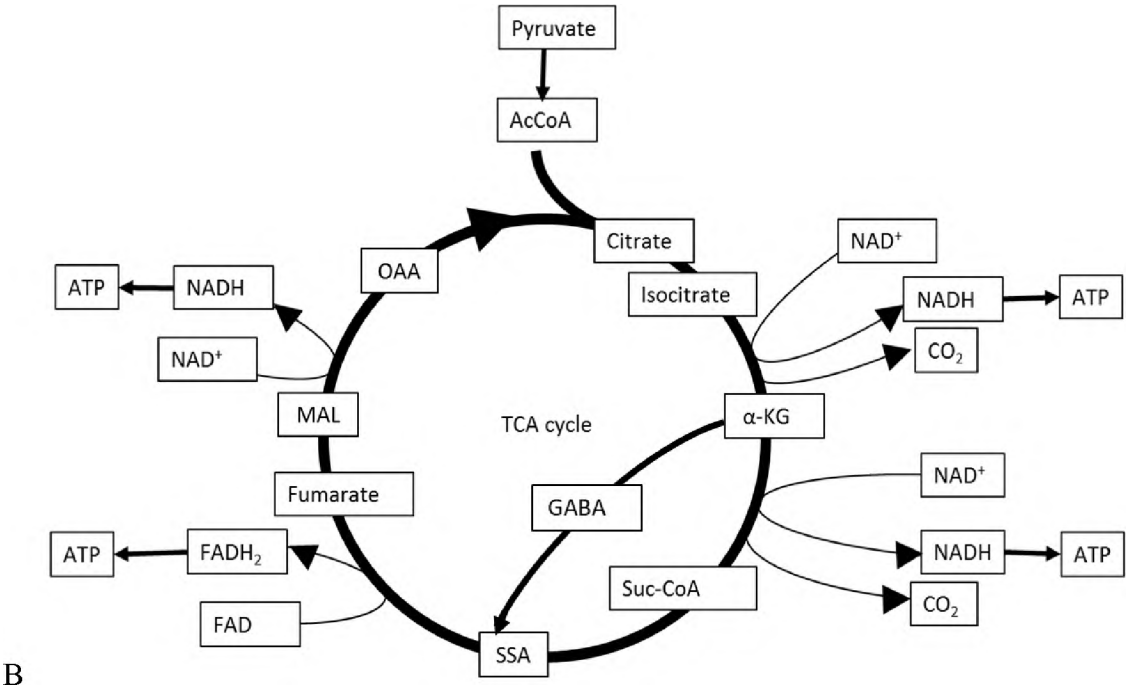

B

Figure II.4. (A) Glycolysis and (B) TCA cycle (Salim, 2017).

Antioxidants can decrease free radical concentration by donating an electron to the unpaired one. If the concentration of free radicals is higher than that of antioxidants, free radicals will over-oxidize the lipids and proteins on the cell membrane. A high concentration of denatured proteins can induce cell dysfunction. An important protein that is susceptible to free radical-induced damage is the complex I protein (NADH ubiquinone oxidoreductase). This protein uses NADH and transports protons and sodium. Denaturation of the complex I is believed to induce a loss of neuronal function. If this happens to the neurons in the substantia nigra, this may potentially cause PD.

Free radicals in brain tissue metabolic phenomena

Glycolysis produces reactive oxygen species (ROS), which contribute to the oxidative stress, which result in mitochondrial depolarization and ,in turn, progressive

neuronal dysfunction (Russell et al., 2002). The accumulation of free radicals generates oxidative stress (Salim, 2017). When mitochondria produce ATP, ROS and free radicals appear simultaneously (Pero et al., 1990). Three primary free radicals are hydroxyl radical (HO•), hydrogen peroxide (H_2O_2), and superoxide (O_2^-) (Sanders & Greenamyre, 2013). Even though ROS are needed for neuronal growth, when ROS concentrations exceed critical levels they have negative effects.

In normal situations, polyphenols can prevent ROS-induced damage during aerobic metabolism (Adefegha et al., 2016). When the amount of ROS exceeds the action of antioxidants, this results in an extensive protein oxidation and lipid over-oxidation; which causes oxidative damage, protein denaturation, and a decrease in cellular function. High concentrations of ROS decrease synaptic transmission (Knapp & Klann, 2002). Oxidative stress has a positive feedback mechanism. When the ROS concentration is high enough to harm the cells by oxidative stress, damaged cells become the sources of ROS.

The brain is susceptible to oxidative stress due to its high content in fat, high energy requirement, and poor anti-oxidative ability (Hulbert et al., 2007). While phospholipids are the primary targets, proteins and DNA are also easily damaged by ROS (Chomyn & Attardi, 2003). Thus, ROS will cause a severe neuronal damage if they accumulate and surpass or bypass the defense mechanisms (Salim, 2017).

Astrocyte-Neuron Lactate Shuttle

Another important metabolic mechanism in the brain is referred to as the astrocyte-neuron lactate shuttle (ANLS). It has been hypothesized that ANLS is an essential pathway for brain tissue to metabolize glucose and a route to sustain neuronal

activity. The lactate shuttle requires the involvement of MCTs. Under adequate glucose supply, and by means of astrocyte-neuron lactate shuttle, neurons generate more than three times the amount of ATP produced in the absence of an active lactate shuttle (Genc et al., 2011). In the presence of a normal lactate shuttle, but under glucose insufficiency, neuronal ATP production rate will be only 20% lower than the one reported under adequate glucose supply and with lactate shuttle activity.

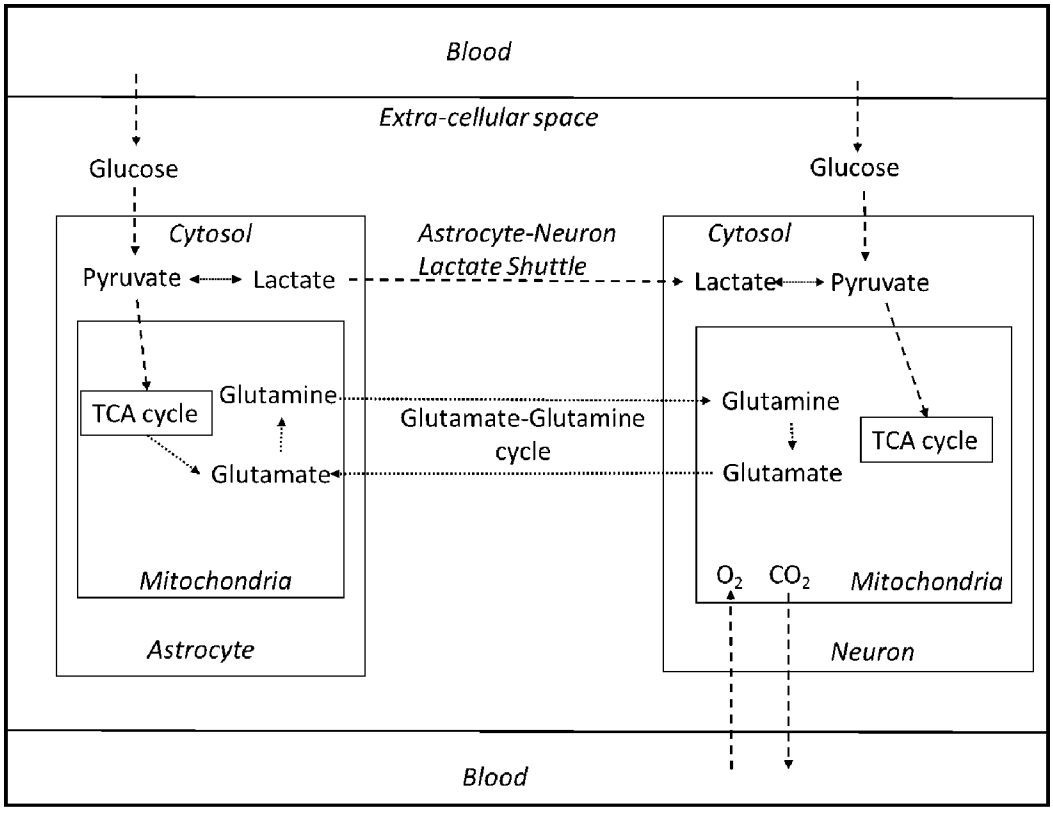

Figure II.5. Neuron-astrocyte lactate shuttle and glutamate-glutamine cycle (Dienel, 2004).

The availability of glucose and lactate in both astrocytes and neurons affects not only the rate of ATP synthesis, but also mitochondrial levels of these metabolites. While each astrocyte just contains 1-2 mitochondria, neurons have more than 10-20

mitochondria. Thus, neurons have larger ATP generation rates than those observed in astrocytes and have a higher ability to metabolize lactate supplied by the ANLS mechanism (Genc et al., 2011).

Glutamate-glutamine cycle

Glutamate is an excitatory neurotransmitter that plays an important role in the TCA cycle. Because neurons do not have glutamine synthetase, these cells cannot transform glutamate into glutamine. Therefore, glutamate is transferred from neurons to astrocytes, where it can be metabolized and complete the cycle (Brekke et al., 2015). This process requires transporters for the release of glutamate from neurons as well for glutamate to enter astrocytes (Danbolt, 2001). The first step of glutamate-glutamine cycle begins with a release of glutamine from astrocytes, and its entry into neurons via absorption by glutamine transporters. Then, the glutamine is catalyzed into glutamate by phosphate-activated glutaminase, and delivered back to astrocytes. Finally, astrocytic glutamine synthetase catalyzes glutamate into glutamine (Hogstad et al., 1988; Norenberg & Martinez-Hernandez, 1979; Varoqui et al., 2000).

Additionally, glutamate is also transformed into α-ketoglutarate that then participates in the TCA cycle (McKenna et al., 1996). The glutamate-glutamine cycle controls the concentration of excitatory glutamate by absorption. Astrocytic regulation of glutamate precursor concentration can diminish the consequences of excitotoxicity by glutamate (Danbolt, 2001).

Transporters and Complex I

GLUTs are the proteins located on the cell membrane that transport specific molecules. GLUT1 in astrocytes and GLUT3 in neurons can transport glucose, 2-deoxyglucose, and so on. The Michaelis constant, Km, in Michaelis–Menten kinetics, represents the affinity between species and transporters. GLUT1 has a Km value 6.9 mM for 2-deoxyglucose, which is higher than the Km value of GLUT3, ~1.4 mM (Simpson et al., 2008). However, the affinity of GLUT3 for glucose is five times higher than that of GLUT1. According to the lactate shuttle hypothesis, lactate provides most energy to neurons, and it is produced by astrocytes that import much more glucose through GLUT1 than neurons (Simpson et al., 2008).

Monocarboxylate transporters (MCT) transport ketone bodies, pyruvate, and lactate (Pellerin et al., 2005). There are 14 isoforms (molecules with the same function but different structures) of MCTs (Halestrap & Meredith, 2004). However, only MCT1 to MCT4 have been confirmed to co-transport protons and monocarboxylates (Manning Fox et al., 2000). The transporters differ in their affinity for lactate, so that MCT4, MCT3, MCT1, and MCT2 have a Km of ~35 mM, ~5.8 mM, ~3.5 mM and ~0.7 mM, respectively (Pellerin et al., 2005), with MCT2 having the highest affinity (Martin et al., 2006). In the brain, astrocytes use MCT1 and MCT4 to export lactate, and neurons use MCT2 to import it.

Four potential models of lactate transfer between astrocytes and neurons by MCTs have been hypothesized (Pellerin et al., 2005).

- The first model states that neurons and astrocytes both export lactate while endothelial cells import it; then, the endothelial cells transform lactate into

glucose, and glucose is imported into neurons and astrocytes by GLUT3 and GLUT1 respectively.

- The second model considers that astrocytic and endothelial cells export lactate, which is then imported by neurons.
- The third model considers that only astrocytes export lactate, and that neurons import it.
- The last model is states that only astrocytes export lactate, and that neurons import lactate by synthesizing more MCT2 in situations of high energy demand.

Since the third option has been heavily favored in the literature, we choose that pathway for the brain tissue model formulation completed in this study.

Complex I is a protein, also called NADH: ubiquinone oxidoreductases type I (NDH-Is) (Brandt, 2006) that acts as an electron transporter in mitochondria and helps the transport of protons and sodium ions (Gemperli et al., 2007). The inhibition of the complex I in the mitochondria in the cells of substantia nigra by an external toxin, for instance rotenone, might induce PD (Beal, 2003). The effect of modulation of the complex I activity on ATP production rate was investigated (Zielinski et al., 2016). Due to complex I act an important role in the cellular metabolism, complex I activity could be a probe of cell normal function.

Role of free radicals

In general, low concentrations of antioxidant enzymes lead to faster free radical production and concentrations. The imbalance of intermediate detoxification and repair

of damage due to oxidative stress activate systematic reactive oxygen species (ROS) expression; which leads to the production of per-oxidants and free radicals that damage protein, lipid, and DNA molecules by interrupting normal redox reactions. Oxidative stresses resulting from oxidation metabolism results in structural damage to DNA. ROS, including super-oxidative free radicals, hydroxyl radicals, and peroxide, indirectly induce structural damage. Furthermore, some reactive oxidants function as intracellular transmitters in redox signal transmission. As a result, oxidative stress is expected to affect normal cell signaling (Ojha et al., 2016).

Role of KB transporter

Proton-linked monocarboxylate transporters (MCT) catalyze transport across plasma membranes of monocarboxylates such as lactate, pyruvate, and ketone bodies (KB) (acetoacetate, beta-hydroxybutyrate (βHB), and acetone). One of the requirements to understand the effect of alternative substrates is to determine the limits of the contribution of these substrates to brain metabolism.

The transport of lactate between neurons and astrocytes have been studied by analyzing the dynamics of lactate plasma concentrations after step perturbations of glucose were introduced to cerebral blood flow (J. C. Lamanna et al., 1992). These authors correlated their experimental data with a Michaelis-Menten-type functionality that correlates the plasma-tissue lactate flux ($J_{b\rightarrow xc,L}$) with plasma lactate concentrations (C_L^P) in the form of the following equation:

$$J_{b\rightarrow xc,L} = \frac{T_{\max} C_L^P}{K_t + C_L^P} \qquad (1)$$

where the maximum transport flux, T_{max}, was found to be in the range 0.9–1.4 μmol g^{-1}_{ww} min^{-1}, and K_t (transport affinity coefficient) ranged between 6 and 12 mM.

It has been reported that, for the baseline (control) βHB plasma levels, the net flux of βHB across the blood-brain barrier is ~ 0.3 μmol g^{-1}_{ww} min^{-1}. Since the total tricarboxylic acid flux under standard diet conditions is ~0.72 μmol g^{-1}_{ww} min^{-1} (~0.57, 79%, in neurons and ~0.15, 21%, in astrocytes) (Shulman et al., 2004), only ~42% (0.3/0.72) of the fuel required to sustain the metabolism of the TCA cycle could be provided by ketone bodies. Indeed, there is experimental evidence that the oxidation of ketone bodies could constitute as much as ~ 53% (0.3/0.57) of the total oxidation of substrates in neurons. As ketone bodies are present in the extra-cellular space under normal diet, it can be concluded that the ketone bodies provide the fuel necessary to sustain 20% of total baseline TCA cycle activity as a baseline condition under normal diet conditions.

This leads to two important conclusions: (i) ketone bodies, being limited by their transporters characteristics, can never sustain 100% of the mitochondrial activity; and (ii) since glucose is the primary energy source for neurons; under conditions in which glucose influx cannot meet the demands of neurons; an additional substrate is needed to substitute glucose as energy source.

Hence, the additional fuel required to sustain TCA cycle activity is derived from the astrocyte and is transported (through the extra-cellular space) via a mechanism called the "astrocyte-neuron lactate shuttle" (or ANLS). These arguments support the hypothesis that the astrocyte-neuron lactate shuttle remains active under all cell conditions.

Ketogenic diet

Under normal diets, the mitochondria of brain cells will oxidize glucose to fuel their metabolism. Although the brain represents only 2% of the adult body weight, it consumes approximately 20% of energy in a static situation. The human brain can metabolize 120 grams of glucose per day.

Ketone bodies can fuel the brain instead of glucose in cases of glucose insufficiency; however, the brain can use ketone bodies only if their concentration exceeds 0.2 mM. Typically, after digesting a dinner and overnight rest, the blood concentration of ketone bodies is between 0.1 and 0.3 mM. This is often referred to as the short time high ketone morning symptom. Thereafter, the concentration decreases soon after eating mixed breakfast, and increases again after completing digestion. The concentration of ketones bodies in diabetic ketoacidosis conditions exceeds 25 mM (Shulman et al., 2004).

Compared to the normal diet, ketogenic diets consist in 80% of lipids (fatty acids) and 20% of carbohydrates and proteins (Adefegha et al., 2016). Low percentage of carbohydrates results in a decreased availability of glucose in the tissue. In contrast, fatty acid ingestion leads to the production of ketone bodies in the liver, which can then be used as substitutes for glucose to fuel cell metabolism. This means that ketone body-derived energy can be used to maintain normal neuronal function during period of glucose insufficiency. In other words, under ketogenic diets, ketone bodies become the main source of energy for brain tissue (Knapp & Klann, 2002). The pathway from fatty acids to ketone bodies is shown schematically in Figure 4 below.

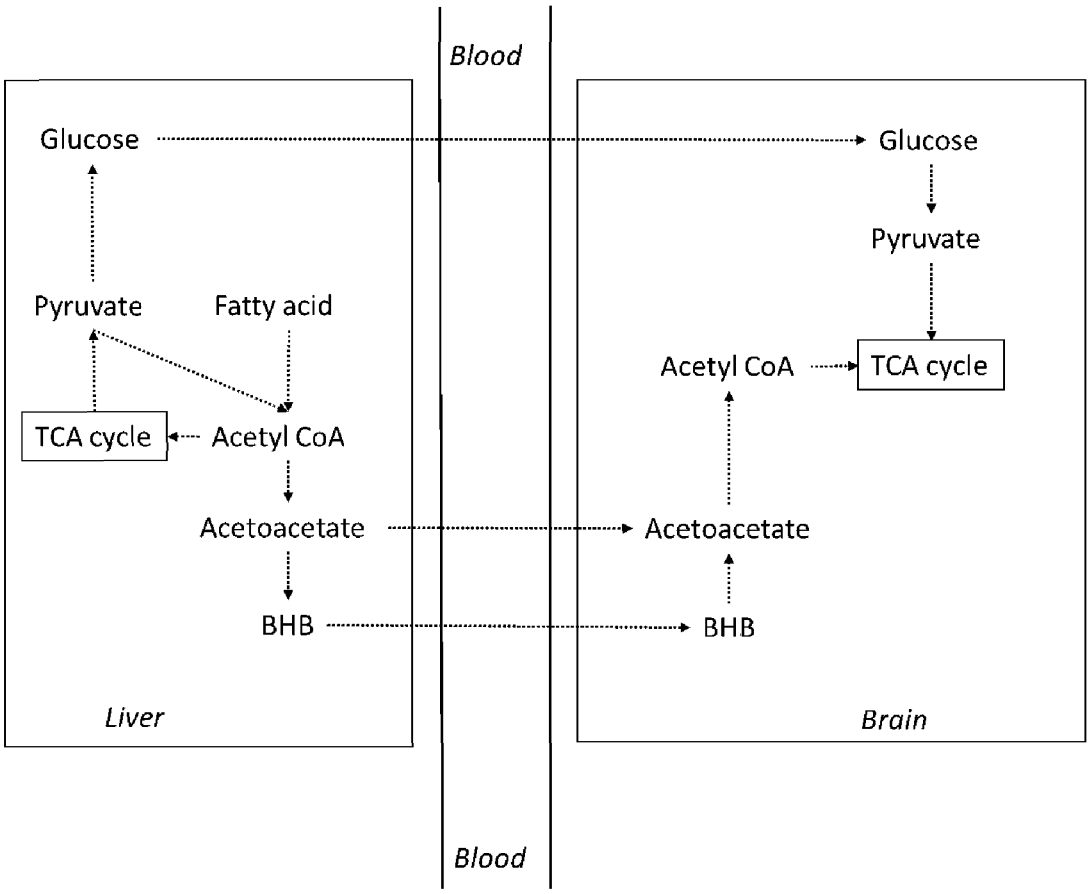

Figure II.4. Fatty acid metabolized to ketone bodies in liver, then transported to brain (Knapp & Klann, 2002).

CHAPTER III

MATHEMATICAL MODEL OF BRAIN TISSUE METABOLISM

Model Overview

This chapter presents the formulation of an *in silico* mathematical model which will include the most relevant metabolic pathways. The main metabolic pathways accounted in this model occur between the following compartments: blood compartments, extra-cellular space, and cytosol and mitochondria in astrocytes and neurons. Each compartment includes pathways considered essential, i.e. those associated with metabolic fluxes directly responsible with deterioration of cell functionality. Therefore, the model includes the following pathways: glycolysis, TCA cycle, ANLS, GABA shunt, and glutamine-glutamate cycle as shown schematically in Figure III.1.

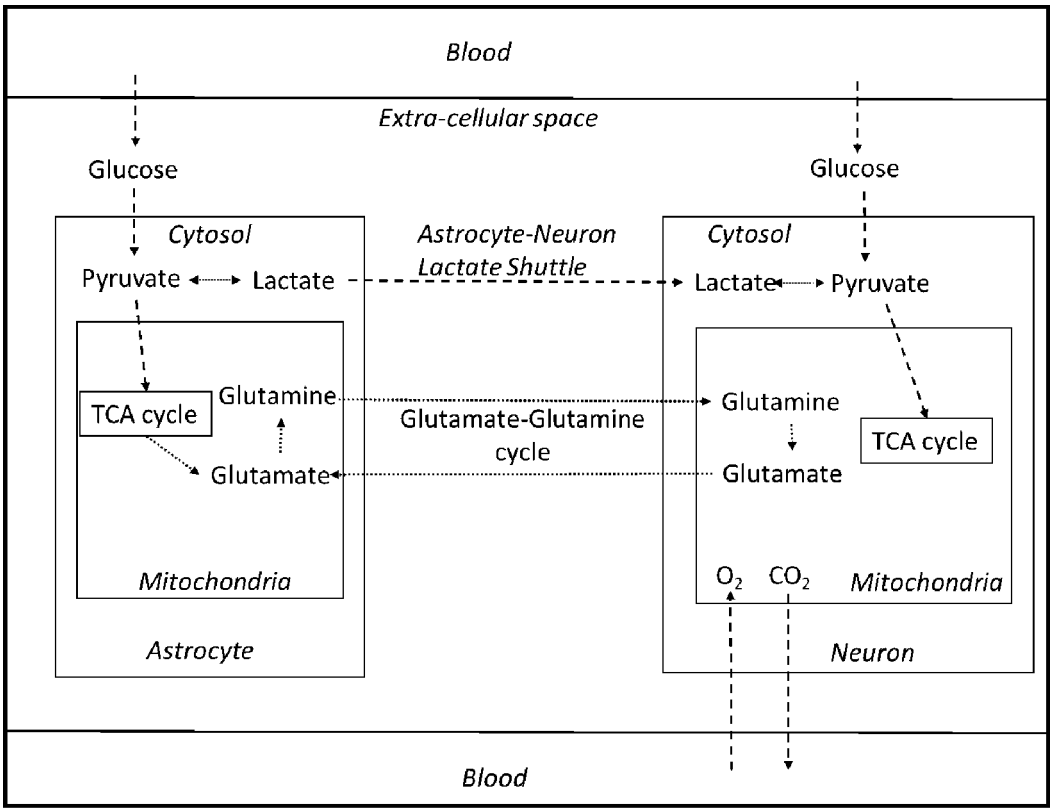

Figure III.1. Neuron-astrocyte lactate shuttle and glutamate-glutamine cycle (Dienel, 2004).

Glycolysis is a ten steps metabolism starting at glucose and ending in pyruvate. Each glucose molecule will produce two pyruvate molecules and two NADH molecules. The full glycolysis reactions are listed in appendix I. This pathway, along with the ANLS, is shown in Figure III.2 below.

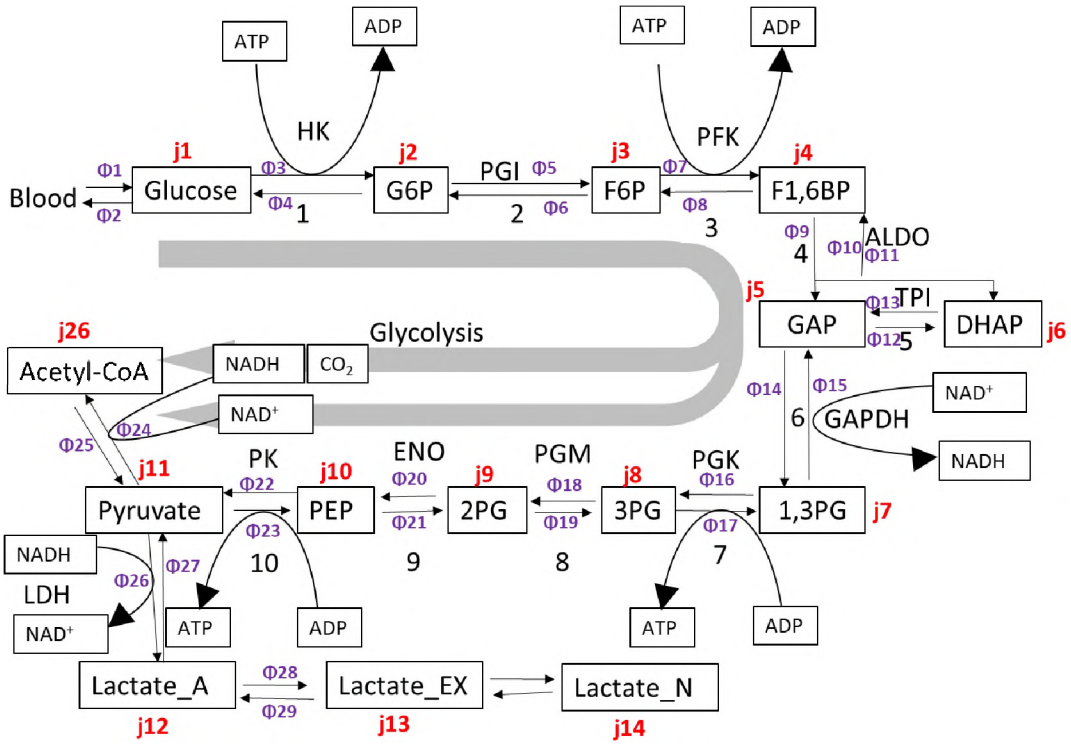

Figure III.2. Metabolic reactions and fluxes corresponding to glycolysis. Here Φ and j represents flux and species, respectively .

The tricarboxylic acid cycle (TCA) cycle begins from pyruvate through acetyl-CoA to Oxaloacetic acid (OAA). This cycle includes ten species and 11 reactions (cf. Figure III.3). The complete list of reactions, fluxes, and species corresponding to the TCA cycle are tabulated in appendix II.

A

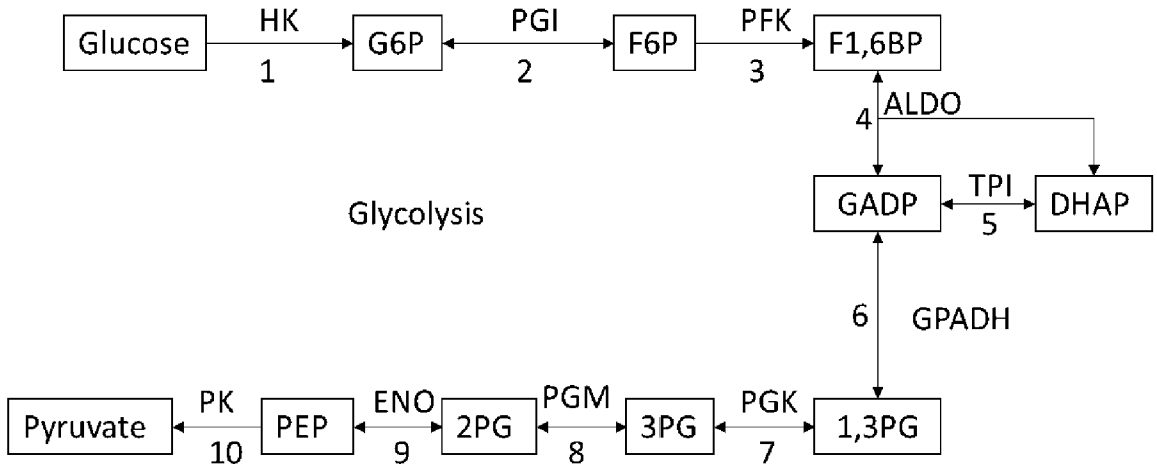

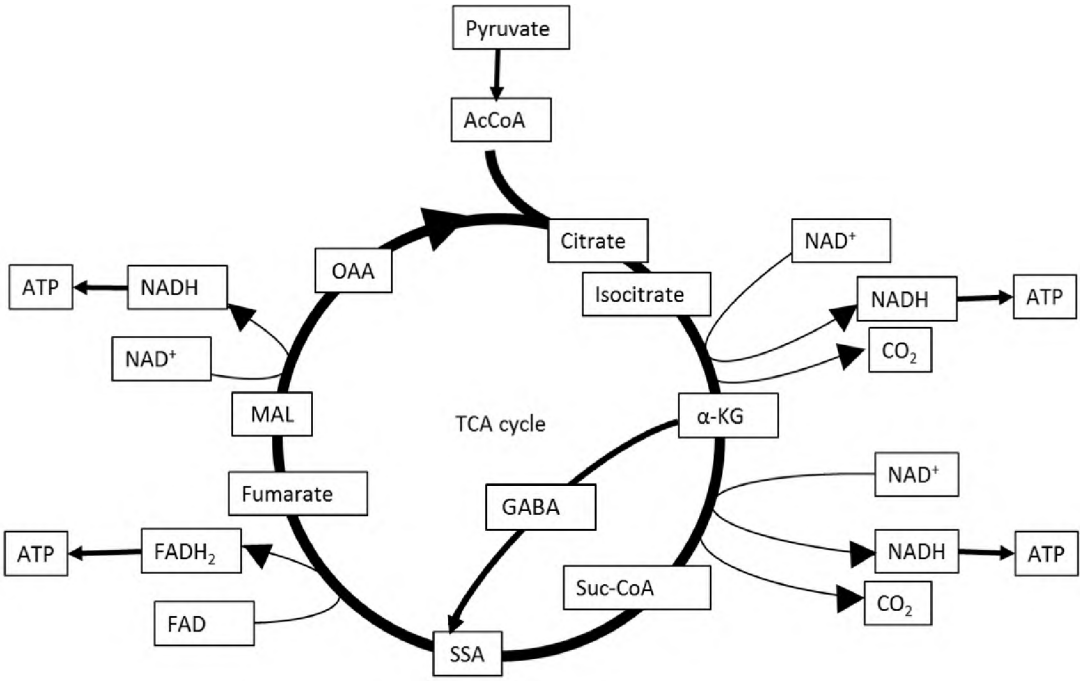

B

Figure III.3. (A) Glycolysis and (B) TCA cycle (Salim, 2017).

In addition, these two pathways are assisted by complementary pathways: the astrocyte-neuron lactate shuttle (ANLS), the GABA shunt, and the glutamine-glutamate cycle (cf. Figures III.1 to 3).

The astrocyte-neuron lactate shuttle (ANLS) is the pathway responsible to transport the lactate produced in astrocytes as fuel to sustain the energy generating pathway in neurons. This shuttle can supplement the deficiency of pyruvate required to sustain neuronal metabolism. Indeed, the ANLS-transported lactate is metabolized from astrocytic pyruvate and the neuronal lactate metabolizes to pyruvate in the neurons.

The GABA shunt is a pathway starting with α-Ketoglutarate (αKG) through γ-Aminobutyric acid (GABA) to succinic semialdehyde (SSA). This shunt can bypass succinyl-CoA. The glutamine-glutamate cycle, glutamate produces glutamine through the glutamine synthetase in astrocytes, and then the glutamine is transported to neurons and metabolized to glutamate via the glutaminase. This cycle overcomes the absence of glutamine synthetase in neurons.

The advantages of a model with this level of complexity are that it enables to estimate the concentration and flux dynamics for all major species of interest in brain tissue. However, the disadvantages of a model like this is its dependence on a large number of parameters; which, more often than not, have a large degree of uncertainty.

Moreover, in models of this dimension it becomes difficult to assess which species and/or parameters play the most significant role in affecting specific species levels or flux rates of interest. For instance, if we needed to adjust the extra-cellular lactate level, we would need to know which parameter will be the most significant in inducing changes to the lactate level in that compartment. In this type of models, a formal analysis will yield a large set of parameters, often identifying a different set for dynamic or steady-state effects. These shortcomings will be illustrated later in this chapter.

A number of specific metabolic pathways occur within each cell compartment. The dynamics of substrate concentrations under isothermal conditions can be described by simple mass balances as shown in Equation (3). Some species are transported between compartments and require special attention. Indeed, while most species participate in metabolic reactions, glucose, lactate, and ketone bodies migrate between compartments. Thus, for instance the dynamics of glucose in the cytosol (both of neurons and astrocytes) will be governed by a general equation as shown below in Equation (2)

$$\frac{dC_{1,c}}{dt} = \emptyset_1 - \emptyset_2 - \emptyset_3 + \emptyset_4 \qquad (2)$$

$$\emptyset_1 = \frac{T_1\left(C_{1,xc}\right)}{M_1 + C_{1,xc} + C_{1,c}} \qquad (3)$$

$$\emptyset_2 = \frac{T_2\left(C_{1,c}\right)}{M_1 + C_{1,xc} + C_{1,c}} \qquad (4)$$

$$\emptyset_3 = \frac{V_1 \frac{C_{1,c}}{K_1}}{1 + \frac{C_{1,c}}{K_1} + \frac{C_{2,c}}{K_2}} \left[\frac{PS^+/\mu^+}{1 + PS^+/\mu^+}\right] \qquad (5)$$

$$\emptyset_4 = \frac{V_2 \frac{C_{2,c}}{K_2}}{1 + \frac{C_{1,c}}{K_1} + \frac{C_{2,c}}{K_2}} \left[\frac{PS^-/\mu^-}{1 + PS^-/\mu^-}\right] \qquad (6)$$

where $C_{1,c}$ is the concentration of species *1*, glucose, in the *c*, cytosol; $\emptyset_1$ is the flux of glucose transported from *xc*, extra-cellular space, to *c*; T_1 is maximum transport rate for mechanism responsible for transporting glucose from extra-cellular space to cytosol; M_1 is affinity of glucose of transporter GLUT; $\emptyset_2$ is the flux of glucose transporting from *c* to *b*; T_2 is transport mechanism rate constant of glucose from cytosol to extra-cellular space; $\emptyset_3$ is the flux of glucose metabolize to species 2, G6P; V_1 is rate constant of glucose to G6P; K_1 is glucose affinity for HK; K_2 is G6P affinity for HK; $PS^+ = C_{ATP}/C_{ADP}$; C_{ATP} is ATP concentration of cytosol; $\mu^+ = \mu^-$ is corresponding controller coefficients; $\emptyset_4$ is the

flux of *2* metabolize to *1*; $PS^{-} = 1/PS^{+}$.

$\emptyset_3$ and $\emptyset_4$ are intra-compartmental fluxes, while $\emptyset_1$ and $\emptyset_2$ are inter-compartmental fluxes. The corresponding pathways for these fluxes will be discussed later in this chapter.

The metabolic reaction mechanism for the glycolysis and TCA cycle are detailed and listed in appendix.

Each intra-compartmental flux will then include 4 parameters, *K* and *V* for each of the two fluxes, which need to be measured, recovered from literature, or calculated. In each of the cellular metabolic pathways there will be ten glycolytic steps, the ten TCA cycle steps, the pyruvate-lactate reduction, and the glutamine-glutamate reaction, the adding reactions and the corresponding parameters as listed below in Table III.1.

Table III.1. Detail of the distribution of fluxes (reactions and/or transport) and the number of parameters associated with each major intra-compartmental metabolic pathway.

Metabolism	# of Reactions	# of Parameters	# of Parameters of metabolisms	Compartment	Cumulative # of Parameters
Glycolysis	10	4	40	2	80
TCA cycle	10	2	20	2	40
Pyruvate-lactate	1	4	4	2	8
Glutamine-Glutamate cycle	1	4	4	2	8
GABA shunt	2	2	4	2	8
Summation	24		72		144

INTER-COMPARTMENTAL TRANSPORT PATHWAYS

In addition to the main metabolic reaction mechanisms: glycolysis and TCA cycle in neurons and astrocytes, there are two additional transport pathways between these two types of cells that need to be considered: (1) the astrocyte-neuron lactate shuttle (ANLS), and (2) the glutamate-glutamine cycle. These pathways are essential features in the model formulated in this research. This study is focused on the role of alternate substrates to substitute or complement glucose as the primary fuel source for cell metabolism.

The ANLS pathway illustrates the supporting role of astrocytes to maintain neuronal activity. Indeed, TCA activity in neurons is known to be primarily sustained by lactate metabolized in the cytosol of neurons. As shown in the schematic in Figure III.1 (and Table III.1), the total TCA flux under standard diet conditions is ~0.72 μmol g^{-1}_{ww} min^{-1}, which is partitioned as ~0.57 μmol g^{-1}_{ww} min^{-1} (79%) in neurons and ~0.15 μmol g^{-1}_{ww} min^{-1} (21%) in astrocytes (Shulman et al., 2004). The ANLS is also a natural route to supplement glycolytic activity in neurons and, therefore, a potential mechanism to control free-radical levels in neurons.

Two inter-compartmental transport mechanisms essential in the ANLS act as essential steps in this pathway. Glucose transport occurs between blood and the extra-cellular space, and between the extra-cellular space and the cells, ie equation (1) $\emptyset_1$ and $\emptyset_2$. Pyruvate transport, on the other hand, occurs between the extra-cellular space and cells, as well as between the cytosol and the mitochondria outer membrane, glutamine or glutamate transport occurs between the extra-cellular space and cells. Table III.2 below

shows a summary of the transport processes and parameters involved in inter-compartment transport mechanisms.

Table III.2. Detail of metabolic fluxes and parameters for inter-compartmental metabolic pathways.

Transport mechanisms	Transport Process	# of Parameters	# of Parameters of metabolisms	Compartment	Cumulative # of Parameters
Glucose	2	2	4	2	8
Lactate	1	2	2	2	4
Pyruvate	1	2	2	2	4
Glutamine or glutamate	1	2	2	2	4
Summation	5		10		20

Figures III.1-3 provide schematics of a complete model of brain tissue metaboilism. It includes glycolysis and TCA cycle metabolic reaction mechanisms and transport phenomena associated with intra and inter-compartmental fluxes. Tables III.1-2 provide a detail of the parameters associated with this model.

Flux Balance Analysis

One parameter estimation methodology currently in use involves employing a Flux Balance Analysis (FBA) (Schilling et al., 2000; Varma & Palsson, 1994) to obtain viable reaction flux values and thereby reduce the number of unknown parameters in the metabolic model. The unknown reaction rate parameters of the model are then obtained by adjusting them in such a way as to correspond to known characteristic times for key substrates in the metabolic system (Kaliappan, 2006).

The goal of FBA is to solve a system of steady state mass conservation equations (flux balances) via optimization of a linear objective function, Φ, that corresponds to a meaningful pathway objective (e.g. maximization of ATP production), i.e.

$$\Phi = \sum_{j=1}^{NR} \nu_{i,j}\phi_j = s_i^T \phi \qquad (7)$$

Here, $\nu_{i,j}$ represents the stoichiometric coefficient for reaction "j" of the species "i"(e.g. ATP) and ϕ_j is the flux corresponding to reaction "j" (s_i, would denote the i-th row of the "stoichiometric matrix" S).

Let us demonstrate some of the shortcoming associated with the FBA methodology by considering the following example. The system illustrated in Figure III.4 represents a reaction network with 12 fluxes and 9 species.

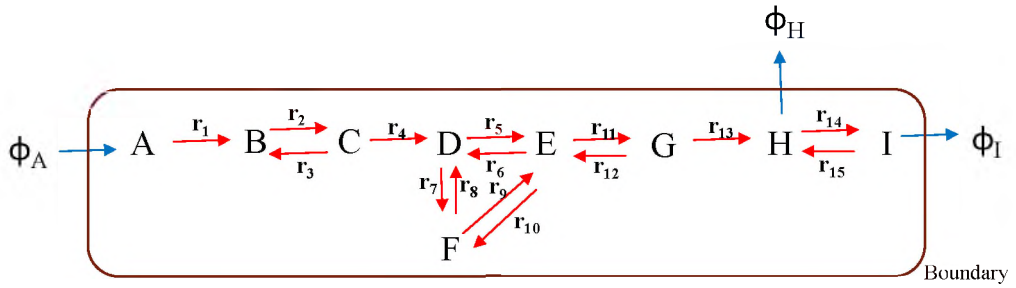

Figure III.4. Sample reaction network

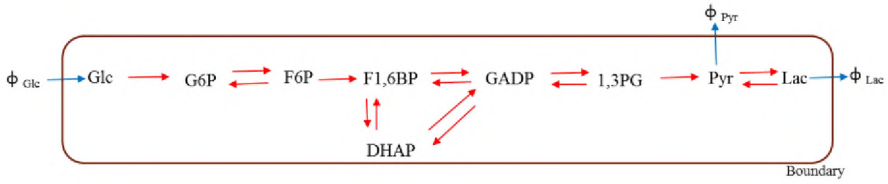

(8)

$$\emptyset = [\ \emptyset_1\ \emptyset_2\ \emptyset_3\ \emptyset_4\ \emptyset_5\ \emptyset_6\ \emptyset_7\ \emptyset_8\ \emptyset_9\ \emptyset_A\ \emptyset_H\ \emptyset_I]^T \tag{9}$$

$$S = \begin{bmatrix} -1 & 0 & 0 & 0 & 0 & 0 & 0 & 0 & 0 & 0 & 0 & 0 & 0 & 0 & 0 & 1 & 0 & 0 \\ 1 & -1 & 1 & 0 & 0 & 0 & 0 & 0 & 0 & 0 & 0 & 0 & 0 & 0 & 0 & 0 & 0 & 0 \\ 0 & 1 & -1 & -1 & 0 & 0 & 0 & 0 & 0 & 0 & 0 & 0 & 0 & 0 & 0 & 0 & 0 & 0 \\ 0 & 0 & 0 & 1 & -1 & 1 & -1 & 1 & 0 & 0 & 0 & 0 & 0 & 0 & 0 & 0 & 0 & 0 \\ 0 & 0 & 0 & 0 & 1 & -1 & 0 & 0 & 1 & -1 & -1 & 1 & 0 & 0 & 0 & 0 & 0 & 0 \\ 0 & 0 & 0 & 0 & 0 & 0 & 1 & -1 & -1 & 1 & 0 & 0 & 0 & 0 & 0 & 0 & 0 & 0 \\ 0 & 0 & 0 & 0 & 0 & 0 & 0 & 0 & 0 & 0 & 1 & -1 & -1 & 0 & 0 & 0 & 0 & 0 \\ 0 & 0 & 0 & 0 & 0 & 0 & 0 & 0 & 0 & 0 & 0 & 0 & 1 & -1 & 1 & 0 & -1 & 0 \\ 0 & 0 & 0 & 0 & 0 & 0 & 0 & 0 & 0 & 0 & 0 & 0 & 0 & 1 & -1 & 0 & 0 & -1 \end{bmatrix} \tag{10}$$

For a given nominal input (J_A), the system would be not under-determined and it will have a unique solution. This is often found in the analysis of metabolic pathways where there will typically be more fluxes than species. The problem can now be solved by standard linear programming methods. The system of equations presented above, nevertheless, will have unique solutions.

In the complete model, at steady state, glycolysis flux rate is at a stable level, here we refer to "stable" as the scenario where all reaction flux rates of glycolysis are the same (steady-state). If this were *in vivo* steady state model, the stable flux rate would equal the cerebral metabolic rate (CMR, 0.58 mM/min), the glucose net transport flux, Typically, in brain tissue, 85% of the CMR of glucose is considered metabolized in astrocytes, while the CMR of glucose left is transported to neurons. With this partition of glucose influx to brain tissue, the FBA problem presented above can be solved both for astrocytes and neuros, the results are listed in Table III.3 below.

Table III.3. Detail of the distribution of fluxes (reactions and/or transport) of astrocytes and neurons.

Flux	Reaction	Flux Rate of Astrocyte(mM/min)	Flux Rate of Neuron(mM/min)
$\emptyset_A$	$Glc_{xc} \rightarrow Glc_c$	0.493	0.087
$\emptyset_1$	$Glc_c \rightarrow G6P_c$	0.493	0.087
$\emptyset_2$	$G6P_c \rightarrow F6P_c$	0.493	0.087
$\emptyset_3$	$F6P_c \rightarrow F1{,}6BP_c$	0.493	0.087
$\emptyset_4$	$F1{,}6BP_c \rightarrow GADP_c$	0.493	0.087
$\emptyset_5$	$F1{,}6BP_c \rightarrow DHAP_c$	0.493	0.087
$\emptyset_6$	$DHAP_c \rightarrow GADP_c$	0.986	0.174
$\emptyset_7$	$GADP_c \rightarrow 1{,}3PG_c$	0.986	0.174
$\emptyset_8$	$1{,}3PG_c \rightarrow Pyr_c$	0.986	0.174
$\emptyset_9$	$Pyr_c \rightarrow Lac_c$	0.87	-0.87
$\emptyset_H$	$Pyr_c \rightarrow Pyr_m$	0.116	1.044
$\emptyset_I$	$Lac_c \rightarrow Lac_{xc}$	0.87	-0.87

From the solution, we got the fluxes values of astrocytes and neurons based on different glucose partition ratio. Figure III.4 presents a simplified schematic of metabolic fluxes at steady-state, where CMR is clearly connected to glycolytic metabolic fluxes. The fluxes shown in this schematic are the result of the flux balance analysis (cf. Table III.3). The substrate partition assumed in the model (Fig. III.5) demonstrates the FBA results for glucose partitioned between the glial and neuron cells for a reference net flux value (or cerebral metabolic rate, CMR) of 0.58 μ-mol $g^{-1}{}_{ww}$ min^{-1} of glucose to brain tissue for a standard 5 mM plasma glucose concentration.

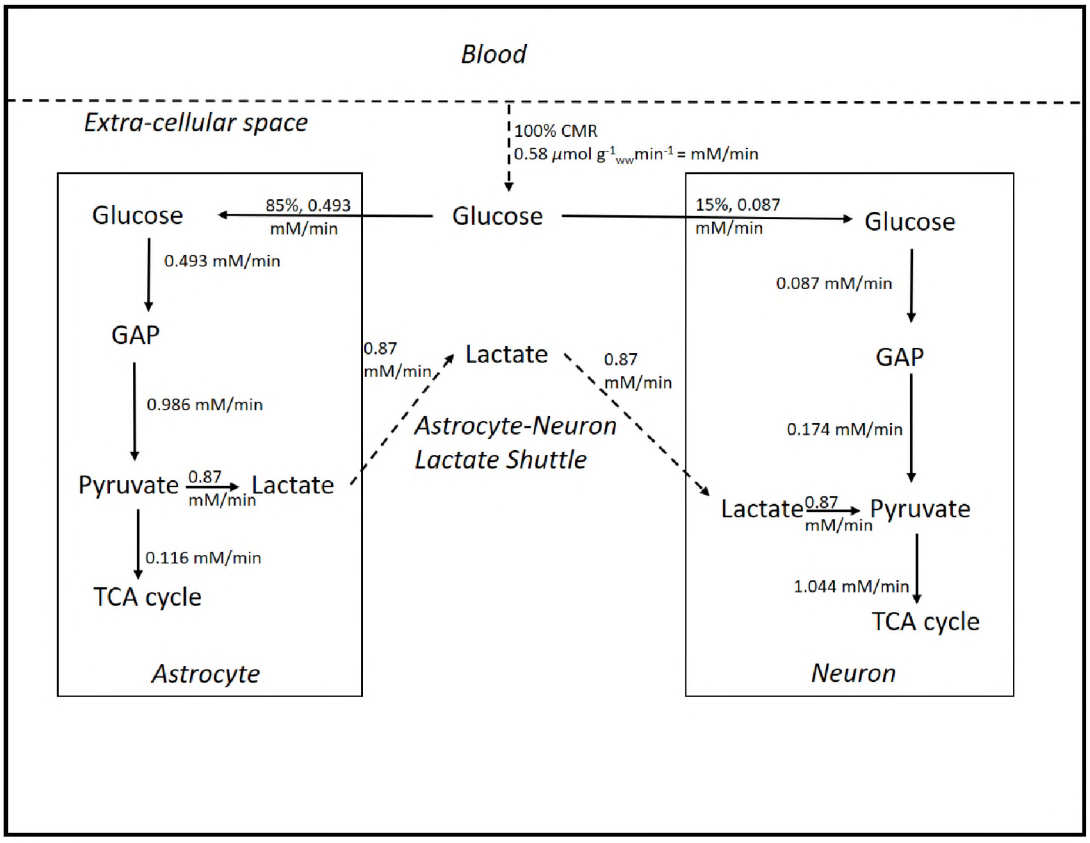

Figure III.5. Flux analysis of simplified schematic diagram model.

The largest fraction of glucose is taken up by the astrocyte where it is broken down to pyruvate and lactate. Lactate, in turn, is transported to the extra-cellular space. Depending on neuronal demand, lactate is driven from the extra-cellular space to the cytosol of neuron, where it is converted to pyruvate to fuel neuronal (TCA) activity. A small fraction of glucose sustains glycolytic activity in the neuronal cytosol, which complements the lactate-generated pyruvate and completes the supply of fuel (pyruvate) required by mitochondrial activity in the neuron.

Results reported by Shulman and coworkers (Shulman et al., 2004) suggest a close interrelationship between neuronal activity, glucose transport, and glycolytic activity in neurons. According to these authors, the glycolytic path (glucose transporters activity, or a combined effect) in neurons becomes activated in response to neuronal

activity. Indeed, glycolytic activity in neurons was reported to follow a linear correlation with neuronal activity, as indicated by the rate of the glutamate-glutamine cycle.

Closer inspection of the results reported by Hyder and coworkers (Hyder et al., 2006) indicates that neuronal glycolysis is persistent even at minimal neuronal activity levels. Their results suggests a baseline glycolytic activity in neurons capable of sustaining 15% of mitochondrial activity in neurons (0.087 μmol g^{-1}_{ww} min^{-1} for a reference value of 0.58 μmol g^{-1}_{ww} min^{-1} net flux of glucose). Neuronal activity is responsible for a ~90% of ATP generated from TCA cycle oxidation (Hyder et al., 2006). Neurons produced ATP is the energy source for clearing glutamate or fueling Na^+ pump of astrocyte (Fernandez-Moncada & Barros, 2014).

With these partitions in mind, FBA shows that approximately 83% of the pyruvate, required to sustain the neuronal metabolism at steady state, is derived from the astrocyte-neuron lactate shuttle (Fig. III.4)(Hyder et al., 2006). Glia reserve 10% of net pyruvate flux for the astrocytic TCA cycle. These reserves include pyruvate carboxylation, oxidation, and recycling. Thus, Hyder and coworkers analysis clearly supports the presence of the astrocyte-neuron lactate shuttle (ANLS), complementing neuronal glycolysis and their functional role under both baseline and neuronal activity conditions.

Research from Lanz and coworkers (Lanz et al., 2013), due to the fact that neurons include GABAergic and glutamatergic neurons, if glia were to reserve a larger fraction of the glucose flux, ANLS will decrease. In a separate work, research by Mangia and coworkers addressed this issue as well; these authors, however approached incorrectly the representation for the *in vivo* neuron-astrocyte lactate shuttle (NALS) by decreasing

astrocytic glucose transporter (GLUT) activity, which result in a smaller glucose influx rate (Mangia et al., 2009). Appendix V shows the steady state inter-compartmental transport fluxes and substrate interaction for standard conditions.

At steady state, the transport of lactate and pyruvate between blood and the extra-cellular space, as well as that between extra-cellular space and the cytosol, are considered negligible. In addition, in the control diet, the transport of ketone bodies (BHB and AcAc) to brain tissue is also neglected. In other words, in the control (or standard) diet, it is assumed that glucose is the only fuel for brain metabolic activity.

Application of Michaelis-Menten kinetics and Haldane relationship

When examining intra-compartmental dynamic model equations it becomes clear that four (4) parameters, $V_1, V_2, K_1,$ and $K_2,$ are required for the characterization of each net metabolic flux (reaction) in reaction pathways. The enzyme affinity values, K_1 and K_2, can be typically found in the literature. The rate constants, V_1 and V_2, on the other hand, need often to be determined from measurements. We will use reaction thermodynamics to reduce the number of unknown (or free) rate constants.

Both dynamic and steady state comparisons between experimental observations and model predictions can benefit from identifying the critical parameters, or steps, in a metabolic pathway. Such an analysis can be formalized using a thermodynamic analysis of the network.

Let's consider the case of a metabolic reaction in a closed system, i.e.

$$\frac{dC_2}{dt} = \emptyset_1 - \emptyset_2 = \frac{V_1\frac{C_1}{K_1}}{1+\frac{C_1}{K_1}+\frac{C_2}{K_2}} - \frac{V_2\frac{C_2}{K_2}}{1+\frac{C_1}{K_1}+\frac{C_2}{K_2}} \quad (11)$$

For example, in the phosphorylation of G6P to F6P, G6P will be denoted as 1 and F6P as 2 in Eq. (11). If we consider the Haldane relationship:

$$K^{eq} = \frac{C_B^{eq}}{C_A^{eq}} = \frac{V_1 K_2}{V_2 K_1} \quad (12)$$

One can substitute one of the reaction rate constants as

$$V_2 = \frac{V_1 K_2}{K^{eq} K_1} \quad (13)$$

And the net flux equation becomes

$$\frac{dC_2}{dt} = \emptyset_1 - \emptyset_2 = \frac{V_1\frac{C_1}{K_1}}{1+\frac{C_1}{K_1}+\frac{C_2}{K_2}} - \frac{V_2\frac{C_2}{K_2}}{1+\frac{C_1}{K_1}+\frac{C_2}{K_2}} = \frac{V_1\left(\frac{C_1}{K_1} - \frac{K_2}{K^{eq}K_1}\frac{C_2}{K_2}\right)}{1+\frac{C_1}{K_1}+\frac{C_2}{K_2}} \quad (14)$$

The equilibrium constant, K^{eq}, can be defined based on thermodynamics as

$$\text{If } K^{eq} = K''^{eq} = \exp\left(-\frac{\Delta G_2''^o - \Delta G_1''^o}{RT}\right) \quad (15)$$

Where K''^{eq} is the further transformed equilibrium constant, and $\Delta G_1''^o$ is the further transformed formation Gibbs free energy of specie 1. As a result, although every metabolic reaction has 4 parameters, only one parameter needs to determined from indirect measurements.

However, we first need to estimate $\Delta G''^o$ for all species.

Calculation of the Transformed Gibbs Free energies.

The Gibbs Free Energy of the reactants is a function of temperature (T), ionic strength (I), and pH, i.e.

$$G = G\,(\mathrm{T,I,pH}) \quad (16)$$

The Gibbs Free Energy for any particular species is calculated using the native thermodynamic data properties data from Alberty (Alberty, 2005). The data consists of a table for various species at a temperature of 310 K, zero ionic strength, and dilute aqueous solution. Values of the standard Gibbs free energies of formation ($\Delta_f G^o$), standard enthalpies of formation ($\Delta_f H^o$), the charge number of the species (z_i) and the total number of hydrogen atoms in the species ($N_H(j)$) are given for each species at these conditions. However, to keep the model as close as possible to physiological conditions $\Delta_f G^o$ had to be calculated at a pH of 7.4, an ionic strength of 0.25, and a temperature of 310 K. By specifying the pH, also referred to as first level Gibbs transformation, the concentration of H^+ becomes fixed thus reducing the complexity of the system as the number of species becomes less. This transformation is achieved by the equation:

$$\Delta_f G_j^{'o} = \Delta_f G_j^o(I=0) + N_H(j)RT\ln(10)pH - \frac{\alpha(z_j^2 - N_H(j))I^{1/2}}{1+1.6I^{1/2}} \quad (17)$$

Let us consider two reactions from glycolysis and show how the transformed reaction Gibbs free energies for the species can be calculated at a pH of 7.4, ionic strength (I) of 0.25, and 310 K temperature. Glucose has the following values of $\Delta_f G^o$,

$\Delta_f H^o, z^i$ and $N_H(i)$ respectively, [-915.90 kJ/mol, -1262.19 kJ/mol, 0, 12], units. Substituting these values in equation (17) , along with the values of I, T, pH and R(0.00831451 kJ/gmol /K), gives a standard transformed Gibbs Free Energy ($\Delta_f G_j^{'o}$) for glucose of 426.71 kJ/mol. Using the data (appendices) the transformed Gibbs Free Energies for the remainder of the species are calculated. They are summarized in Table III.4 below.

Table III.4. Transformed Gibbs values at 310 K, 7.4 pH and 0.25 ionic strength.

Species	$\Delta_f G_j^{'o}$ (kJ/mol)	**Species**	$\Delta_f G_j^{'o}$ (kJ/mol)
GLC	-426.71	NADH	1120.1
G6P	-1318.8	ATP	-2291.9
F6P	-1315.6	ADP	-1424.2
FCT16P	-2206.7	H2O	-155.66
G3PH	-1095.7	Pi	-1058.6
13BPG	-2206	DHPH	-1088
PHPYR	-1189.4	2PHG	-1346.8
PYR	-350.78	3PHG	-1340.6
LAC	-313.7		
NAD	1059.1		

Where GLC denotes glucose, ATP is adenosine triphosphate, G6P is glucose 6-phosphate, ADP is adenosine diphosphate, G6P is glucose 6-phosphate, F6P is fructose 6-phosphate,

FCT16P is fructose 1, 6-biphosphate, G3PH is glyceradehyde 3-phopshate, NAD is oxidized nicotinamide adenine dinucleotide, DHPH is dihydroxyacetone phosphate, NADH is reduced nicotinamide adenine dinucleotide, Pi is phosphate, 13BPG is 1, 3-biphosphoglycerate, 3PHG is 3-phosphoglycerate, 2PHG is 2 phosphoglycerate, PHPYR is phosphoenolpyruvate, PYR is pyruvate and Lac is lactate.

Calculation of the Further Transformed Gibbs Free Energy

Some of the possible simplifications include specifications for the concentrations of some of the species. For example, it is possible to assume a fixed proton concentration, hence fixed pH. To account for this specification while still maintaining the thermodynamic information of the chemical reactions involved in these species, a Legendre transformation of the Gibbs Free Energy is used. The general equation for this is,

$$G' = G - \sum_i n_c(A_i)\mu(A_i) \qquad (18)$$

Where, $n_c(A_i)$ is the number of times species A_i appears in the reaction, and $\mu(A_i)$ is its chemical potential. In the model, the concentrations of the coenzymes NAD, NADH, ATP, ADP, and Pi are considered constant for the sake of simplicity. The effect of the coenzymes concentrations on the systems equilibrium composition is analyzed later in this section. Table III.5 below lists the n_c values of each coenzyme for all the species involved in the pathway.

Table III.5. n_c Values of the different species in the pathway.

	G6P	F6P	FBP	DHAP	GAP	BPG	3PG	2PG	PEP	PYR	LAC
ATP	1	1	2	1	1	1	0	0	0	-1	-1
ADP	-1	-1	-2	-1	-1	-1	0	0	0	1	1
NADox	0	0	0	0	0	1	1	1	1	1	0
NADred	0	0	0	0	0	-1	-1	-1	-1	-1	0
Pi	0	0	0	0	0	1	1	1	1	1	1

The following specified coenzyme concentrations ATP = 2.36, ADP = 0.91, NAD = 1.05, NADH = 0.2, and Pi = 0.24, expressed in mM. These concentrations correspond to astrocytes, and were taken from the literature (Williams et al., 1980; Xie et al., 2009). The further Transformed Gibbs Free Energy can now be calculated. Table III.6 below summarizes these values.

Table III.6. Further transformed Gibbs free energy values at specified coenzymes concentration.

Species	$\Delta_f G_j'^0$
GLC	-426.71
G6P	-453.48
F6P	-450.34
FCT16P	-476.15
DHPH	-230.39
GADP	-222.73
13BPG	-225.5
3PHG	-231.5
2PHG	-225.34
PEP	-74.145
PYR	-100.8
LAC	-122.55

In summary, we can use the standard Gibbs Free Energy of formation for each species, and then estimate the further Transformed Gibbs Free Energy through the approach formulated by Alberty (Alberty, 2005; Zimmerman, 2003).

The table for the Gibbs Free Energy for the reactions in the glycolysis for astrocytes are shown below along with the corresponding equilibrium constants.

Table III.7. Further transformed reaction Gibbs Free Energy (kJ/mole) for Glycolysis in Astrocytes.

Source	Product	Astrocytes
Glucose	G6P	-26.77
G6P	F6P	3.14
F6P	F1,6BP	-25.81
F1,6BP	GAP	253.42
DHAP	GAP	7.66
GAP	1,3PG	-2.77
1,3PG	3PG	-6
3PG	2PG	6.16
2PG	PEP	151.195
PEP	Pyruvate	-26.655
Lactate	Pyruvate	21.75

A complete detail of the reaction Gibbs Free Energy $\Delta_r G_j'^0$, equilibrium constant K^{eq}, rate constants V and affinity constants K for the glycolysis and TCA cycle both in astrocytes and neurons are listed Appendix V.

CHAPTER IV

MODEL VALIDATION

In chapter III, a mathematical model of brain tissue metabolism was formulated. We would like to use this model to predict potential responses to stimuli and or changes in metabolism resulting from diet changes. Before applying this model for prediction or detailed assessment of metabolic fluxes, however, we need to ensure this model is reliable. In other words, the model needs to be validated to ensure it can be used to study real-world physiological metabolisms. The meaning of validation is comparing the results of mathematical model with the corresponding experimental results, both qualitatively and quantitatively (Volland et al., 2017). In our model, which includes glycolysis, TCA cycle, ANLS, and glutamine-glutamate cycle. We can select some condition to validate our model, for instance, comparing reaction fluxes rate and species concentrations. For reaction fluxes rate, we need to know reaction equations and parameters. For species concentrations, we need measure the level of species. For the monitoring (or tracing) of the concentrations of species participating in the glycolysis (in cytosol) and TCA cycle (in mitochondria), traditional detecting method rely on NMR (Nuclear Magnetic

Resonance) to measure the labeled ^{13}C species in each step of the metabolic reactions (Brand et al., 1992; Campbell-Burk et al., 1987; Mackenzie et al., 1984). However, for ANLS and glutamine-glutamate cycle, some studies in the literature report on the lactate, glutamine, or glutamate levels in the extra-cellular space (Hu & Wilson, 1997; Lacreuse et al., 2018).

Since free radicals have been identified as the root cause for certain brain diseases (LeWitt & Fahn, 2016). The model formulated in this dissertation is focused on the glycolysis flux rate, as it might affect the free radicals production rate. The glycolysis metabolic rate has relationship with ANLS and expressing dynamic oscillations in the extra-cellular space lactate levels (Hu & Wilson, 1997).

A wealth of literature data can be found on brain metabolism. These experimental studies address a variety of issues in brain tissue metabolism. Lactate has been identified as an efficient substrate in neurons. Indeed, lactate not only supports respiration but also maintains ATP levels during intense levels of activation (Pellerin et al., 1998). In the early 1990's, Pellerin and Magistretti suggested a relationship that established tight coupling between neuronal activity and energy metabolism (Pellerin & Magistretti, 1994). They identified a strong balance between synaptic glutamate release and its reuptake into astrocytes that triggers aerobic glycolysis in the astrocytes and produces lactate. These authors stated that, contrary to the classical hypothesis (Maher et al., 1994), lactate is shuttled to the neuron through the mechanism which they termed the Astrocyte-Neuron Lactate Shuttle, or ANLS (Magistretti & Pellerin, 1999). More recently, Magistretti presented evidence highlighting strong astrocyte-neuron cooperation to deal with high energy demands of neurons, which suggest that under certain circumstances

neuronal demands will be satisfied by lactate produced in astrocytes (Magistretti & Allaman, 2018). Dienel's recent research shows that astrocytes produce lactate by metabolizing glucose and glycogen (Dienel, 2019). Barros and Weber issue that ANLS has connection with neuron activity (Barros & Weber, 2018). Since the astrocytes number is 10 times that of neurons, glucose will be metabolized primarily by astrocytes instead of neurons, and produce high levels of pyruvate in astrocytes' cytosol. High levels of pyruvate in astrocytes will drive the production of lactate, which, in turn, is then transported to the extracellular space and subsequently to neurons, where is metabolized into pyruvate. The pyruvate concentration gradient is the driving force induces different equilibrium between lactate and pyruvate between the neurons and astrocytes. It has been proposed that the lactate transport from the astrocyte to the neuron is based on a demand-based regulatory mechanism. This theory not only unified coupling between brain activity and the astrocytic and neuronal metabolisms, but also proved to be an important breakthrough in the metabolic modeling of the brain.

This theory received mixed reactions, including strong criticisms (Chih et al., 2001) that challenged the ANLS. However, most of these publications did not show experimental data to support their theories. Studies were done to further this claim of lactate being the preferential substrate of the neurons and it was shown that when neurons were incubated in media containing glucose and lactate separately, the relative contribution of lactate towards neuronal oxidation was higher (Bouzier-Sore et al., 2003).This implies that lactate can enter both neurons and astrocytes, but lactate is preferentially metabolized in neurons.

To understand the metabolite dynamics that are directly associated with brain energetics, some researchers developed models that would attempt to understand the various (metabolic, hemodynamic and electrophysiological) aspects of the brain. Aubert and coworkers (Aubert et al., 2002), for instance, formulated a model based on differential equations derived from mass balances to simulate the dynamics of glycolytic fluxes and oxygen exchanges. This group then investigated the ANLS hypothesis from a theoretical view by developing a compartmental model and testing it with external stimuli (Aubert & Costalat, 2005). Simulations of the brain stimuli were performed and the flux of lactate in the sub and extra-cellular compartments was studied. A continuous flux of lactate was seen from the astrocyte to the neuron during basal and excited states, consistent with the ANLS theory. The authors further suggested that the classical and the ANLS theories do not contradict each other; rather they seem to work concomitantly towards explaining the mechanism of metabolism. These authors also studied the dynamic behavior of the neuron in the presence of electrical stimuli. Such an study was based on experimental data gathered by Hu and Wilson (Hu & Wilson, 1997). Hu used electrical stimulus to induce increased neuron uptake of lactate. The experimental study measured the fluctuations in extracellular lactate levels in the brain in response to acute neuronal stimulation. An initial dip in the concentration of lactate in the extra-cellular space was observed at the beginning of each stimulus.

While Newman and coworkers demonstrated that a test where mice were put to negotiate a maze, associated with neuronal stimulation, also induced increased neuron uptake of lactate , Newman's test (Newman et al., 2011), however, did not indicate any initial dip of lactate levels in extra-cellular space.

Aubert's group focused their attention on the understanding of the mechanisms leading to an initial "dip" and subsequent increase in tissue lactate levels during sustained and periodic stimulation. These authors formulated a model capable of reproducing this phenomenon by defining an ad-hoc input function that incorporated parameters accounting specifically for factors that may influence the extra-cellular lactate kinetics such as the intra-cellular lactate and pH variation. This function successfully reproduced the effect caused by the sensors used in Hu and Wilson's experiments to stimulate the brain (Hu & Wilson, 1997).

The initial dynamics of lactate have been studied by other authors (Mangia et al., 2009), who used proton magnetic resonance spectroscopy to understand neuronal energetics during functional activation. They found an initial dip decrease in the lactate concentration during the early phase of neural activation, which could be explained by the increased lactate consumption following neural activation.

These observations led us to the following questions. Is neuronal metabolism primarily oxidative and glial metabolism primarily glycolytic? What is the substrate partitioning of glucose and lactate between the astrocytes and the neurons?

The aim of this work was to combine various modeling efforts and expand on the current modeling strategies reported in literature. Data collected from physiological experiments were used to formulate and validate the model. A multi-domain model that distinguishes between the cytosol and the mitochondria, both in neurons and astrocytes, is presented in this dissertation. The model includes a detailed model pathway emphasizing the role of alternate energy substrates, such as ketone bodies, known to participate in the brain energetics (cf. Fig. IV.1).

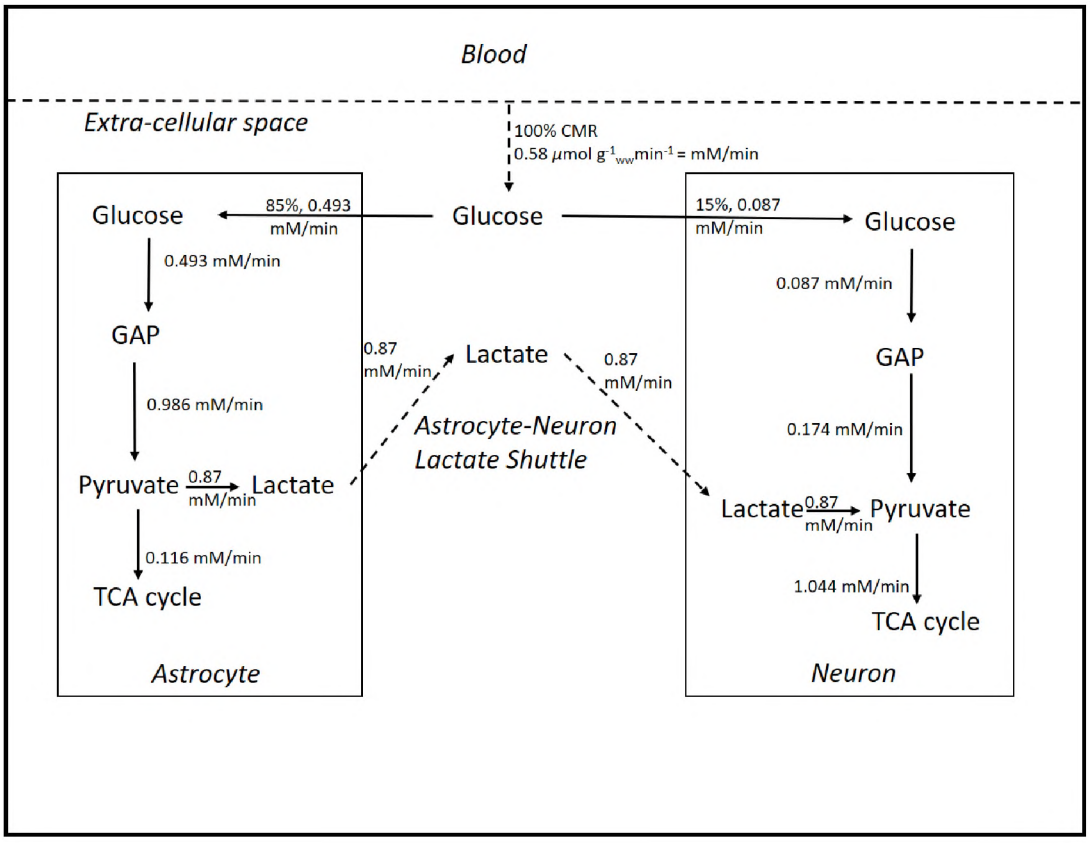

Figure IV.6. Flux analysis of simplified schematic diagram model.

Ketone body metabolism has been thought to affect glucose metabolism by altering carbon fluxes originating from glycolytic activity (neuron and astrocyte). This has been hypothesized to occur through the partitioning of carbon units away from glycolysis and towards the TCA cycle at the level of Acetyl-CoA as shown in the schematic of Fig. IV.2.

A

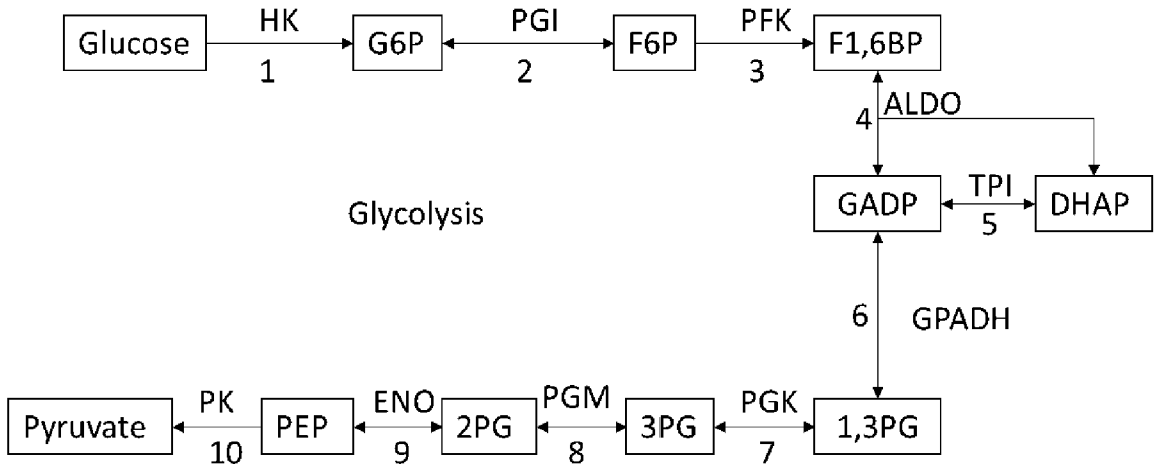

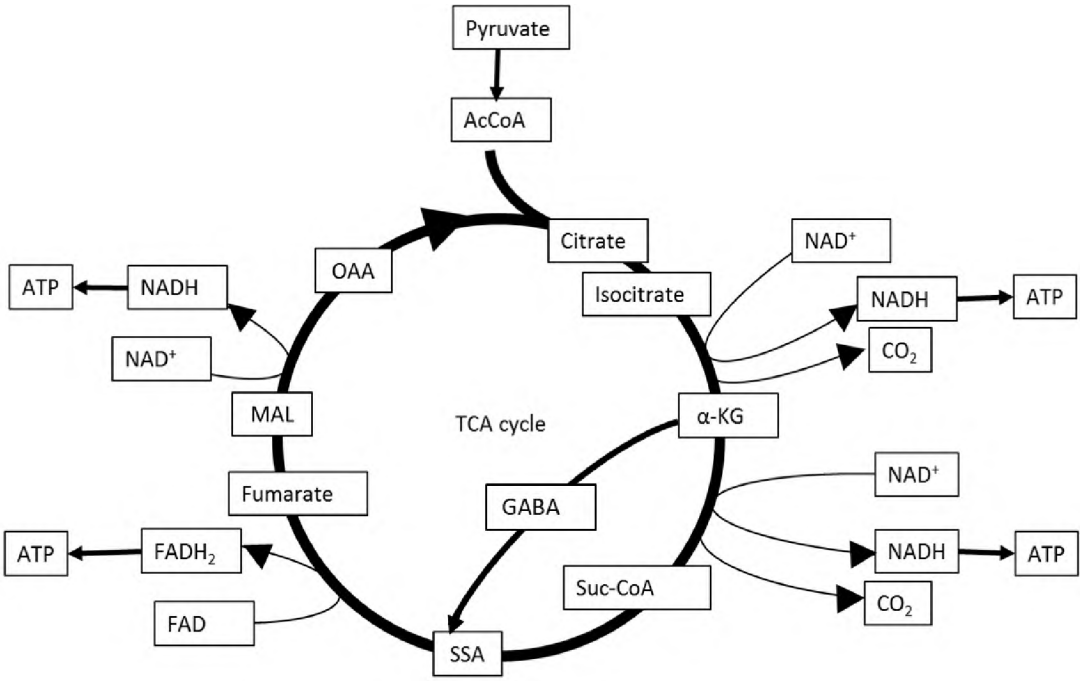

B

Figure IV.7. (A) Glycolysis and (B) TCA cycle (Salim, 2017).

Experimental studies available in the literature, present data in many different forms, such as fluxes, species levels and concentrations, and dynamic responses to different perturbations, among others. The connection with a mathematical model like the

one proposed in this study and the relevance of these observations to lead the model formulation and development, as well as assisting in its validation, present a number of issues.

In a typical study on neuronal activation, Hu and Wilson (Hu & Wilson, 1997) applied electrical stimulation to rats. These authors monitored the dynamics of lactate concentration in the extracellular space of hippocampus following a single electrical stimulus as well as the results for multiple (cyclic) electrical stimuli. Let us examine those two illustrative scenarios.

Lactate dynamics following neuronal activation experiments

In this section, results are compared to experimental data (Hu & Wilson, 1997) followed by the model predictions under conditions corresponding to a single electrical stimulus for rats subject to standard diet.

In vivo experimental data (Hu & Wilson, 1997) of the lactate dynamics induced by a single electrical stimulus and the two models, along with the percent deviations, are presented in figure 8 lactate concentration change during electrical stimulus.

These experimental results indicate a significant (~ 70% relative to the baseline levels) increase in the extra-cellular lactate levels. Figure IV3 below shows the tissue lactate dynamics following a single neuronal stimulation. A 5-s electrical stimulus induces an initial drop of the CMR for 18s, followed by a sharp increase in lactate concentration levels, peaking after 70-s following the stimulus, the dynamics is completed by a period of recovery showing an exponential decrease during which lactate levels return to those corresponding to the pre-stimulus conditions.

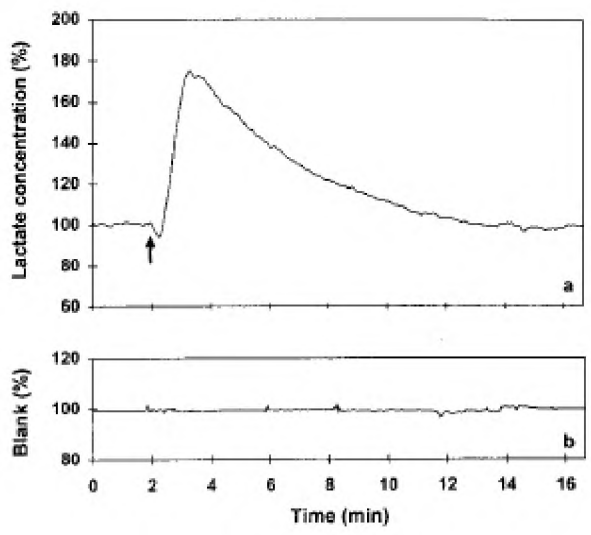

Figure IV.8. Lactate concentration (%) for single-stimulus experiment (figures are made in (Hu & Wilson, 1997)).

We can illustrate the potential and difficulties associated with the use of this type of data to validate a more complex model, as the one formulated in this work. In the following sections the performance of simplified (Aubert et al., 2005) and complex (this work) models are compared with Hu and Wilson (Hu & Wilson, 1997) experimental measurements of lactate concentration in the extra-cellular space during neuronal activation induced by a single and multiple electrical stimuli experiments.

Using Dynamic Data for Model Validation

Aubert and coworkers (Aubert et al., 2005) formulated a simplified model to mimic brain metabolism under neuronal stimulation. The model simulated lactate levels in the extra-cellular space following perturbations to the fluxes through the blood-brain barrier, and in the capillaries network irrigating the brain.

This model was a simple mathematical model of lactate concentration dynamics induced by perturbations to the extra-cellular space lactate concentration. The authors concentrated their attention on the lactate transport mechanism between capillary, blood-brain barrier, and brain tissue, but they did not consider the physiological metabolism of glycolysis and pyruvate-lactate redox reactions. The model contained only 19 parameters and 11 equations, and the model could qualitatively and quantitatively reproduce the lactate dynamics observed experimentally for single electrical stimulus as reported by Hu and Wilson (Hu & Wilson, 1997). However, although Aubert's model could reproduce qualitatively the experimental dynamics for multi electrical stimuli, the quantitative agreement with experimental measurements was very poor in this latter scenario.

Indeed, the results for a single electrical stimulus were very close to experimental observations, resulting in a coefficient of determination of approximately 92% (R^2=0.917). For multiple electrical stimuli scenario, on the other hand, the simulated results resulted only in a coefficient of determination of 45% (R^2=0.4512). Figure IV.4 shows the comparison between simulations of extra-cellular lactate concentration dynamics induced by multiple step perturbations to lactate influx to tissue (Aubert et al., 2005) with *in vivo* experimental data (Hu & Wilson, 1997).

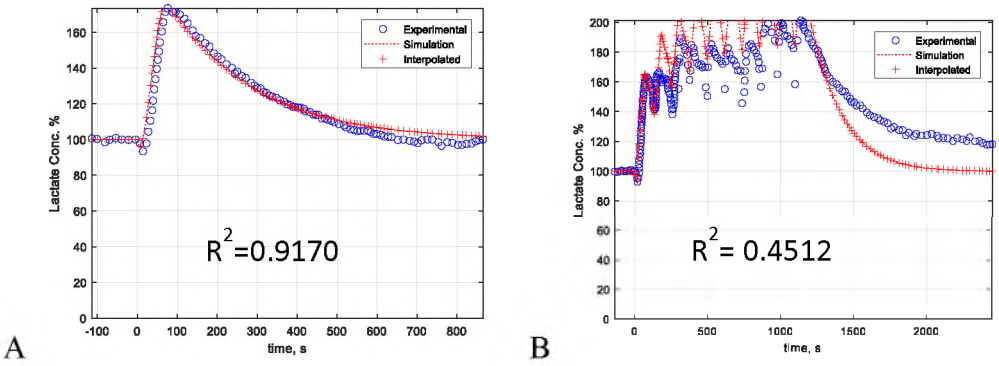

Figure IV.9. Comparison between flux-induced extra-cellular lactate dynamics (red crosses (Aubert et al., 2005)) with *in vivo* experimental data resulting from neuronal activation by electrical stimuli (blue circles (Hu & Wilson, 1997)).
(A) Single electrical stimulus and (B) Multi electrical stimuli.

As shown above, poor quantitative agreement was reported in Aubert's research and lactate levels in extra-cellular space observed experimentally for multi electrical stimuli. This suggests that some of the model parameters need to be adjusted. Since our research model and Aubert's model differ in the degree of complexity, one needs to focus the attention on those parameters common to both models.

We first followed Aubert's (Aubert et al., 2005) approach to mimic extra-cellular lactate dynamics during neuronal activation experiments.

How to ensure that our model could be compared with Aubert's model? Our model includes glycolysis, TCA cycle, ANLS, and glutamine-glutamate cycle. ANLS includes the lactate fluxes between astrocytes, neurons, extra-cellular space, and blood. Aubert's group used 11 equations and 19 parameters to describe lactate fluxes between blood and extra-cellular space. We take these 11 equations and 19 parameters and apply those equations and parameters in ANLS of our model. Among our model 164 parameters, 19 parameter values come from Aubert's model, while the remaining 145

parameters were adapted from the literature. I will refer to this model as the Chan-Aubert model.

Extra-cellular lactate levels dynamics was induced by perturbations to the lactate fluxes between capillary and extra-cellular space of brain tissue in our 164 parameters model, trying to replicate observations reported during single and multi electrical stimuli. The results are shown below in Figure IV.5. The simulation results found with this adapted, or Chan-Aubert's, model showed acceptable qualitative agreement, but quantitative agreement was very poor, both for the single and multiple perturbation exercises.

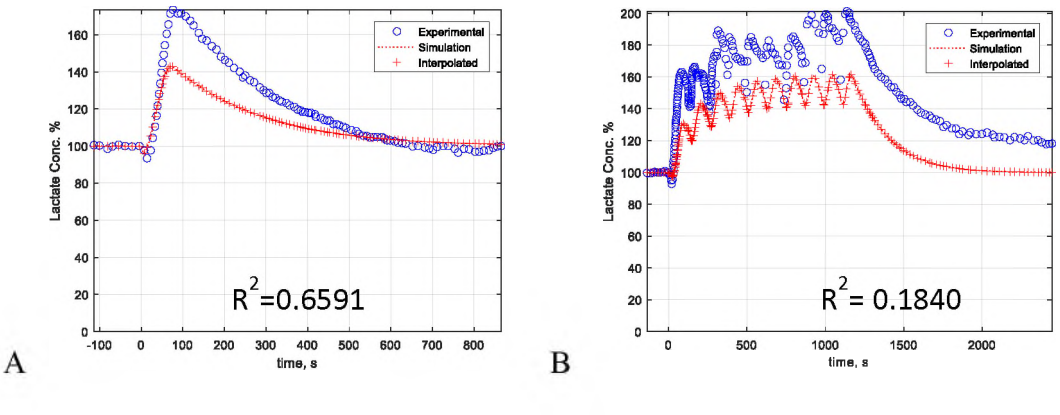

Figure IV.10. Comparison between extra-cellular lactate concentration flux-induced dynamics (red crosses, Chain-Aubert's model) with *in vivo* experimental observations during neuronal activation induced by electrical stimuli (blue circles (Hu & Wilson, 1997)).
(A) Single electrical stimulus and (B) Multi electrical stimuli.

This lack of quantitative agreement was observed when the model used the 19 parameters from Aubert's group. That clearly suggests that the 164 parameters model may be better adjusted by changing a different set of parameters. However, how does the change of these different parameters affect the dynamics of other substrates, for which dynamic data is not available for comparison. These questions obviously need to be

answered before considering the validation exercise successful. In other words, if we want to use Hu and Wilson's (1997) data to validate our model, we need first to find a different method to test (validate) the model.

Two of the 164 parameters in our research model are the cerebral metabolic rate (CMR) and blood flow rate. CMR represents the brain energy consumption rate and blood flow rate will change accordingly to meet the glucose demand associated with a given CMR. Under rest and standard diet conditions, brain energy demands are supported by the metabolism of glucose. Therefore, CMR also represents the net glucose influx to brain tissue.

In a recent modeling effort, Patel and coworkers (Patel et al., 2004), concentrated their attention in some of the inter-compartment (cells) pathways in the glycolysis and the TCA cycle, particularly glutamate-glutamine cycle and GABA shunt, but simplified the basic intra-compartment pathways. This group studied tissue metabolic dynamics for glucose as the main energy substrate. One of the salient features of this study consisted in using CMR to represent glucose consumption. The model formulated by Patel and coworkers consisted of 18 (mass balance) equations and 70 parameters for a simplified brain tissue model. The model could successfully reproduce experimental measurements of the dynamic enrichment of glutamate and aspartate (Patel et al., 2004).

Now, the 164 completed model, 19 parameters come from Aubert's group, and we adjust the CMR and blood flow rate terms by the Patel's method in Chan-Aubert model. This model will now be referred to as the Chan-Aubert-Patel (CAP) model. In this model, neuronal stimulation experiments were mimicked by using CMR dynamics to represent glucose influx changes and blood flow rate changes induced by electrical stimuli. Hu and

Wilson's data (Hu & Wilson, 1997) included glucose dynamic percentage levels both for single and multiple electrical stimuli experiments. Therefore, CMR dynamics can be easily back-calculated based on the net glucose influx to brain tissue in single and multi-electrical stimuli scenarios.

In the CAP model, glucose is metabolized to pyruvate by glycolysis, and pyruvate can be reduced to lactate, then lactate can transported between the cells and the extra-cellular space. The dynamics of lactate concentration levels in the extra cellular space can now be compared to the experimental results reported by Hu and Wilson's research (Hu & Wilson, 1997) as shown in Figures IV.6 and 7 below.

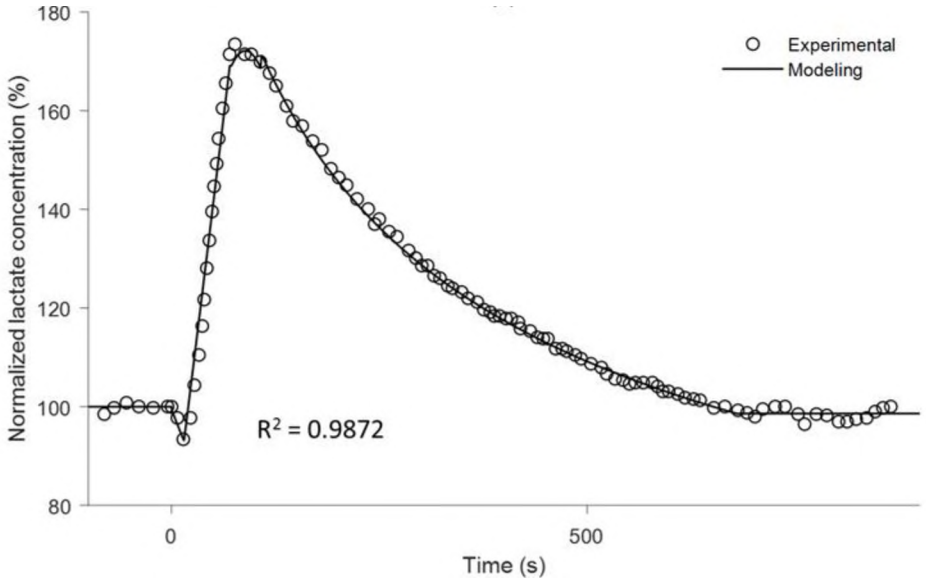

Figure IV.11. Lactate concentration dynamics in the extra-cellular space following a single electrical stimulus of 5-s and recovering peaks at 2 min to 170% of the baseline (pre-stimulus levels at t = 0: min).
Model predictions vs. experimental data (adapted from (Hu & Wilson, 1997))

Figure IV.7 below shows the dynamic response in lactate concentration in the cytosol of the neuron during a sequence of 10 stimuli. Each stimulus consisted of a stimulation period of 5-s followed by a rest interval of 2 min. Lactate levels reached a

maximum of ~70% increase from its baseline values during the activated period. The agreement with the experimental determinations reported in the literature (Hu & Wilson, 1997) showed now a remarkable improvement as evidenced by coefficients of determination larger than 98%, both for a single ($R^2 = 0.9872$) and multiple ($R^2 = 0.9876$) electrical stimuli.

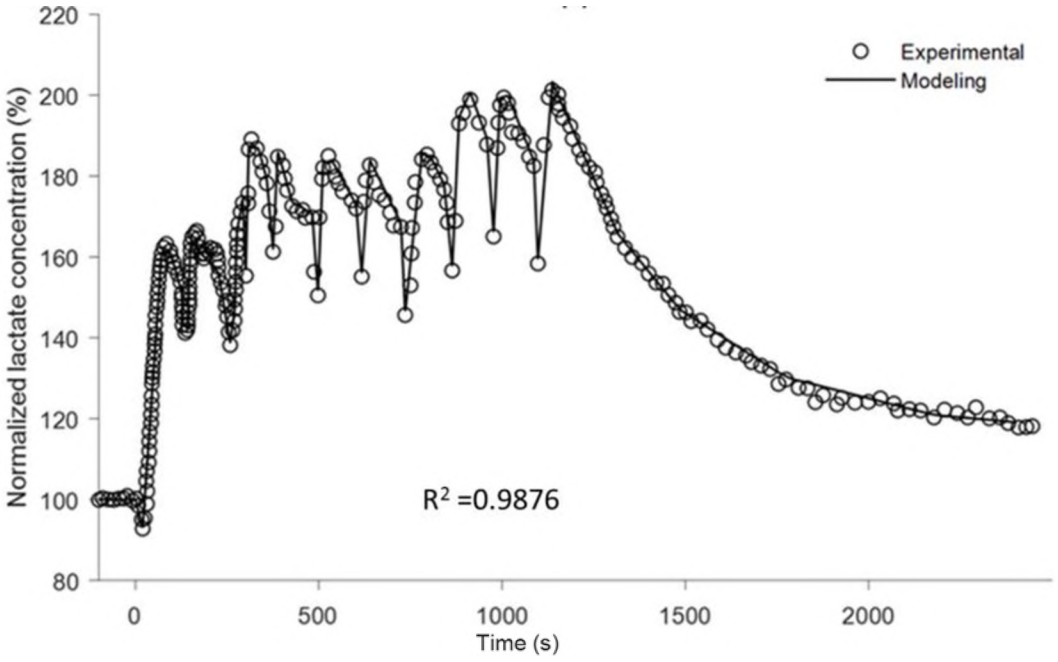

Figure IV.12. Dynamic response in lactate concentration (normalized) during a sequence of 10 repeated stimuli: 5-s stimulus followed by a 2 min rest interval.
Model predictions vs. experimental data (adapted from (Hu & Wilson, 1997)).

These two examples illustrate the relationship between model parameters and predictions, and how the comparison between *in vivo* and *in silico* can be used to adjust/validate the mathematical model.

In summary, CAP model improves the qualitative and quantitative agreement between experiments and model predictions. However, discrepancies provided valuable insight into the deficiencies of the model at each of its formulation stages. Table IV.1 summarizes the similarities and differences among the different models.

Table IV.8. Models Comparison Summary.

Model	Salient features
Hu	Electrical stimulus and CMR *in vivo* experiment (Hu & Wilson, 1997).
Aubert	19 parameters lactate transport mechanism model. Lactate injection from blood to tissue. $$J_{Lac\_BBB} = T_{max}\left(\frac{C_{Lac,EC}}{K_t + C_{Lac,EC}} - \frac{C_{Lac,Blood}}{K_t + C_{Lac,Blood}}\right)$$ J_{Lac_Blood} and J_{Lac_Tissue} are defined in Aubert's literature (Aubert & Costalat, 2005).
Chan-Aubert	Combined 145 parameters model of glycolysis, TCA cycle, ANLS, glutamine-glutamine cycle, and 19 parameters model of lactate injection from Aubert's model, total is a 164 parameters model.
Patel	70 parameters model with CMR represents glucose level (the others include pyruvate-lactate redox, TCA cycle, glutamate-glutamine cycle). The CMR will change with glucose oxidative rate change in neurons and astrocytes (Patel et al., 2004). $$CMR_{Glc\_total} = CMR_{Glc\_ox\_Neuron} + CMR_{Glc\_ox\_Astrocyte}$$
Chan-Aubert-Patel (CAP)	Combined 143 parameters model of glycolysis, TCA cycle, ANLS, glutamine-glutamine cycle, 19 parameters model of Aubert's model, and 2 parameters model of CMR and blood flow rate, total is 164 parameters model.

	$J_{Glc_{Blood \rightarrow tissue}} = K\left(C_{Glc\_Blood} - \sigma C_{Glc\_Tissue}\right)$ K is diffusion coefficient, which will change with blood flow rate, and σ is partition ratio of glucose transports to neurons or astrocytes.

Indeed, under the single electrical stimulus, the lactate concentration increased rapidly following the electrical stimulus, reaching a peak of approximately 180% of the steady state condition, and then decreased slowly back to the steady state condition before the electrical stimulus. Although, the simulation results match the experimental data with R^2 close to 1, one can see that the flux dynamics needs further attention. The high-level CAP model (with 164 parameters and 54 mass balances) can reliably predict the dynamics of the fluxes associated with lactate concentration under neuronal activation conditions without adjusting and model parameters.

The model will next be used to examine dynamic responses under diets that will result in ketone bodies complementing glucose as the main fuel (substrate) to sustain brain energetic demands.

CHAPTER V

MODEL EXPANSION: KETOGENIC DIET

In chapter IV, we validated the CAP model, which includes several pathways: (i) glycolysis, (ii) TCA cycle, (iii) the ANLS, (iv) the glutamate-glutamine cycle, and (v) the GABA shunt. The CAP model proved to be reliable to model the extra-cellular lactate dynamics during electrical stimuli in control (or standard) diets. In this research, however, we would like to study the effects of ketogenic diets (KD on the neuronal glycolytic metabolism. In ketogenic diets (KD), ketone bodies include β-Hydroxybutyrate (βHB), acetoacetate and acetone. Acetoacetate and acetone will metabolize to βHB in liver, and βHB will be transport to brain tissue as an energy fuel. In order to consider the effect of KD, we need add some additional reactions and transport mechanisms in the CAP model. The KD-related reactions and transport mechanism are listed in Table V.1. We will refer to the expanded model as the Chan-Aubert-Patel-Ketogenic (CAPK) model.

Table V.9. Reactions involving ketone bodies and required parameters (A) Metabolism and (B) Transport mechanism.

A

Source	Product	Parameter Number
βHB	Acetyl-CoA	4
Acetyl-CoA	Glutamate	4

B

Species	From	To	Parameter Number
βHB	Blood	Extra-cellular	4
βHB	Extra-cellular	Cytosol (A & N)	8

The expanded CAP, or CAPK, model includes the flux of ketones as a complementary or alternate substrate to sustain energetic demands in neuros. The question that remains unanswered is what portion of the flux of ketone bodies (βHB and acetoacetate) will metabolize to acetyl-CoA. There is experimental evidence that states that the oxidation of ketone bodies could support as much as ~ 60% of the total oxidation (Siesjo, 1979). This leads to two important conclusions: (i) ketone bodies, being limited by their transport characteristics, can never sustain 100% of the mitochondrial activity, and (ii) there is always a need for an additional influx to the TCA cycle apart from that provided by the glycolysis in the neuron. This is because the glycolysis in the neuron is directly related to the activity levels of neuron and, alone, it would not be sufficient to meet the demands of the neuron (Shulman et al., 2004). Hence, the additional fuel required to sustain the Krebs cycle activity is derived from glycolytic activity in

astrocytes, and is transported to neurons (via the extra-cellular space) through the mechanism referred to as the "astrocyte-neuron lactate shuttle" (ANLS). These arguments support the hypothesis that under all conditions, the astrocyte-neuron lactate shuttle remains active. Ketosis cannot increase unlimited to replace the brain glucose demand.

We will assume 80% lipid diet just produce 0.24 mM/min net flux of βHB metabolize to acetyl-CoA. 0.24 mM/min βHB metabolic flux is about 23% of neuronal TCA cycle flux (1.044 mM/min). βHB come the ketone bodies which produced by lipid metabolism in liver. Why ketogenic diet with 80% lipid and 20% protein plus carbohydrate just occupied 23% neuronal TCA cycle? Because some lipid will metabolic to fatty acid and glycerin for storage, and some lipid will metabolize to glucose for energy demand, the left will produce ketone bodies. The most ketone bodies will metabolize to βHB. Then βHB transports to brain, diffuses to extra-cellular space, transport to neuronal cytosol, due to the limitation number of MCT (Monocarboxylate transporters), only 23%, 0.24 mM/min flux shows in βHB→acetyl-CoA reaction. 0.24 mM/min is the maximum βHB→acetyl-CoA metallic rate, and even higher lipid percentage (> 80%) of ketogenic diet will not contribute any extra βHB→acetyl-CoA metabolic rate. Higher than 80% ketogenic diet is unreasonable, and out of our model design. Then we compare the flux rate of βHB→acetyl-CoA reaction and ANLS, 0.24 mM/min vs. 0.87 mM/min, even the maximum βHB→acetyl-CoA reaction rate is not high enough to reverse ANLS direction.

A net plasma-to-tissue influx of 0.58 μmol g^{-1}_{ww} min^{-1} of glucose (or CMR) is used as a reference in this study for the baseline condition (i.e., standard or control diet conditions).

Shulman and coworkers reported that the total (neuron and astrocyte) tricarboxylic acid flux can vary between 1.0 to 1.6 μmol g^{-1}_{ww} min^{-1} (Shulman et al., 2004). Therefore, a value of 0.24 μmol g^{-1}_{ww} min^{-1}, considered as the maximum net ketone influx to neurons in the CAPK model, could sustain as much as ~20% of the TCA activity at steady-state in ketogenic diet.

In the CAP and CAPK models, both standard and ketotic diets will reserve a portion of the CMR to sustain a 10% TCA activity in astrocytes. TCA activity includes pyruvate oxidation to acetyl-CoA as well as pyruvate carboxylation to OAA. If we calculate the astrocytic pyruvate oxidation only based on the total pyruvate neuronal and astrocyte oxidation (TCA activity deduct pyruvate carboxylation), the contribution of the astrocytic pyruvate oxidation will increase. This increased contribution will depend on how much of pyruvate carboxylation. In other words, the tricarboxylic acid flux of neurons and astrocytes under standard diet conditions would correspond to 1.16 μmol g^{-1}_{ww} min^{-1}, which is partitioned as 1.044 and 0.116 μmol g^{-1}_{ww} min^{-1} for neurons and astrocytes, respectively.

Under ketogenic diet conditions, neuronal and astrocytic TCA cycle fluxes are assumed to remain at the same levels shown for standard diets. The net glucose influx under ketotic conditions, however, decreases as the fuel influx is partially sustained by ketone bodies. Lactate transport parameters are kept constant and as reported by

LaManna and coworkers (J.C. LaManna et al., 1992). Figure V.1 presents a simplified schematic diagram of fluxes in the CAPK model.

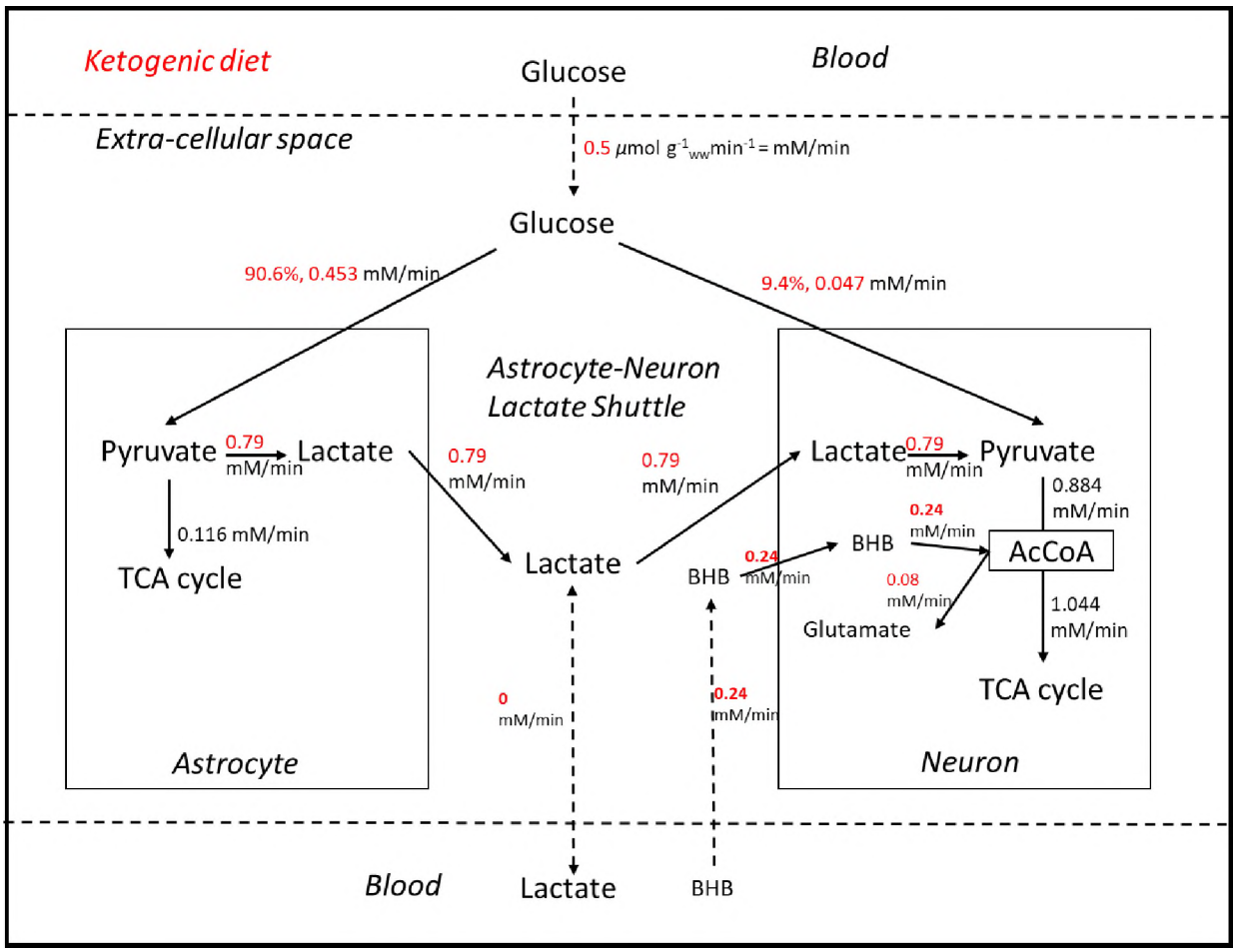

Figure V.13. Flux analysis of simplified schematic diagram of CAPK model.

Determination of substrate Steady-State levels by Optimization

This section consists in determining the steady-state substrate levels under ketogenic diets. The method applied here is based on the research reported by Beard and Qian (2005) (Beard & Qian, 2005). These authors proposed to minimize the total Gibb's free energy based on the enzyme activity. This approach is based on the fluxes (transport and kinetics) and steady state species concentrations for the CAP and CAPK models.

Beard and Qian's approach consisted in defining the enzyme activity as follows:

$$E_j = \left(\frac{\phi_j}{C_{t,j}(\bar{C})}\right)\left(\frac{e^{\frac{\Delta G_j''(\bar{C})-\Delta G_j''^0}{RT}}}{1-e^{\frac{\Delta G_j''(\bar{C})}{RT}}}\right) \quad (19)$$

Where $C_{t,j}$ is total concentration of *j*th reaction, $\bar{C}$ is concentration vector of reactants, ϕ_j is flux of *j*th reaction, $\Delta G_j''$ and $\Delta G_j''^0$ are the vectors of *j*th reaction further transformed Gibb's free energy under steady-state and equilibrium condition, respectively. The researchers defined C_t as

$$C_t = \prod_{i=1}^{Ns}(C_i)^{\alpha i} + \prod_{i=1}^{Ns}(C_i)^{\beta i} \quad (20)$$

Here C_i expresses *i*th species concentration, Ns represents number of species, α and β are stoichiometric coefficients of the forward and backward reactions, respectively.

Then we can define $\triangle$G for an open system. The Gibb's free energy can be represented as:

$$\Delta\bar{G}'' = \Delta\bar{G}''^0 - RT\tilde{S}^T ln\bar{C} \quad (21)$$

Where $\tilde{S}^T$ is transpose of the stoichiometric matrix (i.e., excluding the influx and out-flux of system).

The first set of constraints are formulated as follows

$$L_{null}\bar{C}^{ND} = L_{null}\bar{C}^{KD} \quad (22)$$

$$L_{null}X_cS\bar{\phi} = 0 \quad (23)$$

Where L_{null} is left null space of X_cS, and X_c is a diagonal matrix, which represents the species distribution between cytosol and mitochondria, S is stoichiometric matrix of the system, $\bar{\phi}$ is flux vector, $\bar{C}^{ND}$and $\bar{C}^{KD}$ are species concentration vector under normal (ND) and ketogenic (KD) diets conditions, respectively.

Based on the second law of thermodynamics, a constraint on the fluxes can be formulated: namely the metabolic fluxes combined with the change in Gibbs' free energy for each reaction must meet the condition

$$\phi_j \cdot \Delta G_j'' < 0 \qquad (24)$$

In an earlier chapter (Chapter IV), we showed how to calculate the steady-state (and dynamic) species concentrations of ND. By Beard and Qian's (Beard & Qian, 2005) method, we can calculate the steady-state species concentrations of KD.

Indeed, the CPA model was validated and it can therefore be used to find the steady-state conditions (concentration levels) for the ND. The CPA model included, not only the steady-state concentration levels of all the species involved, but all the associated kinetic and transport parameters.

These values can be used to find the Enzyme Activity as defined by Equation (19). Table V.2 below, lists the enzyme activities, the Gibbs free energy changes, and the metabolic fluxes for the glycolysis in astrocytes and neurons under ND conditions.

Table V.10. Enzyme activities, Gibbs free energy changes, and metabolic fluxes for in the cytosol of astrocytes and neurons under ND conditions.

Normal Diet	Enzyme Activity		ΔG		Flux	
Reaction	Astrocyte	Neuron	Astrocyte	Neuron	Astrocyte	Neuron
Glc to G6P	1.38E-01	1.14E-03	-8.553	-25.857	0.493	0.087
G6P to F6P	2.78E-01	1.09E-02	-10.933	2.331	0.493	0.087
F6P to FDP	1.90E-02	3.38E-03	-16.313	-28.842	0.493	0.087
FDP to GAP+DHAP	9.81E-02	1.42E-02	-5.62	24.916	0.493	0.087
DHAP to GAP	5.87E-02	7.81E-03	-8.897	-6.181	0.493	0.087
GAP to 13PG	3.92E-02	4.71E-04	-14.377	8.222	0.986	0.174
13PG to 3PG	2.37E+32	5.45E+32	-12.473	-19.318	0.986	0.174

3PG to 2PG	2.88E-01	2.39E-02	-15.385	11.921	0.986	0.174
2PG to PEP	3.23E-01	1.21E-02	-8.472	150.567	0.986	0.174
PEP to PYR	6.49E+34	1.60E+34	-19.1	-22.609	0.986	0.174
LAC to PYR	-1.37E-02	1.41E-01	-6.362	-18.342	-0.87	0.87
PYR to AcCoA	1.66E-02	1.66E-01	-20	-447.273	0.116	1.044

One can easily see that a minimum in objective functions, as defined by Equation (25) will be achieved if the enzyme activity remained the same under ND and KD conditions. Therefore, the enzyme activity, along with a flux balance analysis of the KD (Table V.3), can be used to find the steady-state concentration levels under KD conditions (Table V.4).

$$f = \sum_{j=1}^{Nr} \frac{\left(E_j^{ND} - E_j^{KD}\right)^2}{\max\left(E_j^{ND}, E_j^{KD}\right)^2} \qquad (25)$$

Where $C_{t,j}$ is total concentration of jth reaction, $\bar{C}$ is concentration vector of reactants, ϕ_j is flux of jth reaction, $\Delta G_j''$ and $\Delta G_j''^0$ are the vectors of jth reaction further transformed Gibb's free energy under steady-state and equilibrium condition, respectively. Table V.3 lists the enzyme activities, the Gibbs free energy changes, and the metabolic fluxes for the glycolysis in astrocytes and neurons under KD conditions.

Table V.11. Enzyme activities, Gibbs free energy changes, and metabolic fluxes for in the cytosol of astrocytes and neurons under KD conditions.

Ketogenic Diet	Enzyme Activity		ΔG		Flux	
Reaction	Astrocyte	Neuron	Astrocyte	Neuron	Astrocyte	Neuron
Glc to G6P	1.49E-02	4.90E-01	-17.708	-30.63	0.453	0.047
G6P to F6P	4.95E-02	4.01E-03	-17.552	2.563	0.453	0.047
F6P to FDP	1.36E-02	2.79E-01	-7.23	-35.27	0.453	0.047

FDP to GAP+DHAP	4.18E-02	8.98E-04	-15.477	28.418	0.453	0.047
DHAP to GAP	5.90E-02	3.12E-03	-11.129	-2.308	0.453	0.047
GAP to 13PG	2.28E-02	3.98E-03	-2.925	5.611	0.906	0.094
13PG to 3PG	4.88E+31	3.36E+35	-13.806	-4.234	0.906	0.188
3PG to 2PG	9.80E-02	1.10E-02	-13.901	5.166	0.906	0.376
2PG to PEP	1.57E-01	7.48E-03	-2.903	126.521	0.906	0.752
PEP to PYR	2.29E+34	1.51E+35	-16.317	-22.546	0.906	1.504
LAC to PYR	-8.03E-03	5.70E-03	-10.626	-3.852	-0.79	0.79
PYR to AcCoA	1.60E-02	5.87E-02	-11.796	-444.728	0.116	1.044

The results for the steady state, i.e. species concentrations under different diets are listed in table V.4.

Table V.12. Steady state species concentration of different diets in neurons (N) and astrocytes (A).

ND	A	N	5% KD	A	N	10% KD	A	N	15% KD	A	N
Glc	8.98E+00	8.82E+00	Glc	9.01E+00	6.69E+00	Glc	5.04E+00	8.02E+00	Glc	9.54E+00	1.67E+00
G6P	8.72E+00	5.92E+00	G6P	4.67E+00	4.34E+00	G6P	9.54E+00	8.06E+00	G6P	1.19E+00	7.78E+00
F6P	3.88E+00	1.47E-01	F6P	6.11E+00	6.32E+00	F6P	9.89E+00	7.48E+00	F6P	1.51E+00	9.22E+00
FDP	6.40E+00	9.29E-01	FDP	4.80E+00	5.37E+00	FDP	4.26E+00	6.78E+00	FDP	7.31E+00	4.84E-01
GAP	2.36E+00	8.10E+00	GAP	5.57E+00	7.47E+00	GAP	3.67E+00	5.97E+00	GAP	4.18E-01	9.80E+00
DHAP	9.39E+00	6.84E+00	DHAP	4.29E-01	8.17E-01	DHAP	2.32E+00	5.42E+00	DHAP	6.97E-01	4.61E+00
13PG	6.45E+00	4.22E+00	13PG	8.42E+00	2.12E+00	13PG	4.90E+00	6.27E+00	13PG	5.80E+00	3.35E+00
3PG	1.78E+00	7.47E+00	3PG	6.23E+00	1.68E+00	3PG	2.42E+00	9.85E-01	3PG	8.27E+00	1.69E+00
2PG	8.35E-01	4.05E-01	2PG	1.76E+00	8.60E+00	2PG	4.32E+00	1.50E+00	2PG	9.97E+00	7.90E+00
PEP	6.02E+00	9.97E+00	PEP	2.87E-01	6.05E+00	PEP	4.90E+00	6.62E+00	PEP	7.53E-02	8.07E+00
PYR	2.26E-01	2.26E-01	PYR	2.27E-01	7.20E+00	PYR	2.26E-01	3.39E+00	PYR	2.26E-01	4.32E+00
LAC	4.99E+00	6.38E-01	LAC	5.00E+00	6.60E+00	LAC	4.99E+00	7.44E+00	LAC	5.01E+00	7.93E+00
ATP	1.42E+00	2.78E+00	ATP	5.40E+00	1.02E-02	ATP	3.23E+00	3.62E-01	ATP	8.30E+00	8.47E+00
ADP	1.22E+00	1.17E-01	ADP	6.88E+00	7.50E-02	ADP	5.76E+00	2.86E-02	ADP	9.31E+00	1.61E-01
NAD+	4.37E+00	4.31E+00	NAD+	5.81E+00	3.65E+00	NAD+	2.66E+00	3.93E+00	NAD+	8.68E+00	4.77E+00
NADH	9.46E+00	7.17E+00	NADH	9.84E+00	9.58E+00	NADH	7.70E+00	6.34E+00	NADH	8.31E+00	7.39E+00
Pi	4.76E+00	8.04E+00	Pi	4.68E+00	2.02E+00	Pi	3.76E+00	9.14E+00	Pi	1.14E+00	6.96E+00
AcCoA_m	9.31E+00	8.10E-01	AcCoA_m	7.16E+00	8.34E+00	AcCoA_m	7.12E+00	8.52E+00	AcCoA_m	3.92E+00	3.45E+00

Next, we will find the BHB concentrations as well as transport and metabolic parameters for normal and ketogenic diets as follows: (1) BHB will transport from blood to extra-cellular space (EC). The diffusive transport mechanism flux can be formalized as

$$J_{BHB_{Blood\rightarrow EC}} = D\left(C_{BHB\_Blood} - \sigma C_{BHB\_EC}\right) \quad (26)$$

Where D is diffusion coefficient or mass transport constant, σ is a unit conversion factor.

$$\sigma = \frac{Brain\ tissue\ weight}{Whole\ body\ blood\ volume} = \frac{1.4\ kg}{4.9L} = 0.286\ (\frac{kg}{L}) \quad (27)$$

The brain tissue weight and blood volume can be readily found in reference materials (Stevanovic, 2019).

We know the BHB flux from blood to tissue, the BHB concentrations in blood, in the EC, and in the mitochondria from literature (Puchowicz et al., 2005), so we can easily calculate the mass transport constant (or diffusion coefficient) D.

The facilitated transport mechanism use following equation

$$J_{BHB_{EC\rightarrow Cyt}} = T_{max}\left(\frac{C_{BHB,EC}}{M_t + C_{BHB,EC}} - \frac{C_{BHB,Cytosol}}{M_t + C_{BHB,Cytosol}}\right) \quad (28)$$

Where T_{max} is rate constant and M_t is affinity of MCT. Here we can assume that lactate and BHB transport is facilitated by the same transporters, MCT, therefore the facilitated transport parameters for BHB are the same as those corresponding to lactate facilitated transport. With the BHB concentration in the EC space, we can calculate the BHB concentration in cytosol.

In the metabolic model one can use the following equation

$$J_{BHB\rightarrow AcCoA_{Mito}} = \emptyset_1 - \emptyset_2 \quad (29)$$

$$\emptyset_1 = \frac{V_1 \frac{C_{BHB\_m}}{K_1}}{1 + \frac{C_{BHB\_m}}{K_1} + \frac{C_{AcCoA\_m}}{K_2}} \quad (30)$$

$$\emptyset_2 = \frac{V_2 \frac{C_{AcCoA\_m}}{K_2}}{1 + \frac{C_{BHB\_m}}{K_1} + \frac{C_{AcCoA\_m}}{K_2}} \quad (31)$$

Where $V_{1\sim2}$ are rate constants, which are unknown, and $K_{1\sim2}$ are affinities, which are known.

These four parameters are all connected with the equilibrium constant via the Haldane relationship, i.e.

$$K^{eq} = \frac{C_2^{eq}}{C_1^{eq}} = \frac{V_1 K_2}{V_2 K_1} \tag{32}$$

Similarly has it was described in Chapter 3, it is simple to demonstrate that only one of the reaction constants will remain unknown. This constant can be related to the metabolic flux as shown below, i.e.

$$V_2 = \frac{V_1 K_2}{K^{eq} K_1} \tag{33}$$

Then we replace V_2 of Eq. (31), and the metabolic flux as shown below. i.e.

$$J_{BHB\rightarrow AcCoA_{Mito}} = \frac{V_1 \frac{C_{BHB\_m}}{K_1}}{1+\frac{C_{BHB\_m}}{K_1}+\frac{C_{AcCoA\_m}}{K_2}} - \frac{(\frac{V_1 K_2}{K^{eq} K_1})\frac{C_{AcCoA\_m}}{K_2}}{1+\frac{C_{BHB\_m}}{K_1}+\frac{C_{AcCoA\_m}}{K_2}} \tag{34}$$

$$J_{BHB\rightarrow AcCoA_{Mito}} = V_1 \left(\frac{\frac{C_{BHB_m}}{K_1} - \frac{C_{AcCoA_m}}{K^{eq} K_1}}{1+\frac{C_{BHB_m}}{K_1}+\frac{C_{AcCoA_m}}{K_2}} \right) \tag{35}$$

The BHB relative concentrations and parameters of transport mechanism and metabolism in normal and ketogenic diets are listed in table V.5.

Table V.13. BHB relative concentrations and parameters of transport mechanism and metabolism in normal and ketogenic diets.

A. Diffusive mass transport parameters for ketone bodies (blood to extra-cellular space).

BHB Diffusive Transport Mechanism	From	To	Flux	Diffusion coe.(1/min)	Blood-EC unit conversion factor
Diet	C_BHB_Blood (mM)	C_BHB_EC (mmole/kg)	J (mM/min)	D (1/min)	σ (kg/L)
ND	0.20	0.04	1.00E-03	0.01	0.286
KD	2.30	0.18	0.24	0.11	0.286

B. Facilitated transport parameters for ketone bodies (extra-cellular space to cytosol).

BHB Facilitated Transport Mechanism	EC->Cytosol		
Diet	Tmax (mM/min)	M (mM)	C_BHB_Cyto_N (mmole/kg)
ND	3.60	2.50	3.93E-02
KD	3.60	2.50	1.24E-03

C. Facilitated transport parameters for ketone bodies (cytosol to mitochondria).

BHB Facilitated Transport Mechanism		Cytosol->Mito	
Diet	C_BHB_Mito_N (mmole/kg)	Tmax (mM/min)	M (mM)
ND	0.10	3.60	2.50
KD	0.25	3.60	2.50

D. Metabolic parameters and ΔG for the reactions involving BHB, AcCoA, and Glutamate in neurons.

Keto Metabolism	Source	Product	KA (mM)	KB (mM)	VA_N (mM/min)	VB_N (mM/min)	$\Delta G''^{0}_{reaction}$
	BHB	AcCoA	0.006	0.006	1.0235	1.0453	76.80
	AcCoA	Glutamate	0.45	1.1	0.042188	0.0074477	752.29

The concentration of glutamate in mitochondria is adapted from the literature (Patel et al., 2004).

E. Glutamate concentration in neuronal cytosol.

Species	C_Cyto_N (mmole/kg)
Glutamate	11.8

CHAPTER VI

LACTATE DYNAMICS DURING NEURONAL ACTIVATION: KETOTIC CONDITIONS

The robustness of the formulated model was demonstrated in Chapter IV. Indeed, the model showed that it could reliably predict metabolic qualitative trends in brain tissue under conditions of activation or neuronal stimulation. In this section, the model is extended to examine metabolic responses under ketotic conditions by investigating the effect of ketone bodies on lactate dynamics. However, recognizing that the actual contribution of ketone bodies to brain metabolism is still unknown, an analysis of lactate dynamics under different conditions of ketosis will be examined.

The analyses performed below were conducted assuming that at baseline conditions the ketone metabolism contributes to ~20% of the total brain metabolism for ketogenic diet conditions. In order to facilitate comparisons, the concentrations of lactate under ketotic conditions were normalized against lactate values corresponding to standard diet (or control) conditions (Fig. VI.1).

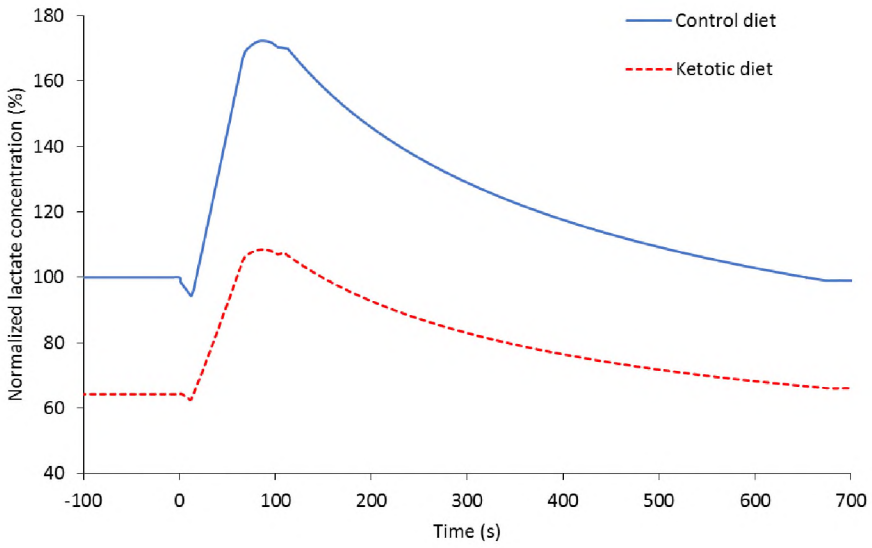

Figure VI.14. Lactate concentration dynamics following a single stimulus of 5-s and recovering peaks at 2 min to 170% of the baseline (pre-stimulus levels at t = 0: min). Dynamic response shown as lactate normalized concentration for standard (control, solid blue line) and ketogenic (red dashed line) conditions. Concentration levels for ketotic conditions were normalized with respect to baseline conditions corresponding to the control diet (concentration $_{\text{stimulus}}$/ concentration $_{\text{baseline-control diet}}$).

The changes in the dynamic behavior of lactate levels in the cytosol of the neuron under the influence of ketogenic diet with a 5-sec sustained stimulus exhibited a ~2% decrease (relative to the baseline condition). Similarly to what was observed in the standard diet conditions, lactate concentration peaks after approximately 2 mins. As compared to standard diet conditions, the lactate levels were ~35% lower under ketotic conditions. This inhibitory effect on lactate accumulation could be explained by the additional flux of ketone bodies in the TCA cycle following a decrease in neuronal activity.

The dynamics of the fluxes associated with lactate mass balances under ketogenic diet demonstrated that the dynamics of these fluxes are similar to those observed for standard conditions (Fig. VI.2).

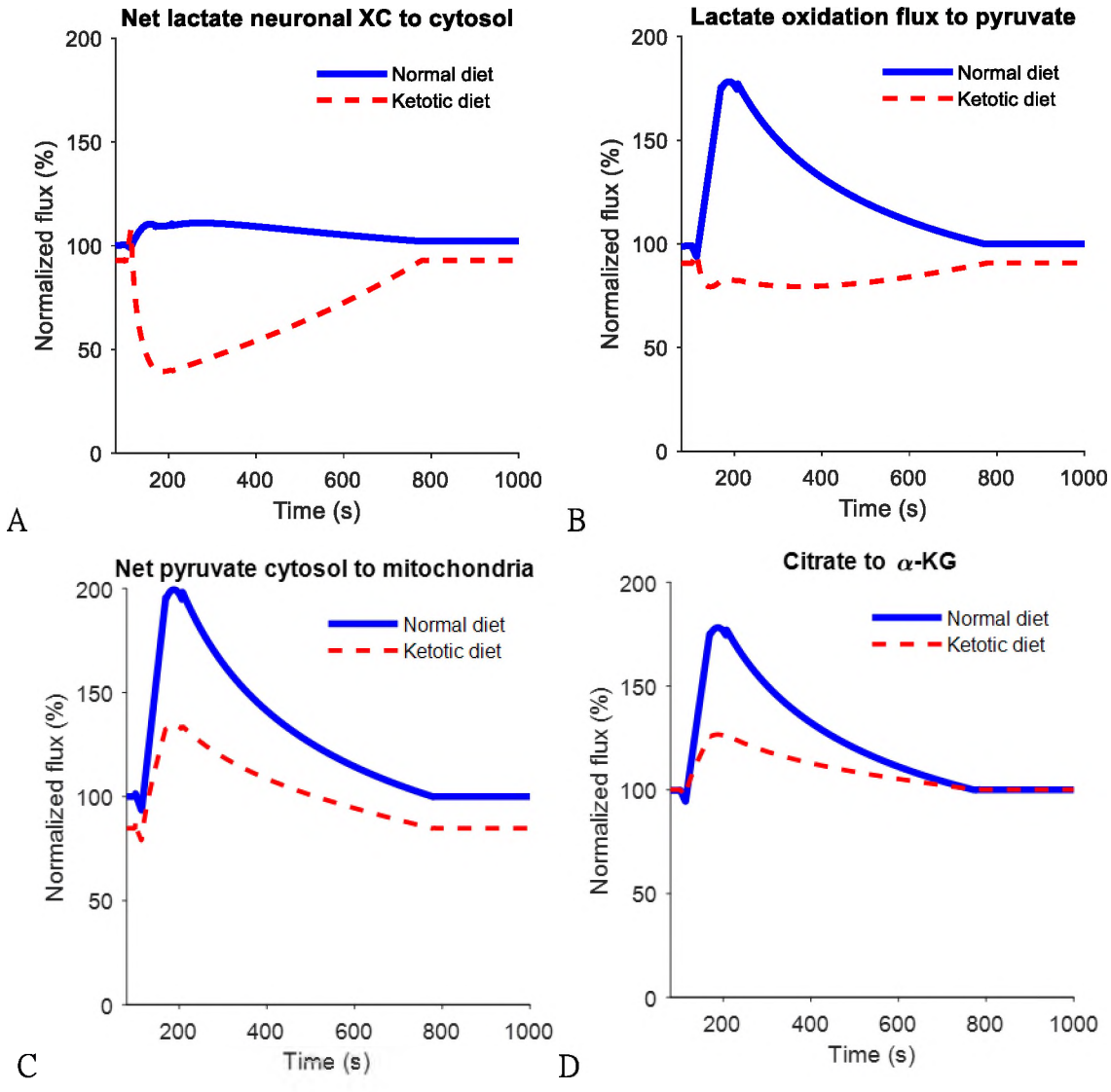

Figure VI.15. Flux dynamics of cytosolic lactate in standard and ketotic conditions. Following a single stimulus of 5-s:
(A) ϕ1: Net flux of lactate entering the cytosol from extra-cellular space; (B) ϕ2: Lactate oxidation flux in the reaction of lactate to pyruvate in the cytosol; (C) ϕ3: Net flux in the transport of pyruvate in the cytosol to the mitochondria increases; and (D) ϕ4: Net flux from citrate to α-KG. The flux values were normalized with respect to normal (control) diet conditions as described in Fig. VI.1.

All flux values are normalized with respect to those of the standard diet (or control) conditions. The dynamics of some of the major TCA cycle fluxes were examined. These fluxes showed the same levels at steady state, but the amplitudes of the deviations from baseline conditions during stimuli were smaller than those observed for standard diet conditions (Fig. VI.2 & 3).

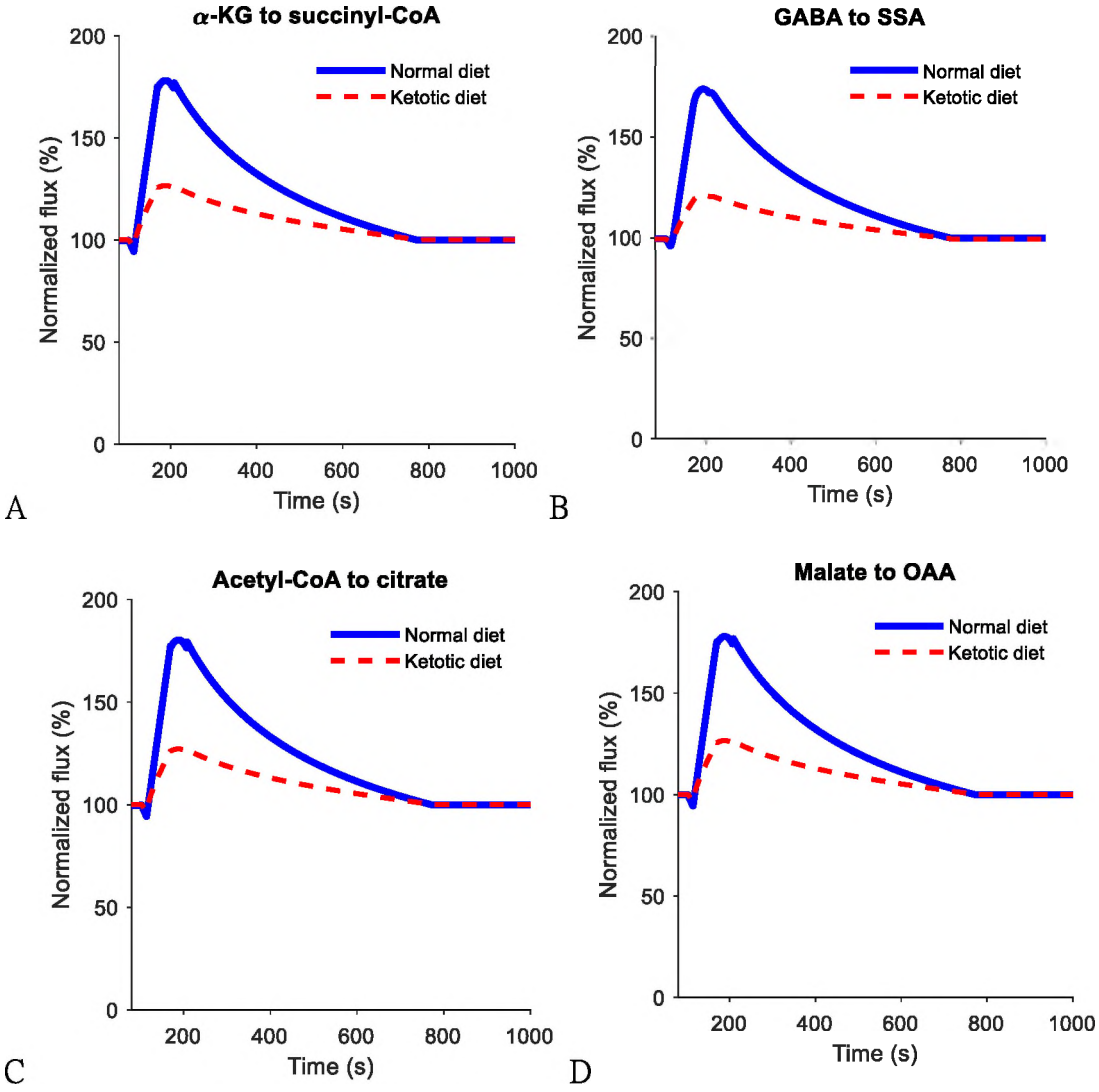

Figure VI.16. Flux dynamics associated with the glutamate-glutamine cycle, the GABA shunt, and malate shuttle in standard and ketotic conditions.
Net fluxes change following a single stimulus of 5-s. (A) ϕ5: Net flux from α-KG to succinyl-CoA; (B) ϕ6: Net flux from GABA to succinic semialdehyde; (C) ϕ7: Net flux

from acetyl CoA to citrate in the TCA cycle; and (D) ϕ8: Net flux from malate to oxaloacetate in the mitochondria.

The dynamics of lactate levels under ketosis during a periodic stimulation of 5 sec followed by a rest periods of of 2 min, were also investigated. The simulations showed similar dynamic profiles for both diet conditions; the magnitudes of the lactate levels deviations, however, were smaller under ketotic conditions as compared to those observed during neuronal activation under standard diet (Fig.VI.4).

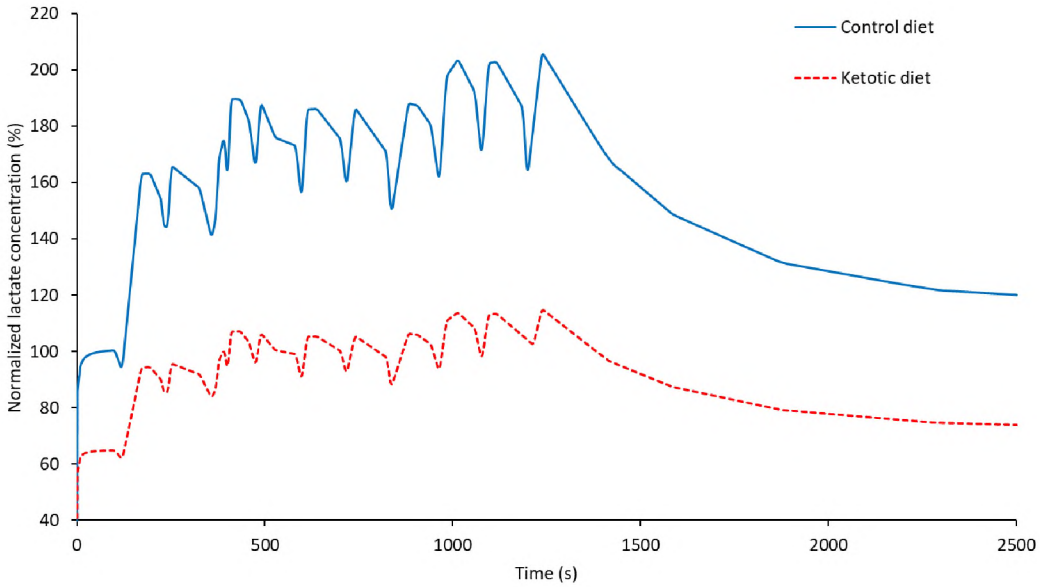

Figure VI.17. Dynamic response in lactate concentration (normalized) during 10 repeated stimuli: 5-s stimulus followed by a 2 min rest interval.
Dynamic response shown as lactate normalized concentration for standard (control, solid blue line) and ketogenic (red dashed line) conditions. Concentration levels for ketotic conditions were normalized with respect to baseline conditions corresponding to the control diet (concentration $_{\text{stimulus}}$/ concentration $_{\text{baseline-control diet}}$).

These findings are consistent with the higher tissue lactate levels observed under standard diet conditions, suggesting that ketone bodies contributions to the regulation of

the TCA cycle activity in the mitochondria, and lower glucose level in blood, result in a decrease of extra-cellular lactate levels.

In normal (or control) diet, the steady state and dynamic total CMRs will provided by a flux of glucose. In ketotic diet, the supply of glucose is not enough to meet the substrate (total CMR) demand, this deficiency is completed by the βHB flux contribution to the total CMR. In our CAPK model, it has been considered that, for conditions of ketone bodies saturation, the ketotic diet can deliver a maximum βHB flux of 0.24 mM/min. A βHB flux (2 carbons per molecule) of 0.24 mM/min will be equivalent to 0.08 mM/min of glucose (6 carbons per molecule) flux, then the βHB contribution to the total CMR will be ~14% (0.08/0.58). To examine the sensitivity of the model to changes in the flux of ketone bodies, we decreased the βHB flux to 0.16 and 0.08 mM/min, i.e. ~9% and ~5% of the total CMR, respectively. These conditions are tabulated below in Table VI.1.

Table VI.14. Conditions (flux of βHB/ Total CMR) used to examine the dynamics in the extra-cellular lactate concentration for a single electrical stimulus.

β HB flux (mM/min)	β HB flux*(2C/6C)	Cerebral glucose metabolic rate (mM/min)	βHB/CMR %
0	0	0.58	0%
0.08	0.027	0.553	5%
0.16	0.053	0.527	9%
0.24	0.080	0.500	14%

The predicted extra-cellular lactate concentration dynamics for a single electrical stimulus is shown in Fig. VI.5.

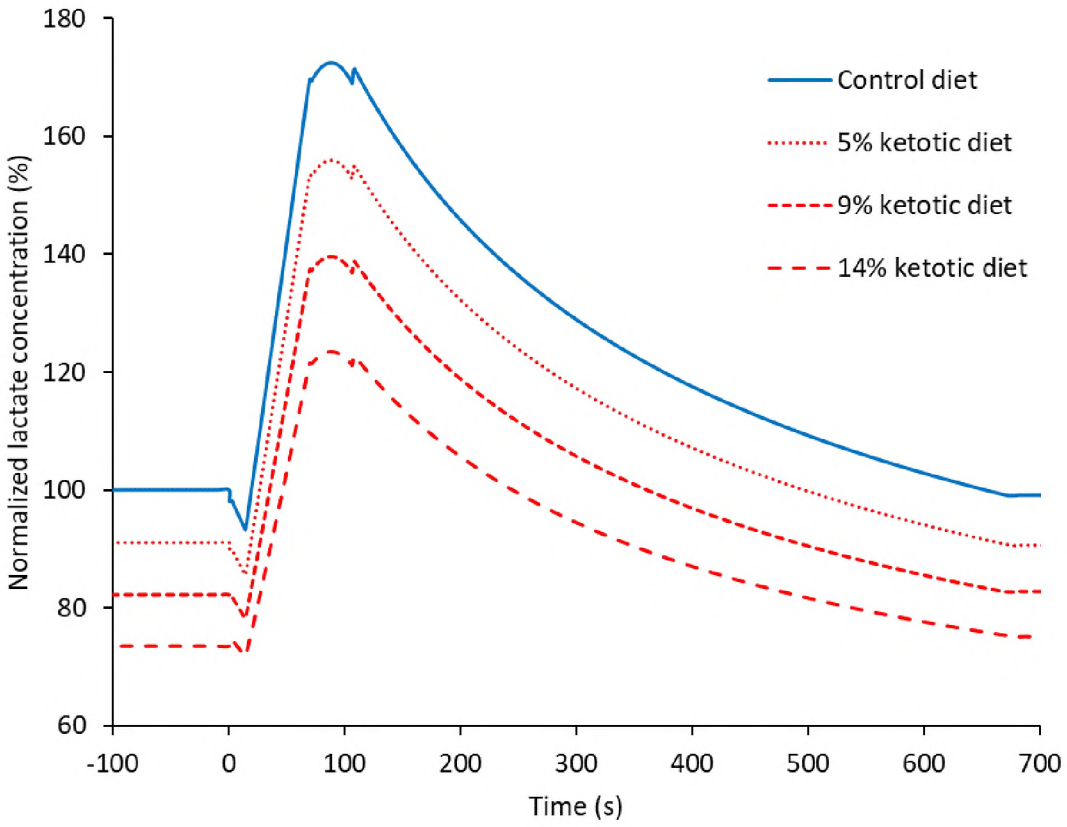

Figure VI.18. Dynamic response shown as (normalized) lactate concentration for different levels of ketosis.
Diets indicated as varying percentages of ketone bodies entering the TCA cycle following a 5-s stimulus show lactate profiles in ketotic conditions to be same as the standard conditions irrespective of contribution from ketone bodies.

Although, we found that the lactate levels decrease under ketotic conditions (Fig. VI.1 and 5), the major finding from these sensitivity studies was that the levels of lactate for varying ketone body contributions to metabolism (5-14%) showed to directly correlate with the contribution of ketone bodies flux to the total CMR.

CHAPTER VII

DISCUSSIONS AND CONCLUSIONS

A phenomenological metabolic model for mammalian brain tissue was formulated in this Dissertation. The model was validated via experimental data (Hu & Wilson, 1997) on the dynamics of lactate in extra-cellular space under conditions of the neuronal activation. The model was validated using reported data for standard diet conditions.

One of the main goals of this study was to examine the carbon flux balance shift stemming from the metabolism of ketone bodies in neurons. This shift was hypothesized to result in a proportional decrease in the glycolytic activity in astrocytes. Model predictions for lactate under standard diet conditions allowed to examine changes in metabolic fluxes both in the mitochondria (TCA) and cytosol (ANLS). The model predicted an increase in the flux of lactate conversion to pyruvate under activated conditions, as well as an increase in the lactate concentration levels following a periodic stimulation pattern.

Dienel's research on a lactate release model, stated that that astrocyte-produced lactate will not only be transported to neurons, but will also be released to blood (Dienel, 2013). Since cerebral metabolic rates (CMR) of glucose consumption can be measured by

following the CO_2 producing rate, this release results in an underestimation of the CMR of glucose consumption, Indeed, if a fraction of the lactate is released to blood instead of being oxidized, CMR will be underestimated by the CO_2 release rates when compared to glucose consumption. In the model formulated in this dissertation the flux rate of the astrocyte-neuron lactate shuttle (ANLS) estimated at steady state suggests that the net lactate release flux to blood is null at steady state.

In the TCA cycle (mitochondria), the model predicted an increased flux from acetyl-CoA to citrate and from citrate to αKG, supporting the bio-chemical mechanism known for the TCA cycle: changes in citrate levels are known to be metabolic regulators of glycolysis and ATP production. Thus, for instance, examination of these fluxes during neuronal activation revealed a negative trend (deceleration) in the flux of citrate to αKG during the recovery from the stimulus, suggesting a decrease in citrate levels. These results also are consistent with an increase in the αKG to succinyl-CoA flux (during stimulus); which accounts for the flux partition from acetyl-CoA towards glutamine (through OAA), which has been reported to increase during ketogenic diet conditions (Melo et al., 2006). The increase in the net flux of malate to oxaloacetate reflects the decreased activity of the malate aspartate shuttle as a result of the stimulus.

Under the state of ketosis, induced by different ketogenic diet levels, model predictions showed a similar increase in the lactate levels in Fig. VII.1 (~ 70%) following a stimulus than those observed under standard diet conditions.

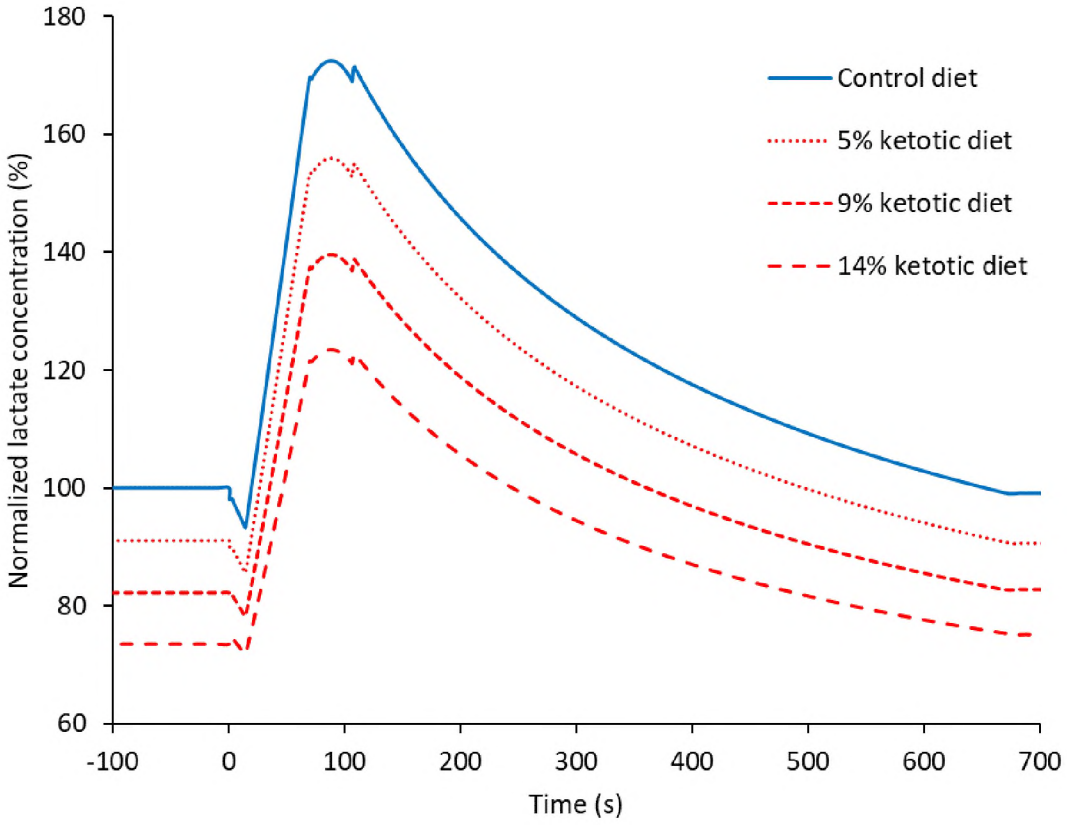

Figure VII.19. Dynamic response shown as (normalized) lactate concentration for different levels of ketosis.
Diets indicated as varying percentages of ketone bodies entering the TCA cycle following a 5-s stimulus show lactate profiles in ketotic conditions to be same as the standard conditions irrespective of contribution from ketone bodies.

This suggests that there is a weak coupling between the ketone bodies metabolism and the glucose metabolism, possibly at the level of glycolysis. Thus, ketone bodies metabolism can be hypothesized to regulate glycolysis (described by the ANLS theory).

These analyses further extend the following observations:

(1) The dynamic response of lactate concentration levels to changes in βHB concentrations for a single stimulus showed similar (~70%) differences with those observed for standard diet conditions. However, with cyclic stimuli,

lactate concentration shows a cumulative effect, and the differences of lactate concentration levels between ketotic and standard diet conditions became markedly different. This suggests that stimulus induced neuronal activity (with the corresponding changes in CMR) may be weakly coupled to ketone-body metabolism as well as to the ANLS.

(2) The net flux of pyruvate from cytosol to mitochondria was found to decrease during ketotic conditions as compared to the values observed for standard diet conditions. This is in correspondence with the assumption that a fraction of the TCA cycle flux (assumed to remain constant at steady-state for both control and ketotic conditions) is sustained by ketone bodies.

(3) Ketotic conditions affect the dynamics of the fluxes associated with the activation of the TCA cycle (acetyl-CoA to citrate) and the GABA shunt/glutamate-glutamine cycle when compared to the dynamics observed for standard diet conditions. However, this study only used the dynamics of extra-cellular lactate levels to validate the metabolic model, and used changes in metabolic fluxes to express distinct outputs in control diet conditions (this study did not validate the extra-cellular lactate levels in ketotic diet). These fluxes reflect the possible change of the species levels under different diets. Since metabolic fluxes depend on the species concentration, as well as kinetic and transport parameters, our modeling dynamic flux curve is similar to the experimental data for the same parameters.

Based on these findings, one could speculate metabolic pathways associated with ketone bodies can be coupled with glycolytic activity (both in astrocytes and neurons); which is independent of the activity of the TCA cycle. While the contribution of the ketone bodies to sustain TCA activity has been widely recognized, the actual contribution of ketone bodies to the TCA cycle is unknown, particularly during activated conditions. However, even with a potential ~14% fuel substitution provided by ketone bodies; the lactate response did not appear to vary significantly qualitatively (Figs. VII.1 and 2).

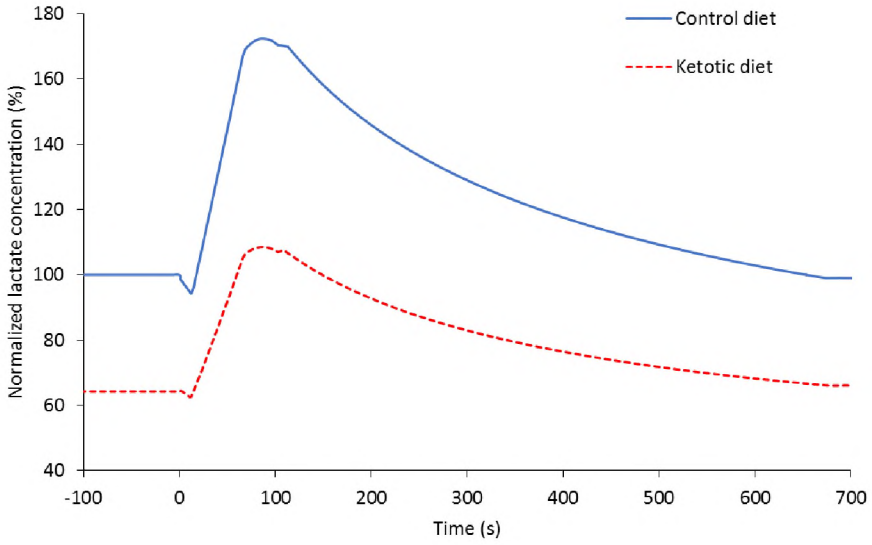

Figure VII.20. Lactate concentration dynamics following a single stimulus of 5-s and recovering peaks at 2 min to 170% of the baseline (pre-stimulus levels at t = 0: min). Dynamic response shown as lactate normalized concentration for standard (control, solid blue line) and ketogenic (red dashed line) conditions. Concentration levels for ketotic conditions were normalized with respect to baseline conditions corresponding to the control diet (concentration $_{\text{stimulus}}$/ concentration $_{\text{baseline-control diet}}$).

We recognize that by incorporating several components (pathways) highlighted in the literature (Shulman et al., 2004) the model presented here is a significant outgrowth to most available metabolic models. However, some of the features seem to suggest that the

model presented may be missing a potential coupling between the metabolism of ketone bodies and the glutamate-glutamine cycle (V_{cycle}).

Aiming to shed light on the intricate mechanisms associated with the metabolism of ketone bodies in brain tissue, this is one the key issues that requires further investigation. The model needs to be expanded to enable examining potential coupling mechanisms between V_{cycle} , glycolysis (neuronal and astrocytic), and ketone body metabolism. At present, one of the main difficulties hindering these developments if the lack of suitable experimental data to compare the output under different diet conditions.

Therefore, in the next Chapter suggested experiments are designed to produce results to validate and extend this model.

CHAPTER VIII

FURTHER RESEARCH

Although the model formulated in this dissertation revealed a number of metabolic phenomena associated with ketone bodies in mammalian brain metabolism, there are a number of unanswered questions.

Indeed, one of the driving motivations for this study was elucidating the effect of ketogenic diets (KD) on metabolic process, which may affect the development and progress of Parkinson's disease. It was shown how the increases in lipid and ketone bodies (KB), accompanied by a decrease in the glucose intake result in a substitution of glucose as the main energy source for brain. This is a natural consequence of ketogenic diets, since the substrate intake during KD cannot provide the brain with sufficient energy from glucose; therefore, requiring of a complement of energy derived from lipids and KB.

Further studies, will require incorporating into the model the connection between glucose and PD progression by connecting glycolytic fluxes with the loss of functionality of complex I. The stages formulating this connection are illustrated in the flowchart shown in Figure VIII.1 below.

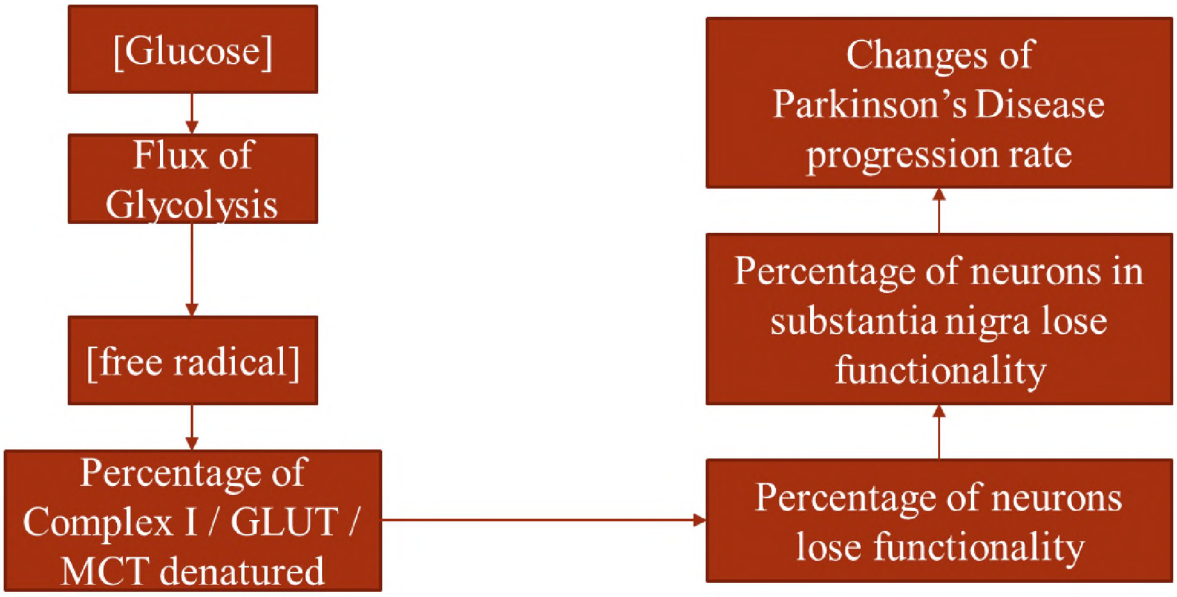

Figure VIII.21. From glucose concentration to PD progression rate.

This aim will require formulating a model capable of reproducing concentration levels of glucose in the extra-cellular space of neurons and validation via experiments including glycolytic flux rate measurements. Fig. VIII.2 below shows the relationship between glucose concentration and the normalized hexokinase reaction rate. Since hexokinase catalyzes the first step in the glycolysis, these data can be used to correlate glycolytic flux with glucose concentration levels.

The normal blood glucose concentration varies between 3–5.5 mM, this concentration range has been identified in Fig. VIII.2, which shows that the glycolytic flux is at its highest level for standard conditions.

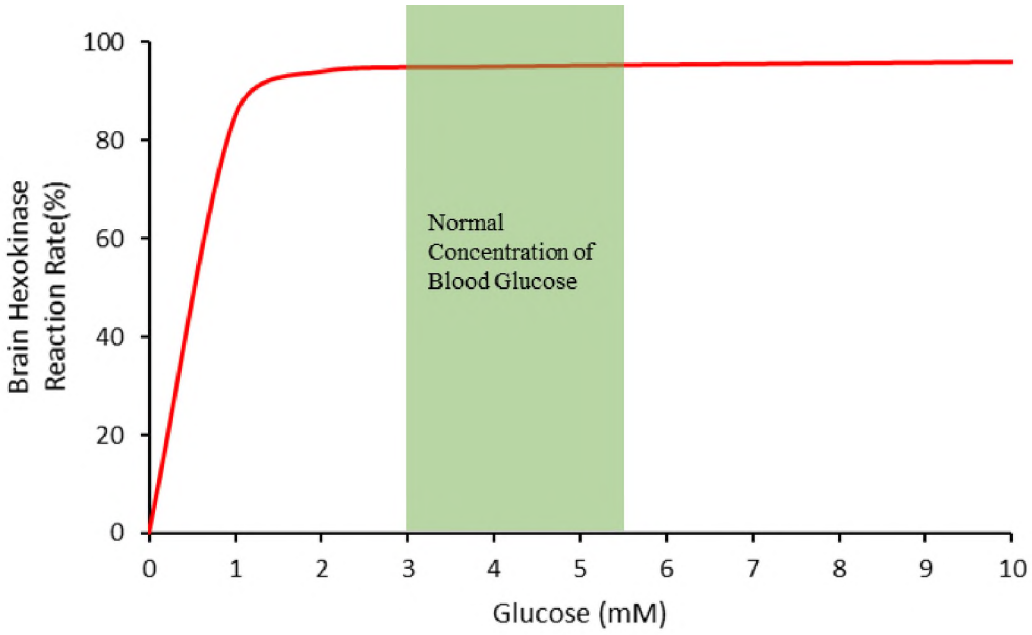

Figure VIII.22. Relationship between glucose and the first step reaction rate of glycolysis (Palmer & Palmer, 2014).

Fig. VIII.3 shows the relationship between the glucose concentration of adipocytes (storage fat cell) and free radical intensity. These measurements were carried out in vitro for adipocytes suspended in phosphate-buffered saline (PBS) solution, which replicates an environment similar to that of the extra-cellular space in brain tissue.

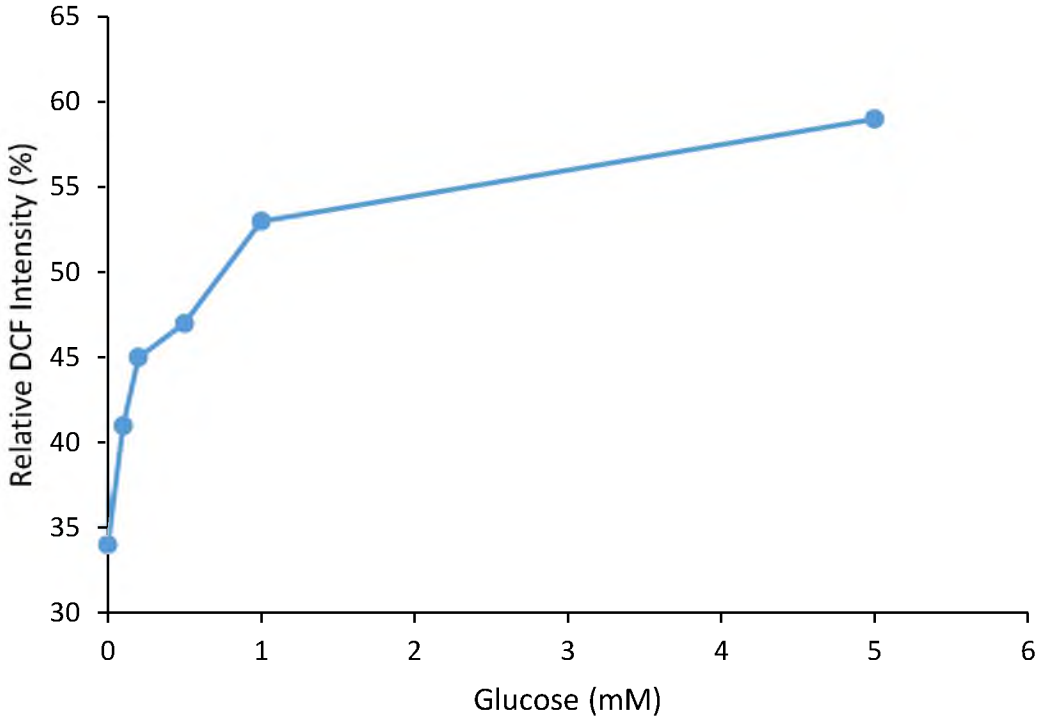

Figure VIII.23. Relationship between glucose concentration and free radical intensity (Talior et al., 2003).
DCF (2',7' –dichlorofluorescin) is the free radicals level probe. In the reaction of 2 DCHF + H_2O_2 → 2 DCF + 2 H_2O, where DCHF is 2',7' –dichlorodihydrofluorescin. The increase of free radicals (H_2O_2) concentration will increase the DCF concentration.

Literature data suggests that there is a direct correlation between the inhibition of complex I and the concentration of free radicals in the cells. Free radicals will block the respiratory chain of complex I, and result to the formation of ubisemiquinone increasing. The increasing of ubisemiquinone, the major electron donor of superoxide production, will induce higher superoxide level. Superoxide is also classified as free radicals. Therefore, more respiratory chain of complex I will be blocked, which will induce the loss of functionality for complex I . Figures VIII.4 (A) and (B) (Li et al., 2003) show two neuronal behavior effects induced by rotenone, a well-known complex I inhibitor.

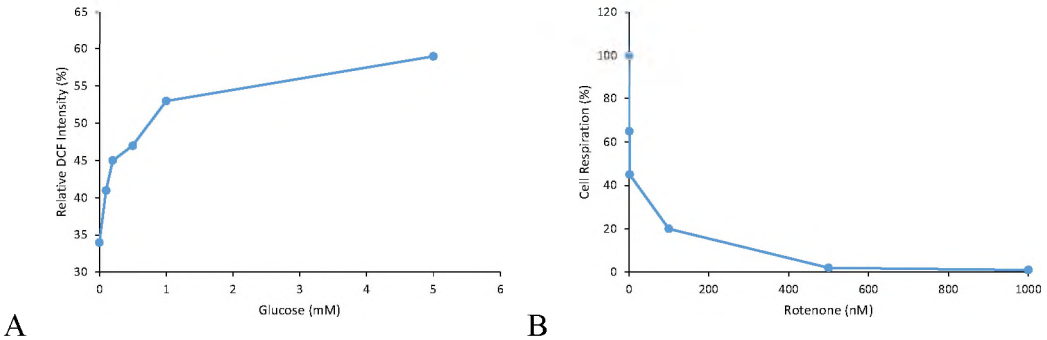

Figure VIII.24. (A) Relationship between complex I inhibitor, rotenone, and free radicals, peroxide, concentration. (B) Relationship between percentage of cell respiration and the concentration of rotenone (Li et al., 2003).

Fig. VIII.4 clearly suggests a relationship between the concentration of free radicals and cell respiration. If we can associate cell respiration with cell functionality, data like this can be utilized to formulate a relationship between glycolytic flux and loss of cell functionality. These observations suggest the need to include the dynamics of the free-radicals concentration in an expanded formulation of the metabolic model.

Since one of the aims of the the metabolic model is to elucidate the connection between glycolytic fluxes and progression of neurological disorders, the relationship between the percentage of neurons that lose functionality and the percentage of neurons whose loss of functionality can be associated with PD needs to be drawn next.

A preliminary connection between these types of neurons can be drawn from glucose utilization data, such as that presented in Table VIII.1 below

Table VIII.1. Glucose utilization rates in brain tissue (Dermon et al., 1990)

	Glucose Utilization Rate (μmol/100mg/min)
Whole Brain	5001 ± 20
Substantia Nigra	104 ± 7
SN/Brain	2.08 ± 0.14 %

A more direct connection can be drawn from a relationship between the substantia nigra cells that are losing functionality and the changes in the PD progression rate. Experimental data relevant for this connection is presented below.

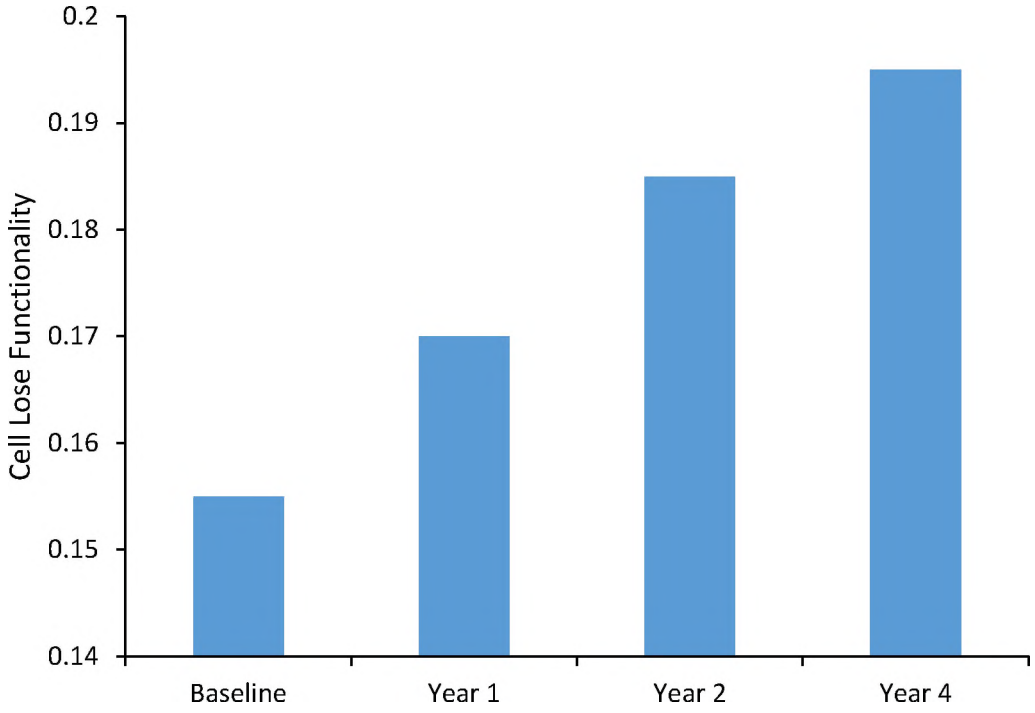

Figure VIII.25. Substantia nigra losing functionality increased with time (Burciu et al., 2017).

Indeed, Burciu's study (Burciu et al., 2017) clearly suggests a relationship between the percent of substantia nigra that has lost its functionality and the progression rate of PD.

In summary, by correlating experimental data as the one presented above, a model for the route between the extent at which glucose sustains brain energy demands (i.e., its metabolism) and its connection to the progression rate PD can be formulated and added to the metabolic model.

Transporters play an essential role in the role of the different substrates in the energy metabolism in brain tissue. Transporters regulating the availability of glucose,

lactate, and ketone bodies to cells are essential in understanding metabolic changes under different diets. One important mechanism affecting facilitated transport fluxes is the transporter self-regulation. For instance, there is evidence that MCT self-regulation might express different activity under different pH, lactate level, and hypoxia conditions (Caruso et al., 2017). These interrelations might prove essential to better correlate diets and tissue substrate levels with metabolic responses in brain tissue and should be incorporated into a more detailed model.

BIBLIOGRAPHY

Adefegha, S. A., Oboh, G., Omojokun, O. S., & Adefegha, O. M. (2016, Oct). Alterations of Na+/K+-ATPase, cholinergic and antioxidant enzymes activity by protocatechuic acid in cadmium-induced neurotoxicity and oxidative stress in Wistar rats. *Biomed Pharmacother, 83*, 559-568. https://doi.org/10.1016/j.biopha.2016.07.017

Alberty, R. A. (2005, May 12). Calculation of thermodynamic properties of species of biochemical reactants using the inverse Legendre transform. *J Phys Chem B, 109*(18), 9132-9139. https://doi.org/10.1021/jp044162j

Aubert, A., & Costalat, R. (2005, Nov). Interaction between astrocytes and neurons studied using a mathematical model of compartmentalized energy metabolism. *J Cereb Blood Flow Metab, 25*(11), 1476-1490. https://doi.org/10.1038/sj.jcbfm.9600144

Aubert, A., Costalat, R., Duffau, H., & Benali, H. (2002). Modeling of pathophysiological coupling between brain electrical activation, energy metabolism and hemodynamics: insights for the interpretation of intracerebral tumor imaging. *Acta Biotheor, 50*(4), 281-295. https://doi.org/10.1023/a:1022620818701

Aubert, A., Costalat, R., Magistretti, P. J., & Pellerin, L. (2005, Nov 8). Brain lactate kinetics: Modeling evidence for neuronal lactate uptake upon activation. *Proc Natl Acad Sci U S A, 102*(45), 16448-16453. https://doi.org/10.1073/pnas.0505427102

Barros, L. F., & Weber, B. (2018, Feb 1). CrossTalk proposal: an important astrocyte-to-neuron lactate shuttle couples neuronal activity to glucose utilisation in the brain. *J Physiol, 596*(3), 347-350. https://doi.org/10.1113/JP274944

Beal, M. F. (2003, Jun). Mitochondria, oxidative damage, and inflammation in Parkinson's disease [Research Support, Non-U.S. Gov't

Research Support, U.S. Gov't, Non-P.H.S.

Review]. *Ann N Y Acad Sci, 991*, 120-131. http://www.ncbi.nlm.nih.gov/pubmed/12846981

Beard, D. A., & Qian, H. (2005, Mar). Thermodynamic-based computational profiling of cellular regulatory control in hepatocyte metabolism. *Am J Physiol Endocrinol Metab, 288*(3), E633-644. https://doi.org/10.1152/ajpendo.00239.2004

Bouzier-Sore, A. K., Voisin, P., Canioni, P., Magistretti, P. J., & Pellerin, L. (2003, Nov). Lactate is a preferential oxidative energy substrate over glucose for neurons in culture. *J*

Cereb Blood Flow Metab, 23(11), 1298-1306. https://doi.org/10.1097/01.WCB.0000091761.61714.25

Brand, A., Engelmann, J., & Leibfritz, D. (1992, Sep-Oct). A 13C NMR study on fluxes into the TCA cycle of neuronal and glial tumor cell lines and primary cells. *Biochimie, 74*(9-10), 941-948. https://doi.org/10.1016/0300-9084(92)90078-s

Brandt, U. (2006). Energy converting NADH:quinone oxidoreductase (complex I) [Research Support, Non-U.S. Gov't

Review]. *Annu Rev Biochem, 75*, 69-92. https://doi.org/10.1146/annurev.biochem.75.103004.142539

Brekke, E., Morken, T. S., & Sonnewald, U. (2015, Mar). Glucose metabolism and astrocyte-neuron interactions in the neonatal brain [Review]. *Neurochem Int, 82*, 33-41. https://doi.org/10.1016/j.neuint.2015.02.002

Burciu, R. G., Ofori, E., Archer, D. B., Wu, S. S., Pasternak, O., McFarland, N. R., Okun, M. S., & Vaillancourt, D. E. (2017, Aug 01). Progression marker of Parkinson's disease: a 4-year multi-site imaging study. *Brain, 140*(8), 2183-2192. https://doi.org/10.1093/brain/awx146

Campbell-Burk, S. L., den Hollander, J. A., Alger, J. R., & Shulman, R. G. (1987, Nov 17). 31P NMR saturation-transfer and 13C NMR kinetic studies of glycolytic regulation during anaerobic and aerobic glycolysis. *Biochemistry, 26*(23), 7493-7500. https://doi.org/10.1021/bi00397a044

Caruso, J. P., Koch, B. J., Benson, P. D., Varughese, E., Monterey, M. D., Lee, A. E., Dave, A. M., Kiousis, S., Sloan, A. E., & Mathupala, S. P. (2017, Feb). pH, Lactate, and Hypoxia: Reciprocity in Regulating High-Affinity Monocarboxylate Transporter Expression in Glioblastoma. *Neoplasia, 19*(2), 121-134. https://doi.org/10.1016/j.neo.2016.12.011

Chen, H. Q., Jin, Z. Y., & Li, G. H. (2007, May 1). Biochanin A protects dopaminergic neurons against lipopolysaccharide-induced damage through inhibition of microglia activation and proinflammatory factors generation. *Neurosci Lett, 417*(2), 112-117. https://doi.org/10.1016/j.neulet.2006.11.045

Chih, C. P., Lipton, P., & Roberts, E. L., Jr. (2001, Oct). Do active cerebral neurons really use lactate rather than glucose? *Trends Neurosci, 24*(10), 573-578. https://doi.org/10.1016/s0166-2236(00)01920-2

Chomyn, A., & Attardi, G. (2003, May 09). MtDNA mutations in aging and apoptosis [Research Support, Non-U.S. Gov't

Research Support, U.S. Gov't, P.H.S.

Review]. *Biochem Biophys Res Commun, 304*(3), 519-529. http://www.ncbi.nlm.nih.gov/pubmed/12729587

Danbolt, N. C. (2001, Sep). Glutamate uptake [Research Support, Non-U.S. Gov't

Review]. *Prog Neurobiol, 65*(1), 1-105. http://www.ncbi.nlm.nih.gov/pubmed/11369436

Dermon, C. R., Pizarro, P., Georgopoulos, P., & Savaki, H. E. (1990, Sep). Bilateral alterations in local cerebral glucose utilization following intranigral application of the GABAergic agonist muscimol [Research Support, Non-U.S. Gov't]. *J Neurosci, 10*(9), 2861-2878. http://www.ncbi.nlm.nih.gov/pubmed/2398365

Dienel, G. A. (2004, Sep). Lactate muscles its way into consciousness: fueling brain activation [Comment

Editorial

Review]. *Am J Physiol Regul Integr Comp Physiol, 287*(3), R519-521. https://doi.org/10.1152/ajpregu.00377.2004

Dienel, G. A. (2013, Oct). Astrocytic energetics during excitatory neurotransmission: What are contributions of glutamate oxidation and glycolysis? *Neurochem Int, 63*(4), 244-258. https://doi.org/10.1016/j.neuint.2013.06.015

Dienel, G. A. (2019, Jan 1). Brain Glucose Metabolism: Integration of Energetics with Function. *Physiol Rev, 99*(1), 949-1045. https://doi.org/10.1152/physrev.00062.2017

Fernandez-Moncada, I., & Barros, L. F. (2014, Jun 15). Non-preferential fuelling of the Na(+)/K(+)-ATPase pump. *Biochem J, 460*(3), 353-361. https://doi.org/10.1042/BJ20140003

Gemperli, A. C., Schaffitzel, C., Jakob, C., & Steuber, J. (2007, Nov). Transport of Na(+) and K (+) by an antiporter-related subunit from the Escherichia coli NADH dehydrogenase I produced in Saccharomyces cerevisiae [Research Support, Non-U.S. Gov't]. *Arch Microbiol, 188*(5), 509-521. https://doi.org/10.1007/s00203-007-0272-3

Genc, S., Kurnaz, I. A., & Ozilgen, M. (2011, Oct 13). Astrocyte-neuron lactate shuttle may boost more ATP supply to the neuron under hypoxic conditions--in silico study

supported by in vitro expression data [Research Support, Non-U.S. Gov't]. *BMC Syst Biol, 5*, 162. https://doi.org/10.1186/1752-0509-5-162

Halestrap, A. P., & Meredith, D. (2004, Feb). The SLC16 gene family-from monocarboxylate transporters (MCTs) to aromatic amino acid transporters and beyond [Research Support, Non-U.S. Gov't

Review]. *Pflugers Arch, 447*(5), 619-628. https://doi.org/10.1007/s00424-003-1067-2

Heiske, M., Nazaret, C., & Mazat, J. P. (2014, Oct). Modeling the respiratory chain complexes with biothermokinetic equations - the case of complex I. *Biochim Biophys Acta, 1837*(10), 1707-1716. https://doi.org/10.1016/j.bbabio.2014.07.013

Hogstad, S., Svenneby, G., Torgner, I. A., Kvamme, E., Hertz, L., & Schousboe, A. (1988, Apr). Glutaminase in neurons and astrocytes cultured from mouse brain: kinetic properties and effects of phosphate, glutamate, and ammonia [Research Support, Non-U.S. Gov't]. *Neurochem Res, 13*(4), 383-388. http://www.ncbi.nlm.nih.gov/pubmed/2899301

Hu, Y., & Wilson, G. S. (1997, Oct). A temporary local energy pool coupled to neuronal activity: fluctuations of extracellular lactate levels in rat brain monitored with rapid-response enzyme-based sensor. *J Neurochem, 69*(4), 1484-1490. https://doi.org/10.1046/j.1471-4159.1997.69041484.x

Hulbert, A. J., Pamplona, R., Buffenstein, R., & Buttemer, W. A. (2007, Oct). Life and death: metabolic rate, membrane composition, and life span of animals [Research Support, N.I.H., Extramural

Research Support, Non-U.S. Gov't

Review]. *Physiol Rev, 87*(4), 1175-1213. https://doi.org/10.1152/physrev.00047.2006

Hyder, F., Patel, A. B., Gjedde, A., Rothman, D. L., Behar, K. L., & Shulman, R. G. (2006, Jul). Neuronal-glial glucose oxidation and glutamatergic-GABAergic function. *J Cereb Blood Flow Metab, 26*(7), 865-877. https://doi.org/10.1038/sj.jcbfm.9600263

Kaliappan, D., S.S. Koppaka, D.L. Magness, M.A. Puchowicz, J.C. LaManna, and J.E. Gatica. (2006). Metabolic Pathways in Mammalian Brain Tissue: A Multi-Compartment Dynamic Model. *Annals of Biomedical Engineering, submitted.*

Kemppainen, J., Aalto, S., Fujimoto, T., Kalliokoski, K. K., Langsjo, J., Oikonen, V., Rinne, J., Nuutila, P., & Knuuti, J. (2005, Oct 01). High intensity exercise decreases

global brain glucose uptake in humans [Research Support, Non-U.S. Gov't]. *J Physiol, 568*(Pt 1), 323-332. https://doi.org/10.1113/jphysiol.2005.091355

Knapp, L. T., & Klann, E. (2002, Oct 01). Role of reactive oxygen species in hippocampal long-term potentiation: contributory or inhibitory? [Research Support, U.S. Gov't, P.H.S.

Review]. *J Neurosci Res, 70*(1), 1-7. https://doi.org/10.1002/jnr.10371

Lacreuse, A., Moore, C. M., LaClair, M., Payne, L., & King, J. A. (2018, Jul 2). Glutamine/glutamate (Glx) concentration in prefrontal cortex predicts reversal learning performance in the marmoset. *Behav Brain Res, 346*, 11-15. https://doi.org/10.1016/j.bbr.2018.01.025

LaManna, J. C., Harrington, J. F., Vendel, L. M., Abi-Saleh, K., Lust, W. D., & Harik, S. I. (1992). Regional Blood to Brain Transport of Lactate. *The Role of Neurotransmitters in Brain Injury* 293-298.

Lamanna, J. C., Harrington, J. F., Vendel, L. M., Abisaleh, K., Lust, W. D., & Harik, S. I. (1992). Regional Blood to Brain Transport of Lactate. *Role of Neurotransmitters in Brain Injury*, 293-298. <Go to ISI>://A1992BX18G00044

Lanz, B., Gruetter, R., & Duarte, J. M. (2013, Oct 28). Metabolic Flux and Compartmentation Analysis in the Brain In vivo. *Front Endocrinol (Lausanne), 4*, 156. https://doi.org/10.3389/fendo.2013.00156

LeWitt, P. A., & Fahn, S. (2016, Apr 05). Levodopa therapy for Parkinson disease: A look backward and forward [Review]. *Neurology, 86*(14 Suppl 1), S3-12. https://doi.org/10.1212/WNL.0000000000002509

Li, N., Ragheb, K., Lawler, G., Sturgis, J., Rajwa, B., Melendez, J. A., & Robinson, J. P. (2003, Mar 07). Mitochondrial complex I inhibitor rotenone induces apoptosis through enhancing mitochondrial reactive oxygen species production. *J Biol Chem, 278*(10), 8516-8525. https://doi.org/10.1074/jbc.M210432200

Lowry, O. H., & Passonneau, J. V. (1964, Jan). The Relationships between Substrates and Enzymes of Glycolysis in Brain. *J Biol Chem, 239*, 31-42. https://www.ncbi.nlm.nih.gov/pubmed/14114860

Mackenzie, N. E., Johnson, J., Burton, G., Wagner, G. G., & Scott, A. I. (1984, Sep). 13C NMR studies of glycolysis in intra- and extra-erythrocytic Babesia microti. *Mol Biochem Parasitol, 13*(1), 13-20. https://doi.org/10.1016/0166-6851(84)90097-5

Magistretti, P. J., & Allaman, I. (2018, Apr). Lactate in the brain: from metabolic end-product to signalling molecule. *Nat Rev Neurosci, 19*(4), 235-249. https://doi.org/10.1038/nrn.2018.19

Magistretti, P. J., & Pellerin, L. (1999, Oct). Astrocytes Couple Synaptic Activity to Glucose Utilization in the Brain. *News Physiol Sci, 14*, 177-182. https://doi.org/10.1152/physiologyonline.1999.14.5.177

Maher, F., Vannucci, S. J., & Simpson, I. A. (1994, Oct). Glucose transporter proteins in brain. *FASEB J, 8*(13), 1003-1011. https://doi.org/10.1096/fasebj.8.13.7926364

Mangia, S., Simpson, I. A., Vannucci, S. J., & Carruthers, A. (2009, May). The in vivo neuron-to-astrocyte lactate shuttle in human brain: evidence from modeling of measured lactate levels during visual stimulation. *J Neurochem, 109 Suppl 1*, 55-62. https://doi.org/10.1111/j.1471-4159.2009.06003.x

Manning Fox, J. E., Meredith, D., & Halestrap, A. P. (2000, Dec 01). Characterisation of human monocarboxylate transporter 4 substantiates its role in lactic acid efflux from skeletal muscle [Research Support, Non-U.S. Gov't]. *J Physiol, 529 Pt 2*, 285-293. http://www.ncbi.nlm.nih.gov/pubmed/11101640

Martin, P. M., Gopal, E., Ananth, S., Zhuang, L., Itagaki, S., Prasad, B. M., Smith, S. B., Prasad, P. D., & Ganapathy, V. (2006, Jul). Identity of SMCT1 (SLC5A8) as a neuron-specific Na+-coupled transporter for active uptake of L-lactate and ketone bodies in the brain [Comparative Study]. *J Neurochem, 98*(1), 279-288. https://doi.org/10.1111/j.1471-4159.2006.03878.x

McKenna, M. C., Sonnewald, U., Huang, X., Stevenson, J., & Zielke, H. R. (1996, Jan). Exogenous glutamate concentration regulates the metabolic fate of glutamate in astrocytes [Research Support, Non-U.S. Gov't

Research Support, U.S. Gov't, P.H.S.]. *J Neurochem, 66*(1), 386-393. http://www.ncbi.nlm.nih.gov/pubmed/8522979

Melo, T. M., Nehlig, A., & Sonnewald, U. (2006, May-Jun). Neuronal-glial interactions in rats fed a ketogenic diet. *Neurochem Int, 48*(6-7), 498-507. https://doi.org/10.1016/j.neuint.2005.12.037

Mulukutla, B. C., Yongky, A., Grimm, S., Daoutidis, P., & Hu, W. S. (2015). Multiplicity of steady states in glycolysis and shift of metabolic state in cultured

mammalian cells. *PLoS One, 10*(3), e0121561. https://doi.org/10.1371/journal.pone.0121561

Newman, L. A., Korol, D. L., & Gold, P. E. (2011). Lactate produced by glycogenolysis in astrocytes regulates memory processing. *PLoS One, 6*(12), e28427. https://doi.org/10.1371/journal.pone.0028427

Norenberg, M. D., & Martinez-Hernandez, A. (1979, Feb 02). Fine structural localization of glutamine synthetase in astrocytes of rat brain [Research Support, U.S. Gov't, P.H.S.]. *Brain Res, 161*(2), 303-310. http://www.ncbi.nlm.nih.gov/pubmed/31966

Ojha, S., Javed, H., Azimullah, S., & Haque, M. E. (2016, Jul). beta-Caryophyllene, a phytocannabinoid attenuates oxidative stress, neuroinflammation, glial activation, and salvages dopaminergic neurons in a rat model of Parkinson disease. *Mol Cell Biochem, 418*(1-2), 59-70. https://doi.org/10.1007/s11010-016-2733-y

Palmer, A. L. P. P. P. M., & Palmer, M. (2014). *Human Metabolism Lecture Notes*. Michael Palmer. https://books.google.com/books?id=L8vmoAEACAAJ

Patel, A. B., de Graaf, R. A., Mason, G. F., Kanamatsu, T., Rothman, D. L., Shulman, R. G., & Behar, K. L. (2004, Sep). Glutamatergic neurotransmission and neuronal glucose oxidation are coupled during intense neuronal activation. *J Cereb Blood Flow Metab, 24*(9), 972-985. https://doi.org/10.1097/01.WCB.0000126234.16188.71

Pellerin, L., Bergersen, L. H., Halestrap, A. P., & Pierre, K. (2005, Jan 1-15). Cellular and subcellular distribution of monocarboxylate transporters in cultured brain cells and in the adult brain [Comparative Study

Research Support, Non-U.S. Gov't]. *J Neurosci Res, 79*(1-2), 55-64. https://doi.org/10.1002/jnr.20307

Pellerin, L., & Magistretti, P. J. (1994, Oct 25). Glutamate uptake into astrocytes stimulates aerobic glycolysis: a mechanism coupling neuronal activity to glucose utilization. *Proc Natl Acad Sci U S A, 91*(22), 10625-10629. https://doi.org/10.1073/pnas.91.22.10625

Pellerin, L., Pellegri, G., Bittar, P. G., Charnay, Y., Bouras, C., Martin, J. L., Stella, N., & Magistretti, P. J. (1998). Evidence supporting the existence of an activity-dependent astrocyte-neuron lactate shuttle. *Dev Neurosci, 20*(4-5), 291-299. https://doi.org/10.1159/000017324

Pero, R. W., Roush, G. C., Markowitz, M. M., & Miller, D. G. (1990). Oxidative stress, DNA repair, and cancer susceptibility [Research Support, Non-U.S. Gov't]. *Cancer Detect Prev, 14*(5), 555-561. http://www.ncbi.nlm.nih.gov/pubmed/2121341

Perrillat-Mercerot, A., Bourmeyster, N., Guillevin, C., Miranville, A., & Guillevin, R. (2019, Jun). Mathematical Modeling of Substrates Fluxes and Tumor Growth in the Brain. *Acta Biotheor, 67*(2), 149-175. https://doi.org/10.1007/s10441-019-09343-1

Puchowicz, M. A., Emancipator, D. S., Xu, K., Magness, D. L., Ndubuizu, O. I., Lust, W. D., & LaManna, J. C. (2005). Adaptation to chronic hypoxia during diet-induced ketosis. *Adv Exp Med Biol, 566*, 51-57. https://doi.org/10.1007/0-387-26206-7_8

Russell, J. W., Golovoy, D., Vincent, A. M., Mahendru, P., Olzmann, J. A., Mentzer, A., & Feldman, E. L. (2002, Nov). High glucose-induced oxidative stress and mitochondrial dysfunction in neurons [Research Support, Non-U.S. Gov't

Research Support, U.S. Gov't, Non-P.H.S.

Research Support, U.S. Gov't, P.H.S.]. *FASEB J, 16*(13), 1738-1748. https://doi.org/10.1096/fj.01-1027com

Salim, S. (2017, Jan). Oxidative Stress and the Central Nervous System [Review]. *J Pharmacol Exp Ther, 360*(1), 201-205. https://doi.org/10.1124/jpet.116.237503

Sanders, L. H., & Greenamyre, J. T. (2013, Sep). Oxidative damage to macromolecules in human Parkinson disease and the rotenone model [Research Support, N.I.H., Extramural

Research Support, Non-U.S. Gov't

Review]. *Free Radic Biol Med, 62*, 111-120. https://doi.org/10.1016/j.freeradbiomed.2013.01.003

Schilling, C. H., Edwards, J. S., Letscher, D., & Palsson, B. O. (2000). Combining pathway analysis with flux balance analysis for the comprehensive study of metabolic systems. *Biotechnol Bioeng, 71*(4), 286-306. https://www.ncbi.nlm.nih.gov/pubmed/11291038

Shulman, R. G., Rothman, D. L., Behar, K. L., & Hyder, F. (2004, Aug). Energetic basis of brain activity: implications for neuroimaging. *Trends Neurosci, 27*(8), 489-495. https://doi.org/10.1016/j.tins.2004.06.005

Siesjo, B. K. (1979). Brain energy metabolism. (John Wiley & Sons, New York, 1978 Annals of Neurology 5:308-308.).

Simpson, I. A., Dwyer, D., Malide, D., Moley, K. H., Travis, A., & Vannucci, S. J. (2008, Aug). The facilitative glucose transporter GLUT3: 20 years of distinction [Research Support, N.I.H., Extramural

Research Support, Non-U.S. Gov't

Review]. *Am J Physiol Endocrinol Metab, 295*(2), E242-253. https://doi.org/10.1152/ajpendo.90388.2008

Stevanovic, N. (2019). *Guyton and Hall Textbook of Medical Physiology - 12th-Ed.*

Talior, I., Yarkoni, M., Bashan, N., & Eldar-Finkelman, H. (2003, Aug). Increased glucose uptake promotes oxidative stress and PKC-delta activation in adipocytes of obese, insulin-resistant mice [Research Support, Non-U.S. Gov't]. *Am J Physiol Endocrinol Metab, 285*(2), E295-302. https://doi.org/10.1152/ajpendo.00044.2003

Utsuki, T. (2015). Development of a cerebral circulation model for the automatic control of brain physiology [Research Support, Non-U.S. Gov't]. *Conf Proc IEEE Eng Med Biol Soc, 2015*, 1890-1893. https://doi.org/10.1109/EMBC.2015.7318751

Varma, A., & Palsson, B. O. (1994, Oct). Stoichiometric flux balance models quantitatively predict growth and metabolic by-product secretion in wild-type Escherichia coli W3110. *Appl Environ Microbiol, 60*(10), 3724-3731. https://www.ncbi.nlm.nih.gov/pubmed/7986045

Varoqui, H., Zhu, H., Yao, D., Ming, H., & Erickson, J. D. (2000, Feb 11). Cloning and functional identification of a neuronal glutamine transporter [Research Support, U.S. Gov't, P.H.S.]. *J Biol Chem, 275*(6), 4049-4054. http://www.ncbi.nlm.nih.gov/pubmed/10660562

Volland, M., Blasco, J., & Hampel, M. (2017, Apr). Validation of reference genes for RT-qPCR in marine bivalve ecotoxicology: Systematic review and case study using copper treated primary Ruditapes philippinarum hemocytes. *Aquat Toxicol, 185*, 86-94. https://doi.org/10.1016/j.aquatox.2017.01.003

Williams, V., Grossman, R. G., & Edmunds, S. M. (1980). Volume and surface area estimates of astrocytes in the sensorimotor cortex of the cat. *Neuroscience, 5*(7), 1151-1159. https://doi.org/10.1016/0306-4522(80)90194-3

Xie, W., Xu, A., & Yeung, E. S. (2009, Feb 1). Determination of NAD(+) and NADH in a single cell under hydrogen peroxide stress by capillary electrophoresis. *Anal Chem, 81*(3), 1280-1284. https://doi.org/10.1021/ac802249m

Zielinski, L. P., Smith, A. C., Smith, A. G., & Robinson, A. J. (2016, Nov). Metabolic flexibility of mitochondrial respiratory chain disorders predicted by computer modelling. *Mitochondrion, 31*, 45-55. https://doi.org/10.1016/j.mito.2016.09.003

Zimmerman, J. (2003, 07/01). Thermodynamics of biochemical reactions: Alberty, Robert A. *Biochemistry and Molecular Biology Education, 31*, 275-276. https://doi.org/10.1002/bmb.2003.494031040245

APPENDICIES

APPENDIX A

REACTIONS OF GLYCOLYSIS

$\text{Glucose} + \text{ATP} \xleftrightarrow{Hexokinase(HK)} \text{Glucose 6 phosphate(G6P)} + \text{ADP}$
$\text{Glucose 6 phosphate(G6P)} \xleftrightarrow{Phosphoglucose\ isomerase\ (PGI)} \text{Fructose 6 phosphate (F6P)}$
$\text{Fructose 6 phosphate (F6P)} + \text{ATP} \xleftrightarrow{Phosphofructokinase\ (PFK1)} \text{Fructose 1,6 bisphosphate (F1,6BP)} + \text{ADP}$
$\text{Fructose 1,6 bisphosphate (F1,6BP)} \xleftrightarrow{Fructose-bisphosphate\ aldolase\ (ALDO)} \text{Glyceraldehyde 3 phosphate (GADP)} + \text{Dihydroxyacetone phosphate (DHAP)}$
$\text{Dihydroxyacetone phosphate (DHAP)} \xleftrightarrow{Triosephosphate\ isomerase\ (TPI)} \text{Glyceraldehyde 3 phosphate (GADP)}$
$\text{Glyceraldehyde 3 phosphate (GADP)} + \text{NA}D^{+} \xleftrightarrow{Glyceraldehyde\ phosphate\ dehydrogenase\ (GAPDH)} \text{1,3 Bisphosphoglycerate (1,3BPG)} + \text{NADH}$
$\text{1,3} - \text{Bisphosphoglycerate (1,3BPG)} + \text{ADP} \xleftrightarrow{Phosphoglycerate\ kinase\ (PGK)} 3 - \text{Phosphoglycerate (3PG)} + \text{ATP}$
$3 - \text{Phosphoglycerate (3PG)} \xleftrightarrow{Phosphoglycerate\ mutase\ (PGM)} 2 - \text{Phosphoglycerate (2PG)}$
$2 - \text{Phosphoglycerate (2PG)} \xleftrightarrow{Enolase\ (ENO)} \text{Phosphoenolpyruvate (PEP)} + H_2O$
$\text{Phosphoenolpyruvate (PEP)} + \text{ADP} \xleftrightarrow{Pyruvate\ kinase\ (PK)} \text{Pyruvate (Pyr)} + \text{ATP}$

APPENDIX B

REACTIONS OF TCA CYCLE

$Pyruvate + CoA - SH + NAD^+ \xleftrightarrow{Pyruvate\ dehydrogenase} Acetyl - CoA + CO_2 + NADH$
$Oxaloacetate + Acetyl\,CoA + H_2O \xleftrightarrow{Citrate\ synthase} Citrate + CoA - SH$
$Citrate \xleftrightarrow{Aconitase} cis - Aconitate + H_2O$
$cis - Aconitate + H_2O \xleftrightarrow{Aconitase} Isocitrate$
$Isocitrate + NAD^+ \xleftrightarrow{Isocitrate\ dehydrogenase} \alpha - Ketoglutarate + CO_2 + NADH$
$\alpha - Ketoglutarate + NAD^+ + CoA - SH \xleftrightarrow{\alpha Ketoglutarate\ dehydrogenase} Succinyl - CoA + NADH + CO_2$
$Succinyl - CoA + GDP + Pi \xleftrightarrow{Succinyl-CoA\ synthetase} Succinate + CoA - SH + GTP$
$Succinate + ubiquinone\,(Q) \xleftrightarrow{Succinate\ dehydrogenase} Fumarate + ubiquinol\,(QH_2)$
$Fumarate + H_2O \xleftrightarrow{Fumarase} L - Malate$
$L - Malate + NAD^+ \xleftrightarrow{Malate\ dehydrogenase} Oxaloacetate + NADH$
$\alpha - Ketoglutarate + NADH + NH_4 + H^+ \xleftrightarrow{Transaminases} Glutamate + NAD^+$
$Glutamate_{Astrocyte} \xrightarrow{Glutamine\ synthetase} Glutamine_{Astrocyte} \xrightarrow{MCT} Glutamine_{Neuron} \xrightarrow{Phosphate-activated\ glutaminase} Glutamate_{Neuron}$

APPENDIX C

CHEMICAL FORMULAS OF SPECIES OF GLYCOLYSIS, TCA CYCLE AND SOME RELATIVE REACTIONS

Species	Abbreviation	Chemical Formulas
Glucose	Glc	$C_6H_{12}O_6$
Glucose 6 phosphate	G6P	$C_6H_{13}O_9P$
Fructose 6 phosphate	F6P	$C_6H_{13}O_9P$
Fructose 1,6 bisphosphate	F1,6BP	$C_6H_{14}O_{12}P_2$
Dihydroxyacetone phosphate	DHAP	$C_3H_7O_6P$
Glyceraldehyde 3 phosphate	GADP	$C_3H_7O_6P$
1,3-Bisphosphoglycerate	1,3BPG	$C_3H_8O_{10}P_2$
3-Phosphoglycerate	3PG	$C_3H_7O_7P$
2-Phosphoglycerate	2PG	$C_3H_7O_7P$
Phosphoenolpyruvate	PEP	$C_3H_5O_6P$
Pyruvate	Pyr	$C_3H_4O_3$
Lactate	Lac	$C_3H_6O_3$
Acetyl-CoA	AcCoA	C_2H_3O-CoA $C_{23}H_{38}N_7O_{17}P_3S$
Oxaloacetate	OAA	$C_4H_4O_5$
Citrate	Cit	$C_6H_8O_7$
Isocitrate	Iso-cit	$C_6H_8O_7$
cis-Aconitate	Cis-Aco	$C_6H_6O_6$
α-Ketoglutarate	α-KG	$C_5H_6O_5$
Succinyl-CoA	Suc-CoA	$C_4H_5O_3S$-CoA $C_{25}H_{40}N_7O_{19}P_3S$
Succinate	Suc	$C_4H_6O_4$
Fumarate	Fum	$C_4H_4O_4$
Malate	Mal	$C_4H_6O_5$
Glutamate	Glu	$C_5H_9NO_4$
Glutamine	Gln	$C_5H_{10}N_2O_3$

APPENDIX D

EQUATIONS OF METABOLISM

Species	Equation	Notation	Parameter
Glucose	$\frac{dC_{1,c}}{dt} = \emptyset_1 - \emptyset_2 - \emptyset_3 + \emptyset_4$ $\emptyset_1 = \frac{T_1(C_{1,xc})}{M_1 + C_{1,xc} + C_{1,c}}$ $\emptyset_2 = \frac{T_2(C_{1,c})}{M_1 + C_{1,xc} + C_{1,c}}$ $\emptyset_3 = \frac{V_1 \frac{C_{1,c}}{K_1}}{1 + \frac{C_{1,c}}{K_1} + \frac{C_{2,c}}{K_2}} \left[\frac{PS^+/\mu^+}{1 + PS^+/\mu^+} \right]$ $\emptyset_4 = \frac{V_2 \frac{C_{2,c}}{K_2}}{1 + \frac{C_{1,c}}{K_1} + \frac{C_{2,c}}{K_2}} \left[\frac{PS^-/\mu^-}{1 + PS^-/\mu^-} \right]$	C:Concentration 1: Glucose c: Cytosol Ø: Flux xc: Extra-cellular space B: G6P 2: G6P $PS^+ = C_{ATP}/C_{ADP}$ $PS^- = 1/PS^+$ μ: corresponding controller coefficients	T_1: Transport mechanism rate constant of glucose from blood to cytosol T_2: Transport mechanism rate constant of glucose from extra-cellular space to blood M_1: Affinity of transporter GLUT V_1: Metabolism rate constant of glucose to G6P V_2: Metabolism rate constant of G6P to glucose K_1: Affinity of glucose of HK K_2: Affinity of G6P of HK
G6P	$\frac{dC_{2,c}}{dt} = \emptyset_3 - \emptyset_4 - \emptyset_5 + \emptyset_6$ $\emptyset_5 = \frac{V_3 \frac{C_{2,c}}{K_3}}{1 + \frac{C_{2,c}}{K_3} + \frac{C_{3,c}}{K_4}}$ $\emptyset_6 = \frac{V_4 \frac{C_{3,c}}{K_4}}{1 + \frac{C_{2,c}}{K_3} + \frac{C_{3,c}}{K_4}}$	3: F6P	V_3: Metabolism rate constant of G6P to F6P V_4: Metabolism rate constant of F6P to G6P K_3: Affinity of G6P of PGI K_4: Affinity of F6P of PGI
F6P	$\frac{dC_{3,c}}{dt} = \emptyset_5 - \emptyset_6 - \emptyset_7 + \emptyset_8$ $\emptyset_7 = \frac{V_5 \frac{C_{3,c}}{K_5}}{1 + \frac{C_{3,c}}{K_5} + \frac{C_{4,c}}{K_6}} \left[\frac{PS^+/\mu^+}{1 + PS^+/\mu^+} \right]$	4: F1,6BP	

	$\emptyset_8 = \frac{V_6 \frac{C_{4,c}}{K_6}}{1 + \frac{C_{3,c}}{K_5} + \frac{C_{4,c}}{K_6}} \left[\frac{PS^-/\mu^-}{1 + PS^-/\mu^-} \right]$		
F1,6BP	$\frac{dC_{4,c}}{dt} = \emptyset_7 - \emptyset_8 - \emptyset_9 + \emptyset_{10} + \emptyset_{11}$ $\emptyset_9 = \frac{V_7 \frac{C_{4,c}}{K_7}}{1 + \frac{C_{4,c}}{K_7} + \frac{C_{5,c}}{K_8} + \frac{C_{6,c}}{K_9}}$ $\emptyset_{10} = \frac{V_8 \frac{C_{5,c}}{K_8}}{1 + \frac{C_{4,c}}{K_7} + \frac{C_{5,c}}{K_8} + \frac{C_{6,c}}{K_9}}$ $\emptyset_{11} = \frac{V_9 \frac{C_{6,c}}{K_9}}{1 + \frac{C_{4,c}}{K_7} + \frac{C_{5,c}}{K_8} + \frac{C_{6,c}}{K_9}}$	5: GAP 6: DHAP	
GAP	$\frac{dC_{5,c}}{dt} = \emptyset_9 - \emptyset_{10} - \emptyset_{12} + \emptyset_{13} - \emptyset_{14} + \emptyset_{15}$ $\emptyset_{12} = \frac{V_{10} \frac{C_{5,c}}{K_{10}}}{1 + \frac{C_{5,c}}{K_{10}} + \frac{C_{6,c}}{K_{11}}}$ $\emptyset_{13} = \frac{V_{11} \frac{C_{6,c}}{K_{11}}}{1 + \frac{C_{5,c}}{K_{10}} + \frac{C_{6,c}}{K_{11}}}$ $\emptyset_{14} = \frac{V_{12} \frac{C_{5,c}}{K_{12}}}{1 + \frac{C_{5,c}}{K_{12}} + \frac{C_{7,c}}{K_{13}}} \left[\frac{RS^+/\nu^+}{1 + RS^+/\nu^+} \right]$ $\emptyset_{15} = \frac{V_{13} \frac{C_{7,c}}{K_{13}}}{1 + \frac{C_{5,c}}{K_{12}} + \frac{C_{7,c}}{K_{13}}} \left[\frac{RS^-/\nu^-}{1 + RS^-/\nu^-} \right]$	7: 1,3PG $RS^+ = C_{NADH}/C_{NAD}$ $RS^- = 1/RS^+$ ν: corresponding controller coefficients	
DHAP	$\frac{dC_{6,c}}{dt} = \emptyset_9 - \emptyset_{11} - \emptyset_{13} + \emptyset_{12}$		
1,3PG	$\frac{dC_{7,c}}{dt} = \emptyset_{14} - \emptyset_{15} - \emptyset_{16} + \emptyset_{17}$	8: 3PG	

	$$\emptyset_{16} = \frac{V_{14}\frac{C_{7,c}}{K_{14}}}{1+\frac{C_{7,c}}{K_{14}}+\frac{C_{8,c}}{K_{15}}}\left[\frac{PS^-/\mu^-}{1+PS^-/\mu^-}\right]$$ $$\emptyset_{17} = \frac{V_{15}\frac{C_{8,c}}{K_{15}}}{1+\frac{C_{7,c}}{K_{14}}+\frac{C_{8,c}}{K_{15}}}\left[\frac{PS^+/\mu^+}{1+PS^+/\mu^+}\right]$$		
3PG	$$\frac{dC_{8,c}}{dt} = \emptyset_{16} - \emptyset_{17} - \emptyset_{18} + \emptyset_{19}$$ $$\emptyset_{18} = \frac{V_{16}\frac{C_{8,c}}{K_{16}}}{1+\frac{C_{8,c}}{K_{16}}+\frac{C_{9,c}}{K_{17}}}$$ $$\emptyset_{19} = \frac{V_{17}\frac{C_{9,c}}{K_{17}}}{1+\frac{C_{8,c}}{K_{16}}+\frac{C_{9,c}}{K_{17}}}$$	9: 2PG	
2PG	$$\frac{dC_{9,c}}{dt} = \emptyset_{18} - \emptyset_{19} - \emptyset_{20} + \emptyset_{21}$$ $$\emptyset_{20} = \frac{V_{18}\frac{C_{9,c}}{K_{18}}}{1+\frac{C_{9,c}}{K_{18}}+\frac{C_{10,c}}{K_{19}}}$$ $$\emptyset_{21} = \frac{V_{19}\frac{C_{10,c}}{K_{19}}}{1+\frac{C_{9,c}}{K_{18}}+\frac{C_{10,c}}{K_{19}}}$$	10: PEP	
PEP	$$\frac{dC_{10,c}}{dt} = \emptyset_{20} - \emptyset_{21} - \emptyset_{22} + \emptyset_{23}$$ $$\emptyset_{22} = \frac{V_{20}\frac{C_{10,c}}{K_{20}}}{1+\frac{C_{10,c}}{K_{20}}+\frac{C_{11,c}}{K_{21}}}\left[\frac{PS^-/\mu^-}{1+PS^-/\mu^-}\right]$$ $$\emptyset_{23} = \frac{V_{21}\frac{C_{11,c}}{K_{21}}}{1+\frac{C_{10,c}}{K_{20}}+\frac{C_{11,c}}{K_{21}}}\left[\frac{PS^+/\mu^+}{1+PS^+/\mu^+}\right]$$	11: Pyruvate	
Pyruvate	$$\frac{dC_{11,c}}{dt} = \emptyset_{22} - \emptyset_{23} - \emptyset_{24} + \emptyset_{25} - \emptyset_{26} + \emptyset_{27}$$	12: AcCoA 13: Lactate m:	

	$\emptyset_{24} = \frac{V_{22}\frac{C_{11,c}}{K_{22}}}{1+\frac{C_{11,c}}{K_{22}}+\frac{C_{12,m}}{K_{23}}}\left[\frac{RS_m^+/\nu^+}{1+RS_m^+/\nu^+}\right]$ $\emptyset_{25} = \frac{V_{23}\frac{C_{12,c}}{K_{23}}}{1+\frac{C_{11,c}}{K_{22}}+\frac{C_{12,m}}{K_{23}}}\left[\frac{RS_m^-/\nu^-}{1+RS_m^-/\nu^-}\right]$ $\emptyset_{26} = \frac{V_{24}\frac{C_{11,c}}{K_{24}}}{1+\frac{C_{11,c}}{K_{24}}+\frac{C_{13,c}}{K_{25}}}\left[\frac{RS^-/\nu^-}{1+RS^-/\nu^-}\right]$ $\emptyset_{27} = \frac{V_{25}\frac{C_{13,c}}{K_{25}}}{1+\frac{C_{11,c}}{K_{24}}+\frac{C_{13,c}}{K_{25}}}\left[\frac{RS^+/\nu^+}{1+RS^+/\nu^+}\right]$	Mitochondria	
Lactate	$\frac{dC_{13,c}}{dt} = \emptyset_{26} - \emptyset_{27} - \emptyset_{28} + \emptyset_{29}$ $\emptyset_{28} = \frac{T_3(C_{13,c})}{M_2 + C_{13,c} + C_{14,xc}}$ $\emptyset_{29} = \frac{T_4(C_{14,xc})}{M_2 + C_{13,c} + C_{14,xc}}$	14: Lactate in extra-cellular space	T3 M2
AcCoA	$\frac{dC_{12,m}}{dt} = \emptyset_{24} - \emptyset_{25} - \emptyset_{30}$ $\emptyset_{30} = \frac{V_{26}\frac{C_{12,m}}{K_{26}}}{1+\frac{C_{12,m}}{K_{26}}+\frac{C_{15,m}}{K_{27}}+\frac{C_{16,m}}{K_{28}}}$	15: Citrate 16: OAA	
Citrate	$\frac{dC_{15,m}}{dt} = \emptyset_{30} - \emptyset_{31}$ $\emptyset_{31} = \frac{V_{27}\frac{C_{15,m}}{K_{29}}}{1+\frac{C_{15,m}}{K_{29}}+\frac{C_{17,m}}{K_{30}}}$	17: Iso-citrate	
Iso-citrate	$\frac{dC_{17,m}}{dt} = \emptyset_{31} - \emptyset_{32}$ $\emptyset_{32} = \frac{V_{28}\frac{C_{17,m}}{K_{30}}}{1+\frac{C_{17,m}}{K_{30}}+\frac{C_{18,m}}{K_{31}}}$	18: αKG	

α KG	$\frac{dC_{18,m}}{dt} = \emptyset_{32} - \emptyset_{33} - \emptyset_{34}$ $\emptyset_{33} = \frac{V_{29}\frac{C_{18,m}}{K_{31}}}{1 + \frac{C_{18,m}}{K_{31}} + \frac{C_{19,m}}{K_{32}}}\left[\frac{RS^+/_{\nu^+}}{1 + RS^+/_{\nu^+}}\right]$ $\emptyset_{34} = \frac{V_{30}\frac{C_{18,m}}{K_{33}}}{1 + \frac{C_{18,m}}{K_{33}} + \frac{C_{20,m}}{K_{34}}}$	19: Suc-CoA 20: GABA	K33: affinity of enzyme KG to GABA K34: affinity of GABA to KG
Suc-CoA	$\frac{dC_{19,m}}{dt} = \emptyset_{33} - \emptyset_{35}$ $\emptyset_{35} = \frac{V_{31}\frac{C_{19,m}}{K_{35}}}{1 + \frac{C_{19,m}}{K_{35}} + \frac{C_{21,m}}{K_{36}}}$	21: SSA	
GABA	$\frac{dC_{20,m}}{dt} = \emptyset_{34} - \emptyset_{36}$ $\emptyset_{36} = \frac{V_{32}\frac{C_{20,m}}{K_{36}}}{1 + \frac{C_{20,m}}{K_{36}} + \frac{C_{21,m}}{K_{37}}}$		
SSA	$\frac{dC_{21,m}}{dt} = \emptyset_{36} - \emptyset_{37}$ $\emptyset_{37} = \frac{V_{33}\frac{C_{21,m}}{K_{37}}}{1 + \frac{C_{21,m}}{K_{37}} + \frac{C_{22,m}}{K_{38}}}\left[\frac{RS^+/_{\nu^+}}{1 + RS^+/_{\nu^+}}\right]$	22: Fumarate	
Fumarate	$\frac{dC_{22,m}}{dt} = \emptyset_{37} - \emptyset_{38}$ $\emptyset_{38} = \frac{V_{34}\frac{C_{22,m}}{K_{38}}}{1 + \frac{C_{22,m}}{K_{38}} + \frac{C_{23,m}}{K_{39}}}$	23: MAL	
MAL	$\frac{dC_{23,m}}{dt} = \emptyset_{38} - \emptyset_{39}$ $\emptyset_{37} = \frac{V_{35}\frac{C_{23,m}}{K_{39}}}{1 + \frac{C_{23,m}}{K_{39}} + \frac{C_{16,m}}{K_{40}}}\left[\frac{RS^+/_{\nu^+}}{1 + RS^+/_{\nu^+}}\right]$		K40: affinity of OAA to MAL
OAA	$\frac{dC_{16,m}}{dt} = \emptyset_{39} - \emptyset_{30}$		

Glutamate	$\frac{dC_{24,c}}{dt} = \emptyset_{40} + \emptyset_{41} - \emptyset_{42}$ $\emptyset_{40} = \frac{V_{36}\frac{C_{18,m}}{K_{41}}}{1 + \frac{C_{18,m}}{K_{41}} + \frac{C_{24,c}}{K_{42}}}\left[\frac{RS^{-}/_{\nu^{-}}}{1 + RS^{-}/_{\nu^{-}}}\right]$ $\emptyset_{41} = \frac{T_5(C_{25,xc})}{M_3 + C_{24,c} + C_{25,xc}}$ $\emptyset_{42} = \frac{V_{37}\frac{C_{24,m}}{K_{43}}}{1 + \frac{C_{24,m}}{K_{43}} + \frac{C_{26,c}}{K_{44}}}$	24:Glutamate in cytosol 25:Glutamate in extra-cellular space 26:Glutamine in cytosol	
Glucose	$\frac{dC_{1,xc}}{dt} = -\emptyset_1 + \emptyset_2 + \emptyset_{43}$ $\emptyset_{43} = D\nabla c$	D: Diffusion coefficient ∇c: Glucose concentration gradient between blood and extra-cellular space	

APPENDIX E

PARAMETER NUMBER VALUES

(Lowry & Passonneau, 1964; Mulukutla et al., 2015)

Source	Product	VA(mM/min)	VB(mM/min)	KA(mM)	KB(mM)	Reference
Glucose	G6P	Calculated	Calculated	0.1	0.47	Mulukutla, 2015
G6P	F6P	Calculated	Calculated	0.96	0.123	Mulukutla, 2015
F6P	F1,6BP	Calculated	Calculated	0.032	0.3	Mulukutla, 2015
F1,6BP	GAP	Calculated	Calculated	0.05	0.189	Mulukutla, 2015
DHAP	GAP	Calculated	Calculated	0.43	0.162	Mulukutla, 2015
GAP	1,3PG	Calculated	Calculated	0.095	0.000671	Mulukutla, 2015
1,3PG	3PG	Calculated	Calculated	0.002	1.1	Mulukutla, 2015
3PG	2PG	Calculated	Calculated	0.168	0.0256	Mulukutla, 2015
2PG	PEP	Calculated	Calculated	0.046	0.11	Mulukutla, 2015
PEP	Pyruvate	Calculated	Calculated	0.225	4	Mulukutla, 2015
Lactate	Pyruvate	Calculated	Calculated	0.87	0.2	Lowry, 1964
Pyruvate	AcCoA	Calculated	Calculated	0.02	1.6	Mulukutla, 2015
AcCoA	Citrate	Calculated	Calculated	0.02	NA	Mulukutla, 2015
OAA	Citrate	Calculated	Calculated	0.68	NA	Mulukutla, 2015
Citrate	Isocitrate	Calculated	Calculated	0.0014	NA	Mulukutla, 2015
Isocitrate	alpha-KG	Calculated	Calculated	0.183	NA	Mulukutla, 2015
alpha-KG	SucCoA	Calculated	Calculated	0.15	NA	Mulukutla, 2015
SucCoA	SSA	Calculated	Calculated	0.055	NA	Mulukutla, 2015
GABA	SSA	Calculated	Calculated	4.1	NA	Mulukutla, 2015
SSA	Fumarate	Calculated	Calculated	0.467	NA	Mulukutla, 2015
Fumarate	Malate	Calculated	Calculated	0.0447	NA	Mulukutla, 2015
Malate	OAA	Calculated	Calculated	0.11	NA	Mulukutla, 2015
Glutamate	glutamine	Calculated	Calculated	0.45	NA	Mulukutla, 2015

Transporter	T(mM/min)	M(mM)	Reference
GLUT	0.767	1.5	Mulukutla, 2015
MCT	Calculated	7.05	Mulukutla, 2015

APPENDIX F

CONCENTRATIONS UNDER STEADY STATE CONDITIONS

Species	Blood and interstitial fluid	Cytosol (Neuron/Glia)	Mitochondria (Neuron/Glia)	Reference
	Conc. [m M]	Conc. [μ mol g^{-1}_{ww}]	Conc. [μ mol g^{-1}_{ww}]	
LAC	1.7#(STD) 1.1#(KTG)	0.79*/5.0# (STD) 0.49*/1.12*(KTG)	-	#Puchowicz, et al., 2004 *calculated
PYR	0.067#	0.15#/0.226* (STD) 0.07#/0.06# (KTG)	0.15#/0.226*	#calculated *Lowry et al., 1964
CoA	-	-	0.687	Deutsch et al., 2002
ACoA	-	-	0.076	Deutsch et al., 2002
CIT	-	-	0.357	Harik et al., 1997
αKET	-	0.3375	0.9	assumed
SCoA	-	-	0.226	assumed
SUC	-	-	0.226	assumed
MAL	-	1.356	0.226	assumed
OAA	-	1.10	1.10	Mason et al., 1992
CO_2	21.7	-	16.18	MIMS
ATP	-	2.36/2.36	2.36/2.36	Lowry et al., 1964
ADP	-	0.91/0.91	0.91/0.91	Lowry et al., 1964
NAD	-	4.37^{+}/2.38*	4.37^{+}/2.38*	+Lowry et al., 1964 *calculated
NADH	-	$4\times10^{-4+}$/1*	$4\times10^{-4+}$/1*	+Lowry et al., 1964 *calculated
O_2	8.8	-	0.963	Zhou et al., 2005
Pi	-	-	0.24	assumed
H^{+}	-	-	1.e-04	assumed

BHB	0.2 2.3*		0.1/0.11 0.25/0.02*	Puchowicz et al., 2005 (* Ketotic conditions)
AcAc	0.12	-	0.12	Puchowicz et al., 2004
PCr	-	4.2	-	Crumrine et al., 1991
Cr	-	6.5	-	Crumrine et al., 1991
Glutamate	-	49.2[+]	11.8	Patel et al., 2004 [+]assumed
Glutamine	-	-	8.4	Patel et al., 2004
Aspartate		0.8925	2.38	Seisjo, 1978
Succinate-semialdehyde	-	-	0.226	assumed
γ-aminobutyric acid	-	-	2.1	Patel et al., 2004

APPENDIX G

STEADY STATE FLUXES FOR CONTROL DIET CONDITIONS

Inter-compartment Transport Processes (Fluxes) and Substrate Interaction		
ϕ	**Transport Process**	**Net Flux, μmol g^{-1}_{ww} min^{-1}**
1	Lactate Transport, C(cytosol, glia) →XC(extra-cellular space)	0.87
2	Lactate Transport, B(blood)⇆XC	Negligible
3	Lactate Transport, XC⇆C(neuron)	0.87
4	Pyruvate Transport, B⇆XC	Negligible
5	Pyruvate Transport, XC⇆C	Negligible
6	Neuronal glycolysis	0.087
7	Pyruvate Transport, C(neuron)→M(mitochondria)	1.044
8	Pyruvate Transport, C(glia)→M	0.116
9	BHB Transport, B⇆XC	N/A
10	BHB Transport, XC⇆C	N/A
11	BHB Transport, C→M	N/A
12	AcAc Transport, B⇆XC	N/A
13	AcAc Transport, XC⇆C	N/A
14	AcAc Transport, C→M	N/A
15	Oxygen Transport, B⇆Tissue	3.48
16	Carbon dioxide Transport, Tissue⇆B	3.48

Reactions in the Neuron and Glia (Mitochondria/ Cytosol)				
ϕ		**Overall Reaction**	**Net Flux μmol g^{-1}_{ww} min^{-1}**	
			Neuron	**Glia**
17	Lactate oxidation/reduction	$LAC + NAD^+ \leftrightarrows PYR + NADH + H^+$	0.87	-0.87
18	Pyruvate Decarboxylation	$PYR + CoA + NAD \rightarrow ACoA + CO_2 + NADH + H^+$	1.044	0.116
19	Citrate Synthesis	$ACoA + OAA + H_2O \rightarrow CIT + CoA + H^+$	1.044	0.116
20	Citrate Utilization	$CIT + NAD^+ \rightarrow \alpha\text{-}KG + NADH + CO_2 + H^+$	1.044	0.116

21	α-KG Utilization	α-KG + CoA + NAD^+ → S-COA + CO_2 + NADH + H^+	0.9396	0.1044
22	Succinate Formation	S-COA + ADP + P_i → SUC + ATP + CoA	0.9396	0.1044
23	Malate Formation	SUC + (2/3)NAD^+ → MAL + (2/3) NADH	1.044	0.116
24	Malate Utilization	MAL + NAD^+ → OAA + NADH + H^+	1.044	0.116
25	AcAc Formation	BHB + NAD^+ ⇆ AcAc + NADH + H^+	N/A	N/A
26	ACoA Formation	AcAc + SCoA → ACoA + SUC	N/A	N/A
27	Glutamate Formation	α-KG + NADH + H^+ + NH_4 ⇆ GLU + NAD^+	N/A	N/A
28	Glutamine Utilization	GLN + ADP + Pi → GLU + ATP	0.0058	-0.0058
29	Oxidative Phosphorylation	0.5 O_2 + 3ADP + 3 P_i + NADH + H^+ → H_2O + 3ATP + NAD^+	1.566	0.174
30	ATP Utilization	ATP + H_2O → ADP + Pi	15.66	1.74
31	Phosphocreatine breakdown and synthesis	PCr + ADP + H^+ → Cr + ATP	Negligible	Negligible
32	ATP/ADP shuttle		Negligible	Negligible
Reactions in the GABA Shunt				
33	GABA Formation	GLU → GABA + CO_2	0.1044	0.0116
34	GABA Utilization	GABA + α-KG → SSA + GLU	0.1044	0.0116
35	SSA Utilization	SSA + NAD^+ → SUC + NADH + H^+	0.1044	0.0116
Malate-Aspartate Shuttle				
Mitochondria				
36	Aspartate Formation	OAA + GLU → α-KG + ASP	1.044	0.116
Inter-compartment Transport				
37	αKG shuttle	$αKG_{MIT}$ ⇆ $αKG_{CYT}$	1.044	0.116
38	Aspartate Transport	ASP_{MIT} ⇆ ASP_{CYT}	1.044	0.116
39	Malate shuttle	MAL_{CYT} ⇆ MAL_{MIT}	1.044	0.116
40	Glutamate Transport	GLU_{CYT} ⇆ GLU_{MIT}	1.044	0.116
Cytosol				
41	OAA Formation (CYTOSOL)	$α\text{-}KG_{CYT}$ + ASP_{CYT} → OAA_{CYT} + GLU_{CYT}	1.044	0.116

42	OAA Utilization	$OAA + NADH + H^+ \rightarrow MAL + NAD$	1.044	0.116

APPENDIX H

FURTHER TRANSFORMED FORMATION GIBBS FREE ENERGY (KJ/MOLE) OF GLYCOLYSIS AND TCA CYCLE IN ASTROCYTES AND NEURONS

Species	Astrocytes	Neurons
Glc	-426.71	-379.16
G6P	-453.48	-409.95
F6P	-450.34	-406.85
F1,6BP	-476.15	-436.71
DHAP	-230.39	-210.72
GADP	-222.73	-203.02
1,3BPG	-225.5	-203.96
3PG	-231.5	-209.87
2PG	-225.34	-203.77
PEP	-74.145	-60.53
Pyr	-100.8	-101.30
Lac	-122.55	-100.78
AcCoA	10.03	10.03
OAA	-424.98	-424.98
Citrate	-599.88	-599.88
Iso-citrate	-593.23	-593.23
α-KG	-444.51	-444.51
SucCoA	-244.87	-244.87
Glutamate	762.32	762.32
Succinate	-321.66	-321.66
Fumarate	-278.05	-278.05
Malate	-429.39	-429.39

APPENDIX I

EQUILIBRIUM CONSTANT (K^{eq}) OF METABOLIC REACTIONS OF GLYCOLYSIS AND TCA CYCLE IN ASTROCYTES AND NEURONS

Metabolic reaction	Astrocytes	Neurons
Glc→G6P	8.16E+05	8.16E+05
G6P→F6P	1.50E+00	1.50E+00
F6P→F1,6BP	1.51E+04	1.51E+04
F1,6BP→DHAP	2.67E+02	2.67E+02
F1,6BP→GADP	2.34E+01	2.34E+01
DHAP→GADP	2.97E-01	2.97E-01
GADP→1,3PG	2.45E-01	6.60E-04
1,3PG→3PG	8.41E-02	1.56E+00
3PG→2PG	2.77E-02	2.43E-01
2PG→PEP	1.23E-25	2.80E-25
PEP→Pyr	7.13E+04	1.14E+08
Pyr→Lac	4.06E+01	1.15E-01
Pyr→AcCoA	3.53E-19	3.53E-19
AcCoA+OAA→Citrate	3.29E-02	3.29E-02
Citrate→Iso-citrate	3.38E+30	3.38E+30
Iso-citrate→ α -KG	5.41E-02	5.41E-02
α -KG→SucCoA	1.36E+41	1.36E+41
SucCoA→Succinate	3.45E-205	3.45E-205
Succinate→Fumarate	1.31E+13	1.31E+13
Fumarate→Mal	3.07E-08	3.07E-08
Mal→OAA	3.47E+25	3.47E+25

APPENDIX J

PARAMETER VALUES OF ASTROCYTES AND NEURONS

		Astrocytes		Neurons				
Source	Product	VA(mM/min)	VB(mM/min)	VA(mM/min)	VB(mM/min)	KA(mM)	KB(mM)	Reference
Glucose	G6P	1.67E+01	3.72E-06	2.95E+00	3.09E-06	0.1	0.47	Mulukutla, 2015
G6P	F6P	9.26E+00	7.90E-01	1.63E+00	1.39E-01	0.96	0.123	Mulukutla, 2015
F6P	F1,6BP	5.16E+01	1.24E-03	9.11E+00	1.03E-03	0.032	0.3	Mulukutla, 2015
F1,6BP	GAP	7.47E-01	1.96E-03	4.47E+00	7.21E-01	0.05	0.189	Mulukutla, 2015
DHAP	GAP	-1.88E+02	1.19E-01	8.30E+01	7.43E+02	0.43	0.162	Mulukutla, 2015
GAP	1,3PG	4.47E+01	8.60E-01	-4.80E+00	-8.72E-02	0.095	0.000671	Mulukutla, 2015
1,3PG	3PG	-1.06E-02	-1.48E+01	-1.35E-01	-2.62E+02	0.002	1.1	Mulukutla, 2015
3PG	2PG	1.00E-01	5.51E-01	-5.35E-01	-3.35E-01	0.168	0.0256	Mulukutla, 2015
2PG	PEP	3.67E-26	7.14E-01	-1.99E-26	-1.71E-01	0.046	0.11	Mulukutla, 2015
PEP	Pyruvate	-2.55E+00	-1.35E-04	-8.98E-01	-3.61E-06	0.225	4	Mulukutla, 2015
Lactate	Pyruvate	1.68E+01	1.66E+00	5.59E-02	2.31E+00	0.87	0.2	Lowry, 1964
Pyruvate	AcCoA	2.50E+00	5.66E+20	2.50E+00	5.66E+20	0.02	1.6	Mulukutla, 2015
AcCoA	Citrate	3.01E+01	2.54E-24	3.01E+01	2.54E-24	0.02	0.004	Mulukutla, 2015
OAA	Citrate	4.58E+02	1.10E+03	4.58E+02	1.10E+03	0.68	1.6	Mulukutla, 2015
Citrate	Isocitrate	6.75E+00	2.28E-42	6.75E+00	2.28E-42	0.0014	0.0238	Mulukutla, 2015
Isocitrate	alpha-KG	6.03E+00	4.03E-34	6.03E+00	4.03E-34	0.183	0.0069	Mulukutla, 2015
alpha-KG	SucCoA	2.20E-02	1.56E+203	2.20E-02	1.56E+203	0.15	0.0069	Mulukutla, 2015
SucCoA	SSA	3.00E-01	2.02E-10	3.00E-01	2.02E-10	0.055	1.275	Mulukutla, 2015
SSA	Fumarate	3.68E+02	9.41E+11	3.68E+02	9.41E+11	0.467	3.5	Mulukutla, 2015
Fumarate	Malate	1.80E+01	2.59E-26	1.80E+01	2.59E-26	0.0447	0.0055	Mulukutla, 2015
Malate	OAA	4.85E+00	3.47E+02	4.85E+00	3.47E+02	0.11	1.6	Mulukutla, 2015

K_A and K_B take from literatures, and V_A and V_B are calculated by K^{eq} and species steady state concentrations.

APPENDIX K

REACTION GIBBS FREE ENERGY $\Delta_r G_j'^0$(KJ/MOLE) FOR GLYCOLYSIS AND TCA CYCLE IN ASTROCYTES AND NEURONS

Source	Product	Astrocytes	Neurons
Glucose	G6P	-26.77	-30.79
G6P	F6P	3.14	3.1
F6P	F1,6BP	-25.81	-29.86
F1,6BP	GAP	253.42	233.69
DHAP	GAP	7.66	7.7
GAP	1,3PG	-2.77	-0.94
1,3PG	3PG	-6	-5.91
3PG	2PG	6.16	6.1
2PG	PEP	151.195	143.24
PEP	Pyruvate	-26.655	-40.77
Lactate	Pyruvate	21.75	-0.52
Pyruvate	AcCoA	110.83	111.33
AcCoA	Citrate	-609.91	-609.91
OAA	Citrate	-174.9	-174.9
Citrate	Isocitrate	6.65	6.65
Isocitrate	alpha-KG	148.72	148.72
alpha-KG	SucCoA	199.64	199.64
SucCoA	SSA	-76.79	-76.79
SSA	Fumarate	43.61	43.61
Fumarate	Malate	-151.34	-151.34
Malate	OAA	4.41	4.41